



**Elisa Manuela Araújo
Fernandes**

**Engenharia biomimética de membranas
estratificadas livres com propriedades mecânicas
controláveis para pensos regenerativos**

**Biomimetic engineering of multilayered freestanding
membranes with tunable mechanical properties for
regenerative patches**



**Elisa Manuela Araújo
Fernandes**

**Engenharia biomimética de membranas
estratificadas livres com propriedades mecânicas
controláveis para pensos regenerativos**

**Biomimetic engineering of multilayered freestanding
membranes with tunable mechanical properties for
regenerative patches**

Tese apresentada à Universidade de Aveiro para cumprimento dos requisitos necessários à obtenção do grau de Mestre em Materiais e Dispositivos Biomédicos, realizada sob a orientação científica da Doutora Sónia Gonçalves Patrício, Bolseira Pós-Doutorada do Departamento de Química da Universidade de Aveiro e do Professor Doutor João Mano, Professor Catedrático do Departamento de Química da Universidade de Aveiro.

o júri

presidente

Professora Doutora Maria Elisabete Jorge Vieira da Costa
professora auxiliar da Universidade de Aveiro

Professor Doutor José Martinho Marques de Oliveira
professor coordenador s/ agregação da Universidade de Aveiro

Doutora Sónia Gonçalves Patrício
bolseira pós-doutorada da Universidade de Aveiro

agradecimentos

Embora a realização de uma tese de mestrado seja, pela sua finalidade académica, um trabalho individual, não posso deixar de frisar que há sempre contributos de natureza diversa, por sua vez muito importantes. Por isso, tudo isto não seria possível sem o apoio, força e energias positivas de várias pessoas, às quais quero deixar aqui expressa a minha gratidão.

Em primeiro lugar, gostaria de agradecer ao professor João Mano pela incrível oportunidade de trabalhar no COMPASS, um grupo de investigação que prima pela excelência e inovação. Em segundo, à Dra. Sónia Patrício, minha orientadora, por toda a sua disponibilidade e orientação durante este ano, permitindo-me sempre todos os recursos necessários e essenciais para a realização desta tese.

Não posso deixar de agradecer também a todo o elenco do grupo COMPASS, que de uma forma ou de outra contribuíram para a possível conclusão deste capítulo. E claro, aos fiéis companheiros de mestrado Mafalda, Liliana, Cátia, Bruno e João. Em especial, agradeço à Rita e à Jéssica por todos os momentos vividos, bons e maus, não só ao longo deste ano, mas também ao longo de todo o meu percurso nesta cidade linda que é Aveiro, foram sem dúvida um excelente pilar. Ao Luís e Lúcia expressei também a minha gratidão por para além de colegas de trabalho se terem tornado excelentes amigos.

A todos os meus amigos que, principalmente durante estes últimos meses, sentiram a minha ausência, queria primeiro dizer que “estou de volta” e depois agradecer toda a paciência, compreensão e apoio, fatores estes essenciais para o meu desempenho. Em especial, queria agradecer à Cristiana, Filipa, Mara, Anabela, Rodolfo, Andreia e Maria João, não descorando as minhas colegas casa, o que conhecido 3º esquerdo, bem como todas as pessoas que cruzaram o meu caminho, seja durante o mestrado, licenciatura ou até mesmo no secundário e afins.

Ao meu namorado, Pedro, por ter caminhado a meu lado, pela sua incessante paciência, compreensão, apoio e ajuda prestada durante a realização da presente tese, e principalmente por me mostrar sempre o lado positivo das coisas por mais difícil que fosse. No entanto, não posso também deixar passar todas aquelas vezes que, sempre com um sorriso na cara, sacrificava os nossos dias, noites, fins-de-semana e feriados em prol da concretização desta etapa. Obrigado por tudo meu amor.

Por último, tendo consciência que sem eles nada disto seria possível, dirijo um especial agradecimento aos meus pais, pelo apoio incondicional, incentivo, amizade e acima de tudo paciência demonstrados não só no decorrer desta tese, mas sim em toda a minha vida. Obrigado por me permitirem ser quem sou hoje e por me terem ensinado superar sempre os meus obstáculos e que há sempre uma luz ao fundo do túnel. Vocês são o meu maior modelo.

palavras-chave

Biomimetismo, *Layer-by-Layer*, biomateriais, membranas, aplicações biomédicas, polissacarídeos.

resumo

Desde a sua introdução, em meados dos anos 90, a técnica de *Layer-by-Layer* tem sido muito utilizada para a produção hierárquica de filmes com múltiplas camadas. É um método versátil e económico que consiste na deposição alternada de diversos materiais sobre um substrato através de forças eletrostáticas e/ou não eletrostáticas. Quando o substrato utilizado possui baixa tensão superficial, este facilita a remoção do filme sem recorrer a qualquer tipo de ajuda externa, permitindo assim a obtenção de membranas autossustentadas. Este tipo de biomaterial pode ser utilizado para mimetizar microestruturas encontradas na natureza ou para aplicação em medicina regenerativa. A inspiração em fenómenos naturais ou até mesmo em organismos é uma forma promissora de obter biomateriais com características únicas, uma área conhecida como biomimetismo. Tendo em conta tudo isto, a alforreca é um animal marinho que possui na sua estrutura uma matriz particularmente dura, porém gelatinosa chamada de mesogleia. Tendo isso em conta, o trabalho aqui apresentado visa a produção de um novo tipo de membranas estratificadas através de biopolímeros de origem marinha como é o caso do quitosano (CHT) e do alginato (ALG). Para simular a estrutura porosa da mesogleia, estes polissacarídeos foram quimicamente modificados com grupos metacrilados (MA) e a sua modificação foi confirmada através da caracterização espectroscópica por RMN e ATR-FTIR. Posteriormente, dois tipos de membranas intercaladas (CHT/ALG/CHT-MA/ALG-MA) foram produzidas e posteriormente fotorreticuladas. Relativamente às condições de deposição dos polímeros, na análise do potencial zeta verificaram-se as cargas de cada composto, enquanto que a microbalança de quartzo (QCM-D) evidenciou a boa interação eletrostática entre o CHT e ALG, bem como entre os polissacarídeos modificados. Uma vez que a alforreca apresenta boas propriedades mecânicas mesmo sendo constituída por quase 99% de água, todas as membranas foram caracterizadas quanto à capacidade de absorção de água, bem como ensaios mecânicos de tração. Assim como a mesogleia da alforreca, as membranas, quando imersas numa solução aquosa mostram alta capacidade de absorção. Por outro lado, enquanto que as membranas de (CHT/ALG)₂₀₀ apresentam um módulo de Young superior, as membranas intercaladas alcançam uma maior extensão. Finalmente, as imagens de SEM mostram que as membranas intercaladas (10/10)₂₀₀ apresentam uma estrutura mais porosa quando comparadas com as membranas (CHT/ALG)₂₀₀, evidenciando, portanto, mais semelhanças com a estrutura da mesogleia presente na alforreca.

keywords

Layer-by-Layer, Biomimetics, freestanding, membranes, polysaccharides, biomedical applications

abstract

Methods for producing multilayered thin films have garnered a powerful scientific interest due to their potential for reinventing multifunctional materials in emerging research fields, like optics, energy, membranes and also biomedicine. Since its introduction in the early 90's, layer-by-layer (LbL) assembly is a versatile method based on the sequential deposition of multivalent materials over an underlying substrate, coordinated by electrostatic and/or non-electrostatic forces. Also, when the substrate possesses low surface energy, it allows for easy film removal without resorting to any post-processing steps, thus allowing the production of free-standing (FS) membranes. Such membranes can be used across several research fields with different applications such as biomimetic membranes and regenerative medicine. Taking inspiration from natural phenomena and living organisms is a promising way of designing and rethinking novel materials with unique features, a thriving research area known as biomimetics. Regarding this, jellyfish is a free-swimming marine organism with a particularly tough, yet gelatinous matrix called mesoglea. Inspired by this, the thesis work here presented envisions the design of novel multilayered FS membranes resorting to marine-derived biopolymers. In order to mimic the jellyfish's mesoglea porous structure, chitosan (CHT), a polycation derived from marine crustaceans, and alginate (ALG), a polyanion derived from brown-algae, were initially modified with pendant methacrylic groups (MA). The successful synthesis of both modified polymers was confirmed by means of ^1H NMR and ATR-FTIR characterization. Afterwards, aiming to recapitulate the jellyfish structure, two types of intercalated (CHT/ALG/CHT-MA/ALG-MA) membranes were produced by selective photocrosslinking. As for the deposition conditions of the natural polymers, zeta potential analysis assured the positive and negative charge of the biopolymers, whereas quartz crystal microbalance with dissipation monitoring (QCM-D) demonstrated effective layer deposition of CHT/ALG, as well as among modified polysaccharides. Moreover, jellyfish is able to maintain great mechanical properties even though it is constituted of nearly 99% wt. of water. Thus, water uptake ability and tensile tests were performed in all of the produced membranes. The FS biomimetic membranes, just like jellyfish's mesoglea, when immersed in a water-like solution show a high-water uptake ability. In addition, (CHT/ALG)₂₀₀ membranes appear to have a higher Young's modulus when compared to the intercalated ones, however, these last ones achieved a greater elongation profile. Finally, scanning electron microscopy images indicate that the bioinspired intercalated membranes (10/10)₂₀₀ appear to have a more porous structure than unmodified control ones, therefore resembling the jellyfish's mesoglea anisotropic structure.

Contents

List of Figures.....	iv
List of Tables.....	viii
List of Abbreviations and Acronyms	ix
Chapter 1: Motivation.....	1
References	7
Chapter 2: Introduction.....	9
2.1. Layer-by-Layer assembly.....	11
2.1.1. Historical perspective on Layer-by-Layer self-assembly.....	11
2.1.2. Biomaterials integrated in LbL assembly.....	12
2.1.3. Interactions driving LbL assembly.....	17
2.1.4. Factors influencing LbL film formation.....	22
2.1.5. LbL Assembly Technologies.....	23
2.1.5.1. Dipping LbL assembly	24
2.1.5.2. Spin LbL assembly	25
2.1.5.3. Spray LbL assembly	26
2.1.6. Biomedical applications using LbL assembly technique	27
2.1.6.1. Multilayered membranes based on chitosan and alginate	27
2.2. Biomimetics	32
2.2.1. Nacre	33
2.2.2. Lobster cuticle	35
2.2.3. Octopus.....	36
References	38
Chapter 3: Materials and Methods.....	49
3.1. Materials.....	51
3.2. Methods.....	51
3.2.1. Synthesis of Methacrylated Polysaccharides	51
3.2.1.1. Modification of Alginate with Methacrylic Anhydride.....	51
3.2.1.2. Modification of Chitosan with Methacrylic Acid.....	52
3.2.2. Characterization of the modified polysaccharides	53
3.2.3. Film Assembly	53
3.2.3.1. Zeta Potential.....	53

3.2.3.2. Quartz crystal microbalance with dissipation monitoring	54
3.2.3.3. Production of multilayered films	54
3.2.3.4. Photocrosslinking	55
3.2.3.5. Scanning electron microscopy	56
3.2.3.6. Water uptake ability.....	56
3.2.3.7. Mechanical test	56
References	59
Chapter 4: Results and Discussion.....	61
4.1. Bioinspired approach to Tune Mechanical Properties of Multilayered Freestanding Membranes for Skin Regenerative Patches	63
Abstract	67
1. Introduction	68
2. Materials and Methods	70
2.1. Materials.....	70
2.2. Synthesis of methacrylated polysaccharides	71
2.2.1 Modification of alginate with methacrylic anhydride	71
2.2.2. Modification of chitosan with methacrylic acid.....	71
2.3. Proton nuclear magnetic resonance spectroscopy	72
2.4. Attenuated total reflectance – Fourier transform spectroscopy.....	72
2.5. Quartz crystal microbalance with dissipation monitoring.....	72
2.6. Production of multilayered films.....	73
2.7. Water uptake ability	74
2.8. Mechanical tests	74
2.9. Scanning electron spectroscopy	74
3. Results and Discussion.....	75
3.1. Synthesis and Characterization of Modified Polysaccharides	75
3.1.1. Methacrylated Alginate	75
3.1.2. Methacrylated Chitosan.....	77
3.2. Build-up of multilayered films	79
3.3. Production of the freestanding membranes	81
3.4. ATR-FTIR analysis	82
3.5. Water uptake ability	83

3.6. Mechanical tests	84
3.7. Scanning electron microscopy analysis.....	85
4. Conclusions	87
References	87
Supplementary information	91
Chapter 5: General Conclusions and Future Perspectives.....	97

List of Figures

Chapter 1: Motivation..... 1

Figure 1. Tissue engineering (TE) triad. The interplay of biomaterials, cells and regulatory signals allows the production of novel materials for TE applications..... 3

Figure 2. Images of jellyfish, a free-swimming marine organism. **(A)** Real photograph of an existing species of jellyfish (*Rhopilema Esculentum*). Image credit to Vladimir Wrangel. **(B)** Sketch of a typical jellyfish cross-section, showing how the gel-like substance, Mesoglea, is sandwiched in between epidermal and endodermal layer. **(C-D)** SEM micrographs of freeze-dried jellyfish mesoglea, **(C)** low magnification showing a layered porous structure and **(D)** high magnification showing many fibers connected to nanostructured layers of the pore walls..... 6

Chapter 2: Introduction..... 9

Figure 3. Schematic illustration of unique physiochemical and biological properties of polysaccharides.....14

Figure 4. Overview of the existing interactions driving LbL assembly, with the most commonly explored ones belonging to the purple quadrant..... 17

Figure 5. Schematic of the production of a multilayered film by sequential absorption of oppositely charged polyelectrolytes, via electrostatic interaction.....18

Figure 6. Schematic assembly process of the layered films using **(a)** post covalent conversion and **(b)** consecutive covalent fabrication..... 21

Figure 7. Effect of salt concentration on intrinsic and extrinsic charge compensation. Charge neutralization happens between polyelectrolyte chains (intrinsic process) or by counterion inclusion in multilayered films (extrinsic process).....23

Figure 8. Schematic overview of LbL assembly technologies, **(a)** Immersive assembly, **(b)** Spin assembly, **(c)** spray assembly, **(d)** Electromagnetic assembly and **(e)** Fluidic assembly..... 24

Figure 9. Overview of some existent organisms in nature that somehow inspired the scientific community due to their properties of commercial interest..... 32

Figure 10. Nacre hierarchical microarchitecture and its toughening mechanism. **a)** Network of CaCO₃ platelets glued together by a biopolymer. **b)** Brick-and-mortar architecture. **c)** Mineral bridges immersed in the polymer layer. **d)** Sketch of the toughening mechanism of nacre. **e)** Crack propagation mechanism within nacre showing obvious crack deflection..... 34

Figure 11. Hierarchical microstructure of lobster cuticle. **a)** American lobster (*Homarus americanus*) morphology. **b)** SEM image of the cuticle cross-section, showing the different layers. **c)** Hierarchical organization: (I) N-acetyl-glucosamine molecules forming (II) anti-parallel α -chitin chains. (III) nanofibrils formed of chitin molecules wrapped with proteins, which cluster to form (IV) chitin-protein fibers. (V) All fibers are oriented in the same direction. (VI) Typical twisted plywood structure chitin-protein fibers. (VII) Three-layered cuticle..... 35

Figure 12. **a)** Image of an octopus sucker (*Octopus vulgaris*) with infundibular and circumferential rim. **b)** Methodological workflow of patch development. **c)** Mechanisms underlying the suction process. **d, e)** Illustrations **d)** and photograph **e)** of octopus-inspired adhesive patches (μ -SCs). **f)** SEM image and cross-sectional optical image of bioinspired μ -SCs. **g)** Pull-off strengths for a PDMS-based μ -SCs and a nonpatterned PDMS-patch against a rough pigskin. **h, i)** Demonstration of the bioinspired adhesive fully supporting a 0.5 kg weight on hairy skin **h)** without sticky residuals after detachment **i)**. **j)** Photographs of the octopus-inspired adhesive on the hairy skin of a volunteer's hand, indicating higher peel-strength than a flat, PDMS-based adhesive..... 37

Chapter 3: Materials and Methods..... 49

Figure 13. Schematic representation of the chemical modification of alginate (ALG) with methacrylate moieties..... 52

Figure 14. Schematic representation of the chemical modification of chitosan (CHT) with methacrylate moieties..... 53

Figure 15. Dipping robot used for LbL assembly. (A) illustration of the steps during the dipping coating. (B) Real photograph of the dipping robot used to produce free-standing (FS) membranes.....	55
Figure 16. Real-time photograph of the Shimadzu MMT-101N, used to performed tensile tests in the membranes.....	57
Figure 17. Stress-strain curve. Young's modulus is obtained by the slope in elastic linear part. Ultimate Strength represents the maximum value of stress that any material could suffer, leading to its fracture.....	58
Chapter 4: Results and Discussion.....	61
Figure 18. Scheme of the multilayered rearrangements within the membrane after UV light exposure (photocrosslinking). Electrostatic interactions are combined with covalent bonds arised from photocrosslinking of methacrylate groups.....	70
Figure 19. ¹ H NMR spectrum of ALG-MA in D ₂ O at 70 °C.....	76
Figure 20. ATR-FTIR spectra of ALG-MA and its reaction components.....	77
Figure 21. ¹ H NMR spectrum of CHT-MA in D ₂ O at 70 °C.....	78
Figure 22. ATR-FTIR spectra of CHT-MA and its reaction components.....	79
Figure 23. Overview of the synthesis route, electrokinetic potential and thin film deposition. (A) Chemical modification of alginate (ALG) and chitosan (CHT) to their methacrylated (MA) counterparts. (B) Zeta-potential analysis of ALG and CHT after methacrylation. (C, D) QCM-D analysis of build-up assemblies of (C) CHT/ALG, and (D) CHT-MA/ALG-MA up to 5 deposition layers in 0.15 M NaCl, normalized frequency Δf ₇ (blue) and dissipation ΔD ₇ (red), obtained at seventh overtone.....	80
Figure 24. ATR-FTIR spectra of the FS membranes made of (CHT/ALG) ₂₀₀ exposed to UV light, red line, (10/10) ₂₀₀ , green line, and (10/10) ₂₀₀ after UV, blue line. The relevant area, after photocrosslinking, is represented in the red band.....	83
Figure 25. (A) Water uptake measurements of (CHT/ALG) ₂₀₀ , (CHT-MA/ALG-MA) ₂₀₀ , (10/10) ₂₀₀ and (25/25) ₂₀₀ FS multilayered membranes immersed in PBS solution for 10 min. (B-D) Mechanical assays performed trough tensile tests in (CHT/ALG) ₂₀₀ , (CHT-MA/ALG-MA) ₂₀₀ , (10/10) ₂₀₀ and (25/25) ₂₀₀ membranes, previously swelled in water,	

frozen in liquid nitrogen and then lyophilized overnight. After that, were hydrated in 2h of PBS solution. **(B)** Representative stress-strain curves. **(C)** Ultimate tensile strength. **(D)** Maximum extension. **(E)** Strain energy density.....85

Figure 26. SEM images of multilayered membranes structure. **(A, B)** Lyophilized membranes cross-sections which were fractured with liquid nitrogen, **(A)** (CHT/ALG)₂₀₀ and **(B)** (25/25)₂₀₀. **(C–E)** Cross-section of the freeze-dried multilayered membranes fractured during the freeze-drying process. (CHT/ALG)₂₀₀ membranes at **(C)** low and **(D)** high magnification comparing with the **(E)** intercalated (10/10)₂₀₀. **(F)** SEM micrographs of freeze-dried jellyfish mesoglea at low magnification showing a layered porous structure.....86

Figure S1†. Overview of steps needed to achieve the bioinspired membranes. **(1)** Schematic representation of the synthesis of the ALG-MA (a) and CHT-MA (b). **(2)** LbL assembly using the dipping robot equipment. **(3)** Detachment method employed to obtain the FS multilayered membrane and a real photograph of the procedure performed in the intercalated membrane (10/10)₂₀₀. **(4)** Photocrosslinking of the FS membranes..... 93

Figure S2†. All types of the produced FS multilayered membranes. **(A-B)** Control membranes: **(A)** multilayered membranes containing CHT and ALG (CHT/ALG)₂₀₀ and **(B)** membranes containing the pendant methacrylic groups (CHT-MA/ALG-MA)₂₀₀. **(C-D)** Intercalated membranes with multilayers alternately deposited with CHT and ALG and CHT-MA and ALG-MA, **(C)** ones with 10 bilayers each (10/10)₂₀₀ and **(D)** ones with 25 bilayers each (25/25)₂₀₀.....94

Figure S3†. Mechanical assays performed trough tensile tests in (CHT/ALG)₂₀₀, (CHT-MA/ALG-MA)₂₀₀, (10/10)₂₀₀ and (25/25)₂₀₀ membranes (without lyophilization), hydrated in 2h of PBS solution. **(A)** Representative stress-strain curves. **(B)** Ultimate tensile strength. **(C)** Maximum extension. **(D)** Strain energy density..... 95

List of Tables

Table 1. Most commonly used polysaccharides in Layer-by-Layer technique.....	15
Table 2. Several studies exploring chitosan and alginate FS membranes and their proposed biomedical applications.....	28

List of Abbreviations and Acronyms

^1H NMR	Proton Nuclear Magnetic Resonance
AFM	Atomic Force Microscopy
ALG	Alginate
ALG-MA	Methacrylated Alginate
ATR-FTIR	Attenuated Total Reflectance Fourier Transformed Infrared
CHT	Chitosan
CHT-MA	Methacrylated Chitosan
D₂O	Deuterium Oxide
DS	Degree of substitution
f-GF	Functionalized graphene nanoflakes
f-GNR	Functionalized graphene nanoribbons
FS	Freestanding
GO	Graphene Oxide
LB	Langmuir-Blodgett
LbL	Layer-by-Layer
MA	Methacrylate Groups
MAc	Methacrylic Acid
Man	Methacrylic Anhydride
o-GFs	Oxidized graphene flakes
o-GNRs	Oxidized graphene nanoribbons
PEMs	Polyelectrolyte multilayered films
QCM-D	Quartz Crystal Microbalance with Dissipation
RT	Room temperature
SEM	Scanning Electron Microscopy
TE	Tissue Engineering
UV	Ultraviolet

Chapter 1: Motivation

Throughout their lifetime, humans can experience several different acute diseases and traumas that distress both cells and their biochemical microenvironment, which can lead to severe degeneration of these living systems, either at cell- or tissue-level, or in a worse scenario, the malfunction of entire organ systems ¹. Taking that in mind, the vision of developing materials with intrinsic healing ability, based on molecular and cellular technologies refined over the years, has been extensively investigated worldwide leading to the advent of advanced regenerative medicine. This is an attractive multidisciplinary field, with current clinical applications and tangible future expectations, which aims to restore, maintain or enhance tissues and hence organ functions ². This type of medicine is the result of intertwining several novel and thriving areas like tissue engineering, stem cell research gene therapy and therapeutic cloning ^{3,4}. Tissue engineering (TE), was first presented to the broad scientific community by Langer and Vacanti in 1993, and interestingly their definitions is still applied until today ⁵. The ultimate paradigm of TE relies on the complex interplay between biomaterials, cells and signaling molecules, with a goal to mimic the well-orchestrated natural complexity and potentially act as a template for tissue regeneration (Figure 1) ^{6,7}. However, so far, the clinical application of tissue engineering has been restricted to a limited number of biomaterials due to slow translation into clinical practice.

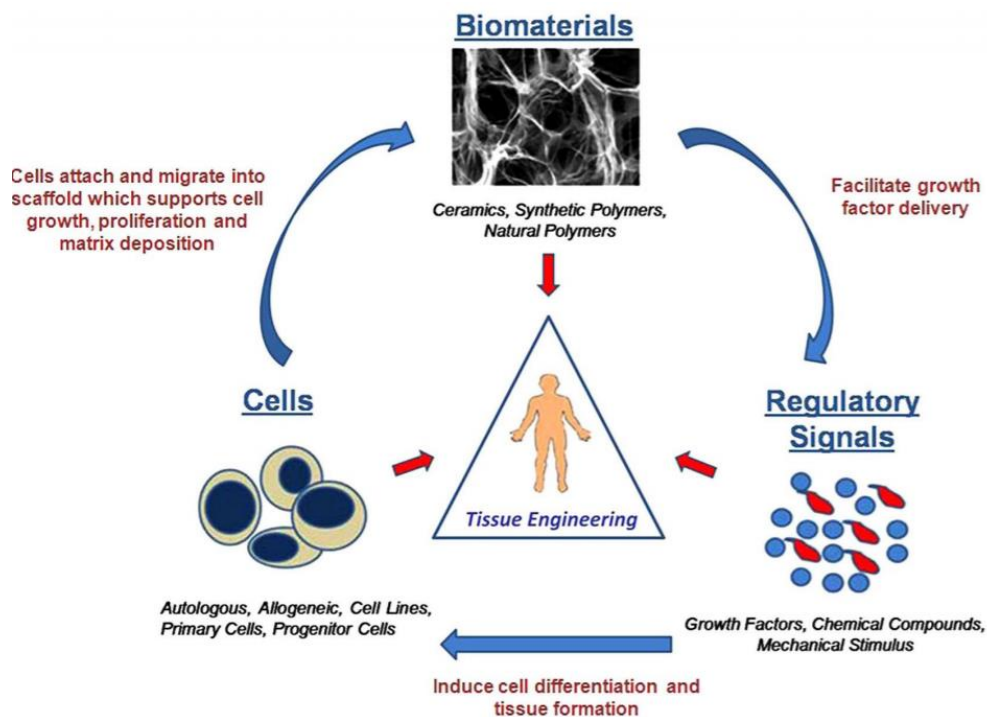


Figure 1. Tissue engineering (TE) triad. The interplay of biomaterials, cells and regulatory signals allows the production of novel materials for TE applications. Retrieved from reference ⁸.

Chapter 1: Motivation

The development of biomaterials plays an important role in most tissue engineering strategies. In the last few decades, several studies have been conducted with the primary focus in the fabrication of new and improved biomimetic materials for a vast range of biomedical applications ^{1,9}. In order to fulfill the demanding requirements for TE, biomaterials should have attractive features such as good mechanical properties, biodegradability, non-toxicity, biocompatibility and similarity with biological tissues ¹⁰.

Among the different classes of materials, polymers have been exploited in a plethora of biomedical applications, including surgical sutures, artificial skin and organs, prostheses, bone repair, dentistry and even in drug delivery systems ¹¹. According to the polymer origin source, polymer-based biomaterials can be mainly classified in synthetic or natural origin-based. Biomaterials obtained from synthetic polymers present as main advantages high quality control and easy ability to tailor physicochemical properties (i.e. degradation). However, most of the synthetic polymers are non-biodegradable containing harmful substances and show poor bioactivity. On the other side, natural polymers have attracted much attention in the scientific community due to their resemblance to the extracellular matrix exhibiting good biocompatibility and biodegradability as well as structural versatility for chemical functionalization.

Polysaccharides from natural marine sources (as algae and arthropods) ^{12,13} have been widely employed as building blocks for the fabrication of biomaterials. For example, apart from cellulose, chitin is one of the most abundant biopolymers in nature and can be extracted from crustacean shells and shellfish wastes (e.g. shrimps). The partial deacetylation of chitin gives rise to chitosan (CHT), which is widely explored in the biomedical field due to its exceptional biocompatibility and biodegradability as well as immunological, antibacterial, bioadhesive and wound-healing activity ¹²⁻¹⁵. Another attractive and well-known marine origin polysaccharide is alginate (ALG). This natural based polymer can be extracted from brown algae and, akin to CHT, possesses essential properties for biomedical applications, such as biocompatibility, non-toxicity, non-immunogenicity and biodegradable behaviors ¹⁶⁻¹⁸. These two natural marine origin polymers are widely combined to produce multilayered freestanding membranes for TE and medicine regenerative purposes ¹⁹. Major drawbacks of the use of these natural building blocks are related with their high-water uptake ability leading to feeble mechanical properties, which impair cell adhesion ²⁰⁻²².

Apart from the use of naturally derived polymers, biomimicry is an elegant strategy for developing novel biomaterials with sophisticated features. Emulating designs and ideas found in nature requires a thorough understanding of the intrinsic properties of natural systems and their relationship with the biological functions. In this context, organisms such as mussels, spiders, octopuses, bees, geckos, among many others, have been used as successful templates for biomimetic research endeavors. Among these, jellyfish is a free-swimming marine organism with a particular umbrella-shaped belonging to the Scyphozoa class that contains a tough, yet gelatinous matrix called mesoglea (see Figure 2A-B) ^{23,24}. It is mainly made up of collagen, which can be comparable to the extracellular matrix of vertebrates, containing about 96–97 wt.% water when swelled to equilibrium. Under such high water content, which can still be as high as 99 wt.% after salt extraction, jellyfish is able to maintain the structural integrity of his body because of its well-developed microstructure (Figure 2C-D), which provides the mechanism to suppress stress concentrations at flaws and crack tips ^{23,25}.

Inspired by the dispersing stress mechanism of the jellyfish, some studies have been developed to improve the mechanical properties with attempts to recreate the well-organized mesoglea porous structure. For example, Wang and co-workers have fabricated a new hybrid hydrogel by combining the biological jellyfish gel with a synthetic one in order to increase the mechanical strength of the double network system ²³. Recently, another hybrid hydrogel based on chitin/PVA with tailored mechanical properties was also successfully developed due to the ordered layered porous structure. More interestingly, they found that the freezing/thawing played a relevant role in the formation of the porous layered network ²⁶.

Exploiting biopolymers found in nature (such as CHT and ALG) to replicate the natural microstructure of jellyfish offers a cleaner and fundamentally bioinspired concept in comparison to previous attempts.

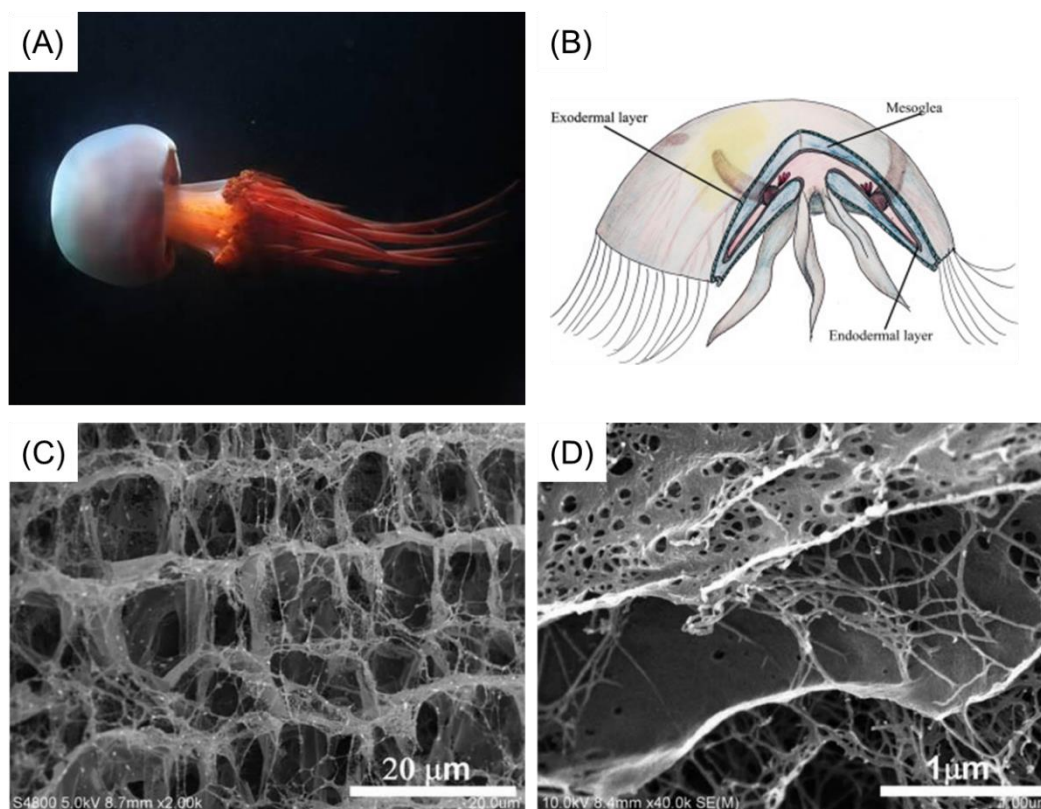


Figure 2. Images of jellyfish, a free-swimming marine organism. **(A)** Real photograph of an existing species of jellyfish (*Rhopilema Esculentum*). Image credit to Vladimir Wrangel. **(B)** Sketch of a typical jellyfish cross-section, showing how the gel-like substance, Mesoglea, is sandwiched in between epidermal and endodermal layer. **(C-D)** SEM micrographs of freeze-dried jellyfish mesoglea, **(C)** low magnification showing a layered porous structure and **(D)** high magnification showing many fibers connected to nanostructured layers of the pore walls. Adapted from references ^{23,27}.

In this context, the aim of this work is the development of novel hierarchical multilayered freestanding (FS) membranes bioinspired on the natural anisotropic structure of jellyfish mesoglea, as an innovative approach to enhance the mechanical properties of CHT and ALG multilayer assemblies. To achieve this purpose, CHT and ALG marine-origin polymers will be electrostatically combined with CHT and ALG functionalized with photopolymerizable double bonds, CHT-MA and ALG-MA, respectively. Upon photocrosslinking, it's expected the formation of interconnected porous layers intercalated with the regular stratification of CHT and ALG bilayers, which could broadly disperse stress near a crack tip, as the jellyfish gel. Such membranes will be characterized regarding their water uptake ability, mechanical properties and microstructural features. These bioinspired hierarchical systems are envisioned to be applied as regenerative patches.

In summary, this master dissertation is divided into the following chapters:

- Chapter 1: *Motivation*, which includes some introductory notes related with the main goal of this work;
- Chapter 2: *Introduction*, a literature review insight to Layer-by-Layer technology and biomimetic systems;
- Chapter 3: *Materials and Methods*;
- Chapter 4: *Results and Discussion*, where new bioinspired freestanding membranes with hierarchical architecture are developed; correlations of the mechanical properties with swelling behavior and microstructural features are also performed.;
- Chapter 5: *Conclusions and Future Perspectives*.

References

1. Iqbal, N. *et al.* Recent concepts in biodegradable polymers for tissue engineering paradigms: a critical review. *Int. Mater. Rev.* 1–36 (2018).
2. Engel, E., Michiardi, A., Navarro, M., Lacroix, D. & Planell, J. A. Nanotechnology in regenerative medicine: the materials side. *Trends Biotechnol.* **26**, 39–47 (2008).
3. Shi, C. *et al.* Therapeutic Potential of Chitosan and Its Derivatives in Regenerative Medicine. *J. Surg. Res.* **133**, 185–192 (2006).
4. Conrad, C. & Huss, R. Adult stem cell lines in regenerative medicine and reconstructive surgery. *J. Surg. Res.* **124**, 201–208 (2005).
5. Langer, R. & Vacanti, J. P. Tissue Engineering. *Science (80-.)*. **260**, 920–926 (1993).
6. Castells-sala, C. & Recha, L. Current Applications of Tissue Engineering in Biomedicine. *J. Biochips Tissue Chips* **S2**, 1–14 (2015).
7. Serban, M. A., Kluge, J. A., Laha, M. M. & Kaplan, D. L. Modular elastic patches - mechanical and biological effects. *Biomacromolecules* **11**, 2230–2237 (2011).
8. Murphy, C., O'Brien, F., Little, D. & Schindeler, A. Cell-scaffold interactions in the bone tissue engineering triad. *Eur. Cells Mater.* **26**, 120–132 (2013).
9. Ma, P. X. Biomimetic Materials for Tissue Engineering. *Adv. Drug Deliv. Rev.* **60**, 184–198 (2008).
10. Feng, Y., Lu, J., Behl, M. & Lendlein, A. Progress in depsipeptide-based biomaterials. *Macromol. Biosci.* **10**, 1008–1021 (2010).
11. Feng, Y. & Guo, J. Biodegradable polydepsipeptides. *Int. J. Mol. Sci.* **10**, 589–615 (2009).
12. Khan, F. & Tanaka, M. Designing smart biomaterials for tissue engineering. *Int. J. Mol. Sci.* **19**, 1–14 (2018).

Chapter 1: Motivation

13. Dutta, P. K., Dutta, J. & Tripathi, V. S. Chitin and chitosan: Properties and applications. *J. Sci. Ind. Res.* **63**, 20–31 (2004).
14. Younes, I. & Rinaudo, M. Chitin and chitosan preparation from marine sources. Structure, properties and applications. *Mar. Drugs* **13**, 1133–1174 (2015).
15. Sashiwa, H. & Aiba, S. I. Chemically modified chitin and chitosan as biomaterials. *Prog. Polym. Sci.* **29**, 887–908 (2004).
16. Yang, J. S., Xie, Y. J. & He, W. Research progress on chemical modification of alginate: A review. *Carbohydr. Polym.* **84**, 33–39 (2011).
17. Gombotz, W. R. & Wee, S. F. Protein release from alginate matrices. *Adv. Drug Deliv. Rev.* **64**, 194–205 (2012).
18. Pawar, S. N. & Edgar, K. J. Alginate derivatization: A review of chemistry, properties and applications. *Biomaterials* **33**, 3279–3305 (2012).
19. Martins, N. I. *et al.* Multilayered membranes with tuned well arrays to be used as regenerative patches. *Acta Biomater.* **57**, 313–323 (2017).
20. Silva, J. M., García, J. R., Reis, R. L., García, A. J. & Mano, J. F. Tuning cell adhesive properties via layer-by-layer assembly of chitosan and alginate. *Acta Biomater.* **51**, 279–293 (2017).
21. Caridade, S. G. *et al.* Myoconductive and osteoinductive free-standing polysaccharide membranes. *Acta Biomater.* **15**, 139–149 (2015).
22. Gaudière, F. *et al.* Genipin-cross-linked layer-by-layer assemblies: Biocompatible microenvironments to direct bone cell fate. *Biomacromolecules* **15**, 1602–1611 (2014).
23. Wang, X., Wang, H. & Brown, H. R. Jellyfish gel and its hybrid hydrogels with high mechanical strength. *Soft Matter* **7**, 211–219 (2011).
24. An, S. *et al.* Bio-inspired, colorful, flexible, defrostable light-scattering hybrid films for the effective distribution of LED light. *Nanoscale* **9**, 9139–9147 (2017).
25. Shaposhnikova, T., Matveev, I., Napara, T. & Podgornaya, O. Mesogleal cells of the jellyfish *Aurelia aurita* are involved in the formation of mesogleal fibres. *Cell Biol. Int.* **29**, 952–958 (2005).
26. He, M. *et al.* Construction of Chitin/PVA Composite Hydrogels with Jellyfish Gel-Like Structure and Their Biocompatibility. *Biomacromolecules* **15**, 3358–3365 (2014).
27. Pedersen, M. T., Brewer, J. R., Duelund, L. & Hansen, P. L. On the gastrophysics of jellyfish preparation. *Int. J. Gastron. Food Sci.* **9**, 34–38 (2017).

Chapter 2: Introduction

2.1. Layer-by-Layer assembly

2.1.1. Historical perspective on Layer-by-Layer self-assembly

In the middle of the 20th century, the design of thin solid films at the molecular level has aroused such a great interest to many scientists, because of their potential for applications in the fields of medicine and biology ¹. Since then, the fabrication of these well-defined nanostructures has gained prominence within the scientific community due to their customizable properties, structures and functions for many relevant applications ². In the meantime, more and more sophisticated approaches and methodological techniques have been engineered to further advance the production of these kind of films, as well as directing their molecular assembly. Moreover, several disciplines of natural sciences have studied the influence of specific surface modifications and their role in promoting fundamental changes in the properties of materials at the building-block level ³.

Historically, Langmuir first realized the monomolecular surface coating of solid substrates ^{4,5}, and then Blodgett further expanded this approach by exploring the production of multilayer coatings to develop what is now known as the Langmuir– Blodgett (LB) technique ⁶. This technique relies on a room temperature deposition process that may be used to produce monolayered and multilayered films of organic materials ⁷. Since then, LB has demonstrated to be an extremely useful method to explore the fundamental interactions of amphiphilic molecules, chemical reactions in confined geometries, and also to conceive model systems in order to calibrate and challenge new experimental techniques. However, the LB-technique seems to be difficult, expensive and limited to only certain colloids ^{8,9}.

Iler, in 1966, reported a method with the alternating surface charge of colloidal particles which could be interactively assembled onto glass substrates ¹⁰ and the work of Nicolau and his colleagues also illustrated that successive layering of substrates with oppositely charged metal ions could also produce polycrystalline coatings ¹¹.

Interestingly, the work of Iler and Nicolau probably inspired the essential breakthrough reported by Decher and his co-workers in 1992 ¹², who are responsible for revitalizing this concept of film production by relying on electrostatic interactions between oppositely-charged synthetic polyelectrolytes with ionizable surface groups. The sequentially-ordered deposition of polycations and polyanions thus resulted in the production of polyelectrolyte

Chapter 2: Introduction

multilayered films (PEMs) onto a substrate. This robust and simple method is well-known until today as Layer-by-Layer (LbL) technique assembly. This method stands out from other known techniques because of its simplicity, versatility, robustness, cost effectiveness, and also offers a massive freedom in both material selection and structural design flexibility^{13,14}. In addition, the PEMs deposition through LbL has emerged as a promising approach because it only requires charged substrates for its application. The substrate may range from flat to non-flat models, such as colloids or microcapsules¹⁵. However, the use of substrates with low surface energy may result in different structures, such as freestanding (FS) membranes. The latter approach represents a practical way to achieve robust multilayer FS membranes without using any sacrificial templates nor dissolving layers¹⁶. Interestingly, these membranes have increasing applications in the biomedical field as drug delivery systems for wound healing and tissue engineering. Moreover, this enabling technique opens up opportunities for exploiting naturally-available biopolymers, such as chitosan, alginate, heparin and hyaluronic acid, and allows researchers to expand the use of these biomaterials to new emerging fields.

Over the past few decades, LbL technique has proven markedly powerful and has demonstrated wide interdisciplinary impact on scientific research¹⁷, with applications in corrosion resistant coatings, metal/protein purification, as well as fabrication of ultratough materials^{18–22}. Moreover, in biomedical fields, LbL currently represents by far the most established strategy to produce thin films for antibacterial coatings or membranes for wound healing and tissue engineering^{23–25}. Furthermore, films with precisely controlled properties can be obtained by simply adjusting the starting experiment conditions (e.g., pH, temperature, polymer molecular weight, polyelectrolyte concentration, deposition time, number of bilayers)²⁶.

2.1.2. Biomaterials integrated in LbL assembly

Throughout more than 400 million years of evolutionary differentiative processes, nature has provided us with an immense library of diverse biomolecules and biopolymers. All these compounds play distinct roles in influencing health/disease status in organisms, owing to its wide variety of mechanical, biochemical and degradable properties. Over the last few decades, scientific efforts have been invested in exploiting such biomaterials for improving

forefront areas with high demand, such as biomedical and technological applications. Furthermore, advances in chemical modification strategies have not only enabled full customization of biomaterial backbones, but also led to the creation of new synthetic polymeric materials with unique features²⁷. In summary, there is a nearly endless variety of available materials that could be applied for LbL assembly, being the polyelectrolytes by far the most prominent ones, such as the polysaccharides (chitosan, alginate, hyaluronic acid, etc.). Nevertheless, there are several other attractive alternatives and most of them with a biological character, such as proteins (soy, collagen, fibrin gels, silk), nucleic acids (DNA and RNA) and virus particles, as well as several organic synthetic polymers, molecular assemblies and inorganic composites^{1,13}.

Among the several classes of polymeric materials that have aroused as an important tool for the biomaterials scientist, the natural origin polymers, namely polysaccharides, have received special attention during the past few decades because of their unique properties such as great abundance, low cost, eco-friendship and more importantly, their ability to confer unique properties to PEMs, such as biodegradability, biocompatibility, low toxicity, the presence of cell recognition sites as well as natural similarity with biological tissues (Figure 3)²⁸⁻³⁰. Interestingly, these biopolymers can be commonly found through diverse natural sources such as marine algae (alginate and carrageenan), plant origin (cellulose, pectin, and guar gum), microbial (dextran and chitin), and animal (chitosan, hyaluronic acid, chondroitin, and heparin)^{31,32}. Moreover, this vast array of natural sources from which these polysaccharides can be extracted from is also critical for pursuing the 2030 agenda for Sustainable Development set by the United Nations General Assembly.

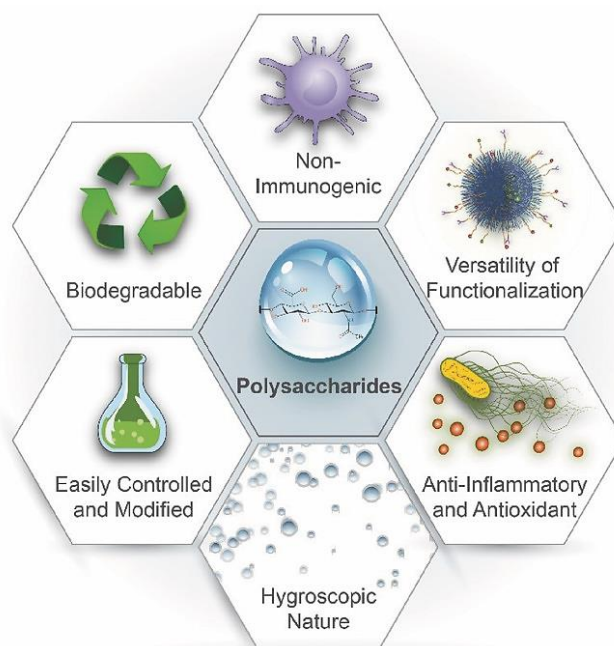
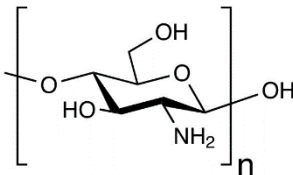
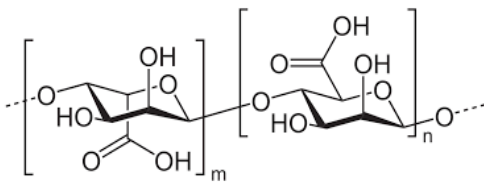
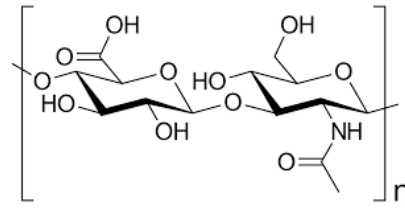
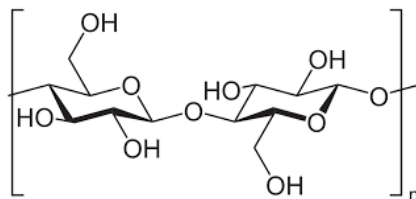


Figure 3. Schematic illustration of unique physiochemical and biological properties of polysaccharides. Retrieved from reference ³³.

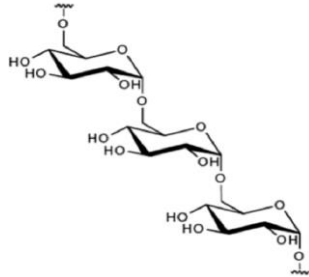
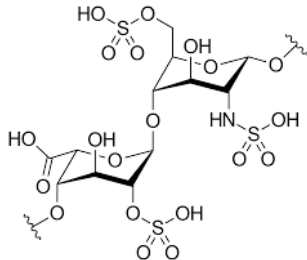
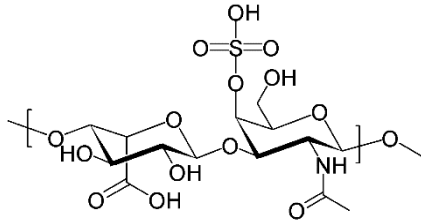
As natural origin biopolymers, polysaccharides are carbohydrates characterized by multiple sugar molecules covalently bonded through glycosidic linkages. They possess a wide range of variable molecular weight and a plentiful number of pendant reactive groups (i.e., amine, carboxyl, hydroxyl and carbonyl groups) on their backbone for chemical modification, amplifying their functional and structural diversity among the different types of polysaccharides ^{30,33,34}. Moreover, their biological synthesis promotes a heterogeneous mixture of different sequences dependent on several climate factors (e.g. seasonal conditions, humidity, place of origin, extraction conditions). However such variability can also impose significant weaknesses in reproducibility and hinder clinical translation, considering that their biological activities are strongly affected by molecular weight, chemical structure and chain conformation ^{30,35}.

Polysaccharides have been used for decades in various industrial applications, e.g. pharmaceuticals, material sciences and biofuels, as well as food and nutrition applications. More specifically, they have also proved their immense potential in the production of multilayered films using LbL assembly techniques ^{3,14,28,36-44}. Taking that in mind, Table 1 encompasses the most commonly used polysaccharides for LbL assembly constructs, as well as a brief description of their chemical structures and their relevant properties.

Table 1. Most commonly used polysaccharides in Layer-by-Layer technique.

Polysaccharide	Source	Repeating unit	Charge	Relevant properties
Chitosan	crustaceans		cationic	pH-sensitive, antimicrobial, hemostatic, muco-adhesive ^{45,46}
Alginate	brown algae		anionic	Ca ²⁺ -sensitive, absorbs wound exudate, non-adhesive ⁴⁷
Hyaluronic Acid	rooster comb, bacteria (<i>Streptococcus equi</i>)		anionic	cartilage component, joint lubricant, non-adhesive ⁴⁸
Cellulose	agricultural feedstock		anionic	ability to self-assembly into fibers via hydrogen bonds, high mechanical properties ⁴⁹

Chapter 2: Introduction

<p>Dextran</p>	<p>bacteria (<i>Leuconostoc mesenteroides</i>)</p>		<p>anionic</p>	<p>Soluble in both water and DMSO, highly available hydroxyls, anti-thrombotic^{50,51}</p>
<p>Heparin</p>	<p>bovine lung, porcine gut</p>		<p>anionic</p>	<p>anti-coagulant, hemocompatibility^{52,53}</p>
<p>Chondroitin sulfate</p>	<p>cartilaginous tissues</p>		<p>anionic</p>	<p>major component of hyaline cartilage, anti-inflammatory⁵⁴</p>

2.1.3. Interactions driving LbL assembly

Since LbL assembly first appeared as a promising way to produce thin films, several types of interactions have been studied and reported as driving forces to direct the assembly process of LbL films, such as, electrostatic, hydrophobic, hydrogen bonding, charge-transfer, covalent bonding, surface sol-gel transitions, host-guest behaviors, biospecific linkages, metallic coordination chemistry and stereo complexation⁵⁵. An overall depiction of all of these driving forces in LbL assembly is represented in Figure 4.

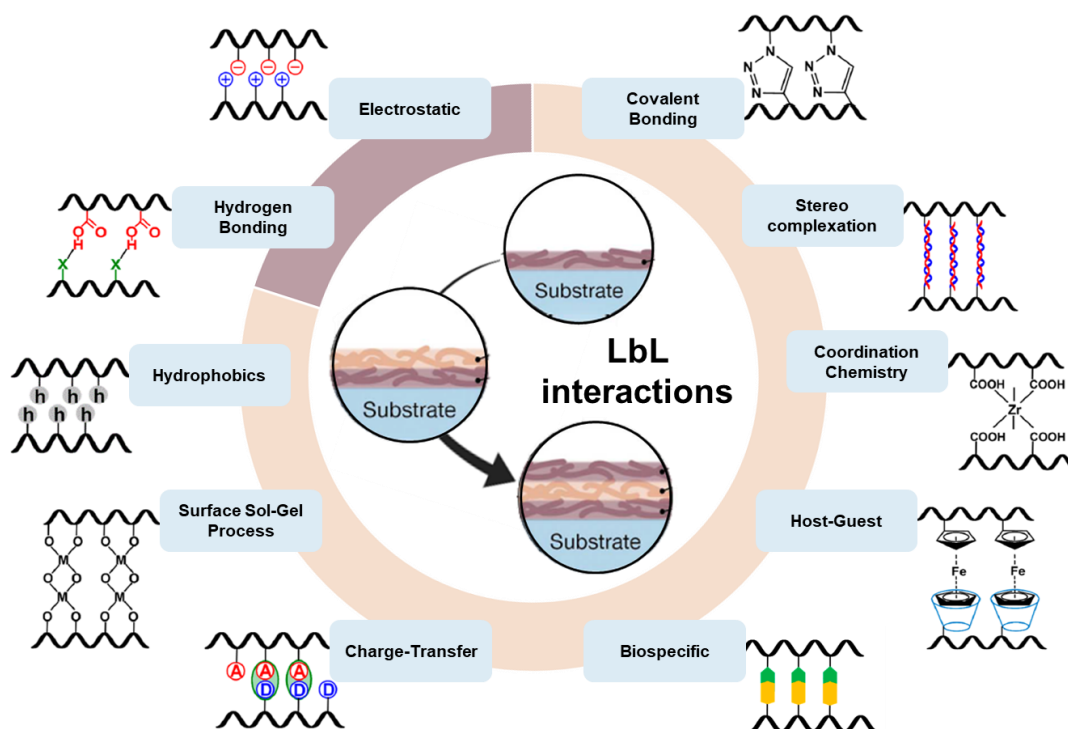


Figure 4. Overview of the existing interactions driving LbL assembly, with the most commonly explored ones belonging to the purple quadrant. Adapted from references^{55,56}.

As experienced in Nature, supramolecular and molecular structural assemblies are brought together with an immense diversity in terms of the type of connection/interaction between them⁵⁷. Likewise, there are several different interactions governing LbL assemblies. However, as demonstrated above, there are driving forces playing more prominent roles, such as the electrostatics and hydrogen bonding^{15,58}. However, while not belonging in the top two, covalent bonding and hydrophobic interactions have emerged over the years. Thus, these four interactions will be focused in more detail in the following subsection. Regarding

Chapter 2: Introduction

the other interactions, for a more extensive description please refer to this excellent review discussing the topic at hand ⁵⁵.

The electrostatic interaction is one of the most explored assembly driving forces, if not the primary one within the LbL approach, as proven by the vast majority of publications throughout the literature ⁵⁵. In fact, Decher when first exploring the LbL technique used this type of driving force to support layer assembly ¹². This kind of interaction entails the fabrication process, entirely in aqueous solutions, of sequential deposition of oppositely-charged monolayers of polymers, colloid or several other materials (virtually any charged material) onto a substrate in order to obtain cohesive and ionically crosslinked thin films ^{55,59}. In other words, this method exemplifies an ordered assembly between cationic and anionic polyelectrolytes, as represented in Figure 5 ¹³.

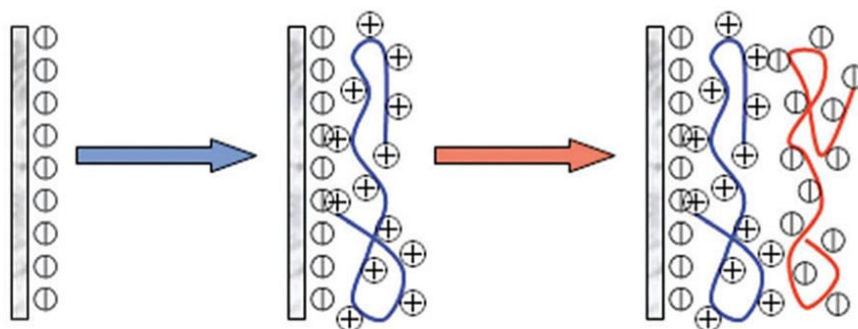


Figure 5. Schematic of the production of a multilayered film by sequential absorption of oppositely charged polyelectrolytes, via electrostatic interactions. Retrieved from reference ⁶⁰.

This type of interaction is a very attractive driving force due to its simplicity and efficiency in film preparation. Moreover, the main advantage of electrostatic forces coordinating LbL assembly is that several film/membrane parameters, including its nanoscale structure, composition, thickness, mechanical and hydration properties can be easily controlled by adjusting, for instance, the immersing solution's pH, ionic strength, temperature, etc. On the other hand, this is only applicable to charged and water soluble materials and the produced multilayered films can be less stable and robust than those obtained through hydrogen or even covalent bonding ⁵⁵. Electrostatic-driven LbL assemblies can also be exploited for the development of hollow capsules, such as those composed of CHT/ALG multilayers for encasing live cells or delivering bioactive compounds ⁶¹⁻⁶³. Moreover, chondroitin

sulfate/poly(-L-arginine) microcapsules were fabricated via electrostatic LbL deposition onto a MnCO₃ core template for encapsulation of DNA molecules ⁶⁴.

Besides electrostatic interactions, hydrogen bonding is one of the most studied and reported driving forces to date. By exploiting this interaction, an array of uncharged materials could be successfully incorporated into the production of multilayered films, which otherwise cannot be accomplished only by electrostatic interactions. Here, their present moieties can act as hydrogen bonding donors and hydrogen bonding acceptors ^{55,65}. Examples include poly(ethylene oxide) (PEO), in which the polymer backbone incorporates oxygen atoms that could act as hydrogen bonding acceptors, or alternatively, temperature-responsive poly(N-isopropylacrylamide) (PNIPAAm) polymer, in which both donor (amine) and acceptor (carbonyl) groups are present ⁶⁵. Due to the nature of this interaction, a key feature from multilayered films produced via hydrogen bonds is its high sensitivity to environmental conditions such as solutions' pH, ionic strength and temperature ⁶⁶. Moreover, the bilayer thickness can range from angstrom to the nanometer scale just by tuning the deposition pH values. Indeed, in a PEO/ poly(acrylic acid) (PAA) system, an increase in pH from 2.8 to 3.5 markedly decreased film thickness, while no film deposition was observed for pH values above 3.5 ⁶⁷. Accordingly, films composed of uncharged polymers and carboxylic acid-containing polymers can be erased by a simple increase in pH, because ionization of carboxylic groups involved in hydrogen bonding disrupts the interpolymer network ⁶⁸. Thus, this pH-triggered dissolution can be exploited to design films with distinct pH stabilities depending on the hydrogen bonding pairs used. Lee and co-workers produced multilayered thin films from poly(vinyl alcohol) (PVA) and PAA hydrogen bonding interactions and observed that the presence of free hydroxyl groups in the multilayer can tune the pH stability of the films ⁶⁹.

Also, another attractive application of hydrogen-bonded LbL assemblies is the development of LbL hollow capsules ⁷⁰. In this strategy, polymeric chains are sequentially deposited on top of a sacrificial particle template until the desired shell thickness of the LbL film is obtained, followed by dissolution of the inner core, leaving a hollow interior ⁶⁶. Similar to the electrostatic-based hollow capsules, the empty volume generated can then be filled with bioinstructive molecules for drug delivery as well as living cells for tissue engineering purposes. An interesting approach to this application is the design of hydrogen-bonded LbL shells for gentle cell encapsulation. This was achieved by Kozlovskaya and co-workers, who

Chapter 2: Introduction

exploited the hydrogen-bonding interaction between poly(N-vinylpyrrolidone) and tannic acid to achieve a high permeable LbL shell with significant biocompatibility⁷¹. Tannic acid is a natural polyphenolic tannin with intrinsic antioxidant and antibacterial properties characterized with a high pKa (*ca.* 8.5), which allows strong hydrogen bonding at physiological pH conditions⁷². Because of this capacity, it has been vastly used in several applications, including the development of LbL coatings, fibers, membranes and capsules^{73–76}. Recently, a tannic acid/poly(N-vinylpyrrolidone bilayer coating was successfully used for nerve tissue engineering purposes⁷⁷.

The hydrophobic interactions play a prominent role in the multilayered film buildup when the adsorbed molecules are uncharged, however both charged and uncharged materials can be used in this scenario⁵⁵. This interaction is well described by the relations between water and nonpolar hydrophobes (low water-soluble molecules), which usually have a long chain of carbons that do not interact with water⁷⁸. A good example of this particular interaction is the resulting mixture of fat and water. Moreover, these driving forces are widely implicated in the formation of large biological structures, since it permits the immobilization of several hydrophobic drugs and biomolecules, as well as hydrophobic protein domains^{55,79}. This driving force can strongly stabilize the internal network between layers during the multilayer buildup, however it is a weak interaction and with a rather short range in comparison to electrostatic interactions. The assembly of amphiphilic carboxymethyl pullulan with different cationic polyelectrolytes showcased the important role of hydrophobic microdomains in stabilizing interlayer formation⁸⁰.

Silk fibroin is one of the most commonly used proteins in hydrophobic-driven LbL assemblies, endowing high permeability and biocompatibility upon incorporation within multilayered films. Recently, PCL electrospun fibers were coated in a LbL fashion with a heparin-disaccharide modified silk fibroin via predominantly hydrophobic interactions with the goal of attenuating foreign body reaction towards the nanofibers⁸¹. Also, the hydrophobic domains within this protein allow anchoring of small hydrophobic drugs and increase the permeability of LbL shells produced this way, thus providing attractive features for therapeutic delivery and support cell attachment in microcapsule applications⁵⁵.

Lastly, covalent bonding has showcased its value as a critical interaction when strong, tough and robust films are desired, since they can impart enhanced strength and stability to the

stratified multilayered construction⁵⁵. Overall, these interactions comprehend two different building strategies, namely one termed “post covalent conversion” and the other “consecutive covalent fabrication”, both represented below in Figure 6.

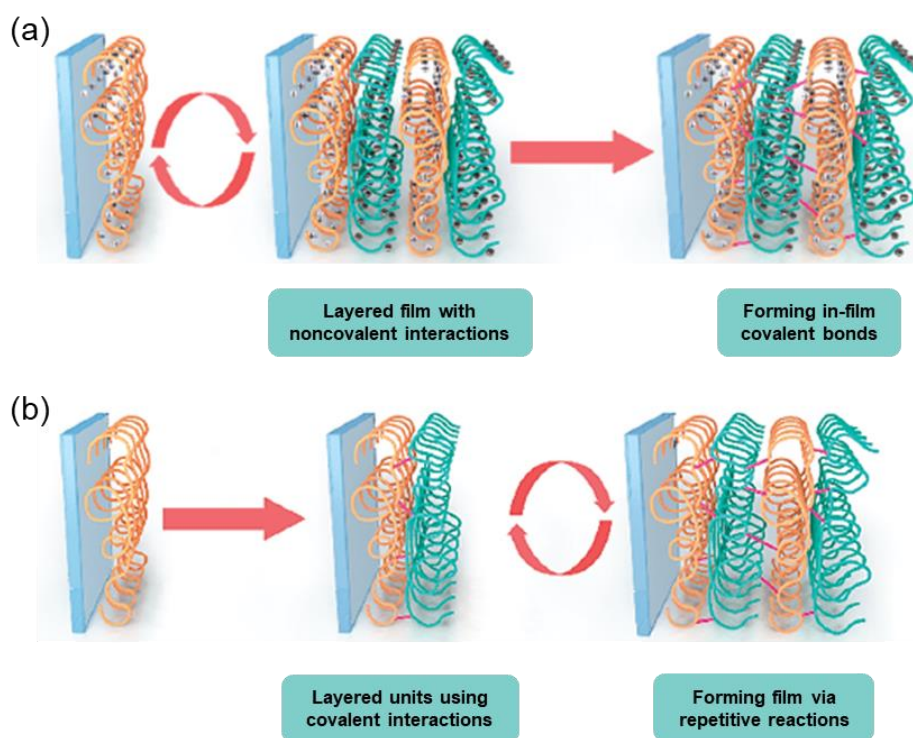


Figure 6. Schematic assembly process of the layered films using (a) post covalent conversion and (b) consecutive covalent fabrication. Adapted from reference⁸².

The first one refers when the multilayered constructions are obtained using non-covalent interactions (e.g. electrostatics) followed by the applications of covalent reaction conditions to successfully convert the non-covalent films into covalent ones. The transition from non-covalent to covalent represents an intertwining across the interlayer network that is typically named as crosslinking. These covalent reaction conditions can be achieved by adding bifunctional reagents (e.g. glutaraldehyde, genipin, EDC), increasing the temperature (for amine to carboxylic acid thermal coupling), using light irradiations (e.g. UV light) for methacrylic or thiol-ene coupling via photocrosslinking, or even enzyme-catalyzed bioconjugations such as transglutaminase and tyrosinase^{27,83,84}. On the other hand, in the second building strategy, the multilayered films are instead built in each step using covalent reaction, in other words, all layers are subsequently and immediately covalently linked to each of their neighbors⁸². This interaction can be performed in aqueous and organic solutions and allows the production of highly stable and resistant multilayer films. On the

contrary of electrostatic and hydrogen-bonded films, the covalent bonded ones can resist harsh conditions such as high temperatures, ionic strength values or even extreme pH. However, is more complex and expensive methodology compared to the other three ⁵⁵. Furthermore, the inherent toxicity of some of its crosslinking agents or conditions can be an obstacle when cell-based applications are envisioned, in which a careful cell-friendly procedure should always be considered when aiming to translate such platforms. Also, the inherently stiff covalent bonds/network introduced to the multilayered films can sometimes significantly alter its flexibility and mechanical properties. In these instances, a well optimized balance between non-covalent and covalent bonds should always be considered, in particular if seeking to incorporate living cells that are biologically predisposed to prefer softer substrates/tissues.

2.1.4. Factors influencing LbL film formation

The immense flexibility that characterizes the LbL assembly process derives from being a convenient method for thin film construction with precise control of film structures at the nano and microscale, as well as different underlying properties, such as thickness, roughness, porosity, growth, flexibility and toughness ³⁶. Taking in mind that electrostatic interactions are one of the most prominent driving forces behind LbL assembly, there are several factors that may directly or indirectly affect the multilayered films main properties. In fact, controlled composition, layer thickness, topography, and intermixing of neighboring layers can be tuned through simple adjustments of assembly parameters including pH, salt concentration, ionic strength and molecular weight, polymer concentration, temperature, humidity or even the solvent qualities ^{26,85-93}. For example, the presence of salt in solutions for LbL assembly can drastically affect the chain configurations of polymers in the bulk solution. When no salt is added to the solutions, the like charges within a single chain may repel each other. On the other hand, in presence of additional salt, the introduced counterions screen some of the charges allowing the single chain to fold into a random coil configuration, as represented below in Figure 7. In addition, films produced under high salt concentrations are usually thicker and have a higher surface roughness. However, the influence of salt concentrations on the structural details will likely be dependent upon the nature of materials used ⁹⁴.

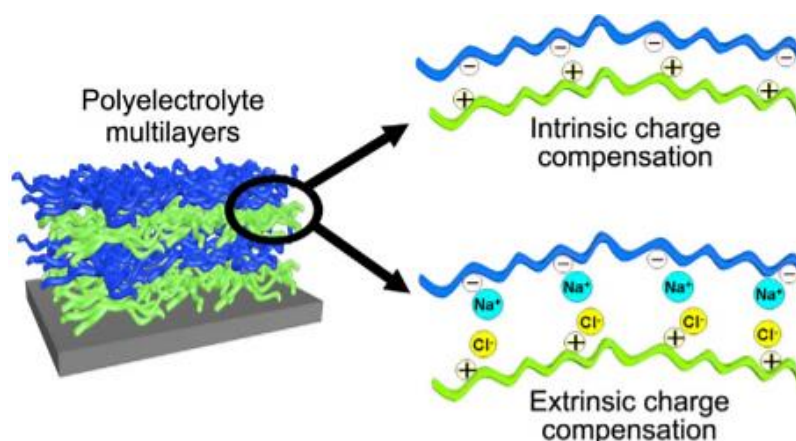


Figure 7. Effect of salt concentration on intrinsic and extrinsic charge compensation. Charge neutralization happens between polyelectrolyte chains (intrinsic process) or by counterion inclusion in multilayered films (extrinsic process). Retrieved from reference ⁹⁵.

2.1.5. LbL Assembly Technologies

Regarding LbL assembly, the production method can be performed in several different approaches, as it will be described below in the following subsections. On the other hand, the characterization of LbL films can include several supporting techniques such as Scanning electron microscopy (SEM), water uptake ability, atomic force microscopy (AFM), profilometry, mechanical properties, quartz crystal microbalance (QCM) or quartz crystal microbalance with dissipation monitoring (QCM-D) ^{14,16,96–101}.

Meanwhile, the LbL technique has undergone an immense technological improvement over the years with different emerging methods that can speed up the exponential assembly of film depositions, promoting rapid and scalable productions of thick functional films ⁸⁷. Overall, five distinct categories have been performed to assemble these type of films, namely: (a) immersive, (b) spin, (c) spray, (d) electromagnetic, and (e) fluidic assembly, all of which are represented in Figure 8 ⁵⁶. These technologies can affect the process methodology as well as the resultant materials properties. Taking this into account, the careful selection of the employed technology is crucial for the success of assembled films and dependent on the intended applications, however, this subchapter will only emphasize the three most commonly used technologies reported in the literature, namely highlighting the immersive, spin and spray assemblies.

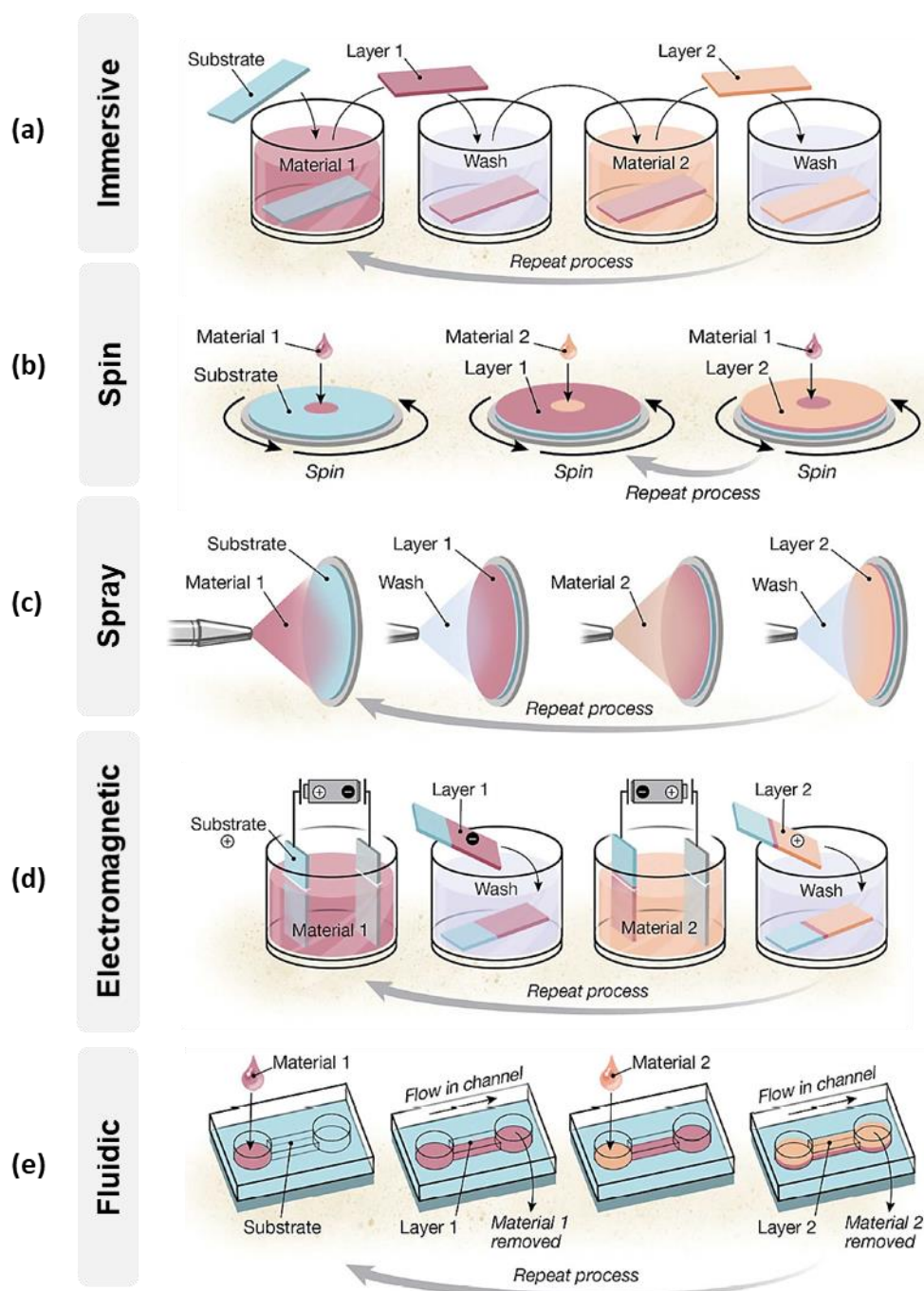


Figure 8. Schematic overview of LbL assembly technologies, (a) Immersive assembly, (b) Spin assembly, (c) spray assembly, (d) Electromagnetic assembly and (e) Fluidic assembly. Adapted from reference ⁵⁶.

2.1.5.1. Dipping LbL assembly

The dipping assembly also referred to as “immersive assembly” is the most commonly used LbL method and usually represents the standard that most newer technologies are compared to ⁵⁶. The process is simple and does not require any specific equipment, but can also be

scalable and automatized with sophisticated dipping robots ⁹. In a typical set-up, planar substrates are sequentially immersed into solutions containing different materials (such as polyelectrolyte solution) and subsequently washed in a determined order, as demonstrated in Figure 8a ^{9,17}. This process can be repeated limitless times, ending only when the desired number of layers is achieved ⁹. The immersion time and speed used in every single process play a key role in determining the multilayered film properties such as thickness, roughness, etc. However, the drying conditions, wettability and substrate movement speed also ultimately require an optimization process in order to produce films with reproducible properties ⁵⁶.

As a manner of making LbL films, dipping assembly has proven to be an attractive option due to its simplicity and versatility. In addition, it allows to achieve several types of film thicknesses just by modifying the final number of bilayers. Secondly, this is a viable method which allows the easy control of the film structure as well as tuning several mechanical properties, such as porosity, roughness or even the Young's Modulus ¹⁰². On the other hand, as an effort to eliminate the likelihood of human error and also to enable the deposition of a high number of layers over extended periods of time, this technique has been automatized over the years. The proof of that is the several studies based on the production of LbL films by using a robot specialized for dipping coating ^{14,16,44,58,96,99}. However, another sophisticated way of dipping automation is the use of QCM, where a gold-coated piezoelectric crystal is used as a substrate, which allows users to follow the layer build-up process with a tremendous resolution just by using a computer monitored feedback loop ¹⁷. Still, despite the use of automated equipment, there are other efficient techniques that can be established to make LbL a viable and translatable technology, which is the case of the spin coating.

2.1.5.2. Spin LbL assembly

LbL assemblies using spin coating (i.e. spin assembly) utilize coating technology of spinning a substrate to promote the rapid deposition of different materials ^{9,56}. In other words, the liquid solution is deposited and scattered onto either a spinning or a stationary substrate that is then spun, represented in Figure 8b ^{103,104}. Despite being a faster way to produce thin manufactured films, this coating approach involves a rapid evaporation of the solvent from the coating material which ultimately leads to the formation of thinner films when compared

to the standard ones ^{9,56}. Nevertheless, spin assembly strategies are advantageous due to an easier obtaining of more homogenous films when compared with dipping coating. This occurs because multilayered assemblies are brought about several driving forces, including electrostatics, which promotes the adsorption and rearrangement of polymers, while in this technology, centrifugal and viscous forces, as well as air shear, promote quick dehydration and desorption of weakly bound polymers of the films ⁵⁶. This is also why spin assembly strategies are typically ordered of magnitude faster than the standard dipping coating.

2.1.5.3. Spray LbL assembly

Spray assembly is another well-established LbL category, where films are typically produced just by sequential spraying of desired solutions onto substrates (Figure 8c) ¹⁰⁵. Interestingly, standard spray assembly is much faster than immersive assembly and the resulting films are usually well organized ¹⁰⁶. Moreover, like spin assembly, the spray coating resulting films have more established and uniform layers than those obtained from dipping coating. Also, in this assembly, the film main properties, such as morphology, composition, uniformity can be optimized in a similar way than those prepared by immersive coating. For instance, film thickness can be influenced by suspension concentrations, spray flow rate, spray and resting duration, as well as whether the solution is sprayed in a horizontal or vertical fashion ¹⁰⁵⁻¹⁰⁹.

Although spraying assemblies remains the fastest and easy method to coat large or nonplanar substrates, immersive assembly is still the chosen method for coating complex three-dimensional (3D) substrates. On the other hand, spray assembly is one of the most highly relevant methods for industrial applications ⁵⁶.

Meanwhile, spray assembly has recently been combined with other assembly technologies to benefit from each technological advantages as well as automating the assembly process ⁵⁶. Thus, a new method namely spin-spray-assisted LbL assembly was developed, which combines the spin and spray LbL technologies, and has been emerging as a promising method due to its tremendously accelerated rate of film production, as well as reducing the material demand and thus minimize operation costs. In this approach, the multilayered films could be produced by directly spraying two oppositely charged solutions in turns on high speed rotating substrates, while the rinsing step is performed in between spraying steps ¹⁷.

2.1.6. Biomedical applications using LbL assembly technique

Currently, production of multilayered systems obtained through LbL assembly techniques have been extremely useful tools for advancing the potential of regenerative medicine and tissue engineering, as well as for different biomedical applications, including medical implants, drug delivery, biomimetic coatings, protein adsorption, biosensors, bioreactors, coating of living cells, or the manipulations of adhesion, differentiation, proliferation and biofunction of the attached cells, and so on^{15,25,58,110–114}. This approach offers the possibility to produce nanostructured ultrathin films as well as the capacity to manipulate their chemical, physical and topographical properties just by adjusting solutions parameters (e.g. concentration, pH, etc.) and achievable through different assembly techniques, as discussed earlier. Throughout the years of LbL innovation and development, literature studies exploring the production of multilayered LbL membranes are converging on those based on natural origin polymers, which have attracted increasingly attention due to their biofriendly features, such as biodegradability, low toxicity and biocompatibility. Among such promising biopolymers, chitosan (CHT) and alginate (ALG) now represent well-established candidates for LbL assembly techniques, allowing the production of natural-based multilayered freestanding membranes.

2.1.6.1. Multilayered membranes based on chitosan and alginate

These two polysaccharides have been widely used due to its stability under physiological conditions and also confer biological properties to the resulting constructs, such as biocompatibility, adhesive, antimicrobial and hemostatic activities⁴⁴. Moreover, multilayered films based on these two biopolymers are stable over a pH range of 3–9, however they exhibit high levels of hydration and low mechanical resistance, thus impairing cell adhesion^{29,44}. These properties can be tuned in order to control cell behavior by adapting the mechanical properties (stiffness, elasticity and viscosity of the matrix), which ultimately influence the dissemination, migration, propagation, differentiation and organization processes of key intracellular structures²⁹.

Studies have shown that FS membranes based on CHT (cationic) and ALG (anionic) can be easily and reproducibly prepared in mild conditions without resorting to any post-processing steps. Caridade and co-workers demonstrated that myoblast cells seeded on CHT/ALG

Chapter 2: Introduction

multilayered membranes exhibited preferential adhesion on the alginate-ending membrane over chitosan-ending membranes or to the substrate side ⁹⁹. This spatially specific adhesion is interesting to control cell adhesion at specific sites and design membranes with controllable adhesive properties. Moreover, the thickness of the obtained dry membrane can vary over a large range from 4 to 35 μm allowing easy handling with tweezers and necessary stability in physiological buffers. Also, these porous membranes enable partial permeation of model drugs throughout their nanostructure, which is critical for delivering bioactive molecules in wound-healing applications. The assembly of thick, detachable, biocompatible, and permeable FS membranes as those achieved in the study, offers new perspectives for applications of membrane-based tissue engineering ⁹⁹. However, a major drawback in the application of natural polymers in LbL films is their low mechanical performance ¹⁶. As discussed in previous subchapters, films based only on electrostatic interactions naturally present lower mechanical properties when compared to films that were mechanically-improved with the incorporation of multiple self-assembly driving forces. Some of the strategies currently used for enhancing the properties of CHT/ALG multilayered films will be presented below, as briefly summarized in Table 2.

Table 2. Several studies exploring chitosan and alginate FS membranes and their proposed biomedical applications.

Author	Membrane	Reinforcement Strategy	Biomedical Application
Caridade, S. <i>et al.</i> ⁹⁹ (2012)	CHT/ALG		Tissue engineering
Caridade, S. <i>et al.</i> ¹⁰⁰ (2015)	CHT/ALG	Crosslinking (EDC)	Bone tissue regeneration
Silva, J. <i>et al.</i> ⁴⁴ (2016)	CHT/ALG	Crosslinking (Genipin)	Biomedical and biotechnological fields.
Moura, D. <i>et al.</i> ¹⁶ (2016)	CHT/ALG	Incorporation of GO	Wound healing, and cardiac and bone engineering applications
Silva, M. <i>et al.</i> ¹⁰¹ (2017)	CHT/ALG	Functionalized Nanotubes	Wound healing and tissue engineering of bone and cardiac tissues.

In another study, Caridade *et al.* produced FS membranes based on CHT and ALG that were chemically crosslinked in order to improve their final mechanical properties¹⁰⁰. In this case, amine-to-carboxyl crosslinking agent EDC was used in different amounts to form a covalent interlayer network between CHT (amine containing) and ALG (carboxyl containing). This covalent crosslinking resulted in significantly improved membrane stability in aqueous conditions. Also, SEM images revealed an increased roughness at higher crosslinking degrees and also showcased the membranes' homogeneous structure. In addition, the proliferation of skeletal myoblasts and their subsequent differentiation in myotubes (myogenic differentiation) was also influenced by the crosslinking degree, with the more crosslinked and tighter membranes being more myoconductive. These membranes also exhibited osteoinductive features and represent promising materials showcasing the attractiveness of CHT/ALG multilayered systems for future *in vivo* studies as tissue-engineered constructs for bioinstructive cardiac patches as well as accelerating the repair of bone fractures¹⁰⁰.

Regarding other crosslinking agents, genipin is a naturally-derived compound extracted from gardenia fruit which has been widely used for enabling the crosslinking of amine-containing polymers' in multilayer films. The main advantages of genipin when compared with other covalent crosslinkers (such as glutaraldehyde) are its low cytotoxicity and anti-inflammatory activities¹¹⁵. In the particular case of CHT/ALG multilayered films, since ALG does not contain primary amines, genipin crosslinking will give rise to the formation of semi-interpenetrating polymer networks with free ALG chains entrapped inside crosslinked CHT multilayers⁴⁴. Adding to this, and relying on the calcium-enabled self-assembly phenomenon of ALG chains, Silva *et al.* studied the combined interaction of covalent and ionic crosslinking on CHT/ALG multilayers, by using natural and cell-friendly genipin and calcium chloride (CaCl₂) as crosslinking agents⁴⁴. The combination of multiple driving forces (i.e. electrostatic, covalent, ionic) within the multilayered membranes lead to increased mechanical properties whilst decreasing water uptake abilities. Moreover, the ionic crosslinking of multilayered CHT/ALG films led to FS membranes with multiple interesting features beyond just mechanical properties, such as calcium-induced adhesion and shape memory ability. The use of CaCl₂ enabled the reversible switching of structural properties by simple immersion in a solution containing EDTA, a calcium-chelating agent.

Chapter 2: Introduction

The authors suggest a great potential for these polysaccharide FS membranes to be used in different research applications, including biomedical and biotechnological fields ⁴⁴.

Graphene Oxide (GO) has appeared as an inorganic filler that can endow higher mechanical performance when embedded within polymeric matrices. Having that in mind, Moura *et al.* investigated FS membranes based on CHT, ALG and GO ¹⁶. GO derived from graphite and multi-walled carbon nanotubes yielded oxidized graphene flakes (o-GFs) and nanoribbons (o-GNRs) and allowed the formation of stable suspensions that could be combined with CHT and ALG solutions by LbL. Interestingly, the addition of o-FGs and o-GNRs achieved more rigid and hydrophilic FS membranes with significantly improved mechanical properties over CHT/ALG films. Also, the presence of o-GFS or o-GNRs did not affect in any way the thermal stability of the films, and in particular, the addition of o-GFs resulted in improved cytocompatibility. The authors suggested that the GO-reinforced multilayered films have a high potential for biomedical applications, especially the o-GFs films for exploring wound healing and cardiac and bone tissue engineering alternatives.

Silva *et al.* studied the incorporation of functionalized graphene nanoflakes (f-GF) or nanoribbons (f-GNR) within CHT/ALG multilayered films via LbL assembly ¹⁰¹. Interestingly, the incorporation of f-GF resulted in smoother films while f-GNR resulted in rougher multilayers, when compared to the CHT/ALG control films. Both graphene-incorporating FS membranes achieved significantly lower porosity and water uptake capacity than control ones. Also, f-GNR containing multilayered membranes showed higher *in vitro* cell adhesion and proliferation of L929 cells over control and f-GF membranes, which may be related to its lower hydrophobicity and higher roughness ¹⁰¹. Still, most of the membranes developed this way still lack important bioadhesiveness, which is a key feature when envisioning biomedical applications of such systems.

Regarding this, a recent study by Sousa and co-workers explored the LbL-assembly of CHT/ALG-based FS films with an elegant mussel-inspired approach aiming to improve the mechanical and adhesive properties of standard CHT/ALG multilayered membranes ¹⁴. To achieve this, the authors incorporated dopamine-modified hyaluronic acid (HA-DN) within the assembly of CHT/ALG membranes. They observed that (CHT/ALG/CHT/HA-DN)₁₀₀ membranes displayed higher Young's modulus and ultimate tensile strength than (CHT/ALG/CHT/HA)₁₀₀. Also, the catechol-containing membranes showed reduced water

content and enhanced cell proliferation and infiltration over the unmodified membranes. This study aimed the production of bioinspired membranes as potential adhesive patches for skin wound healing. Dopamine contains catechol groups that are responsible for the wet adhesive capacity of mussels on rocks. Exploiting nature systems with unique features is a promising way to develop novel materials with sophisticated properties, a field known as biomimetics. Thus, the next chapter will discuss in more detail some biomimetic approaches with successful and impactful applications in this field.

2.2. Biomimetics

Following the perspective of Natural Selection advocated by Charles Darwin and Alfred Russel Wallace, natural systems provide examples of impressive adaptiveness and resilience for enduring the pass of time throughout billions of years of evolutionary processes and harsh environmental conditions. Evolution has given rise to an enormous biodiversity, and living organisms represent machines constantly updated and always seeking new improvements to current features (Figure 9). The key idea is that over the pass of time, unique and valuable features will prevail over less efficient ones.

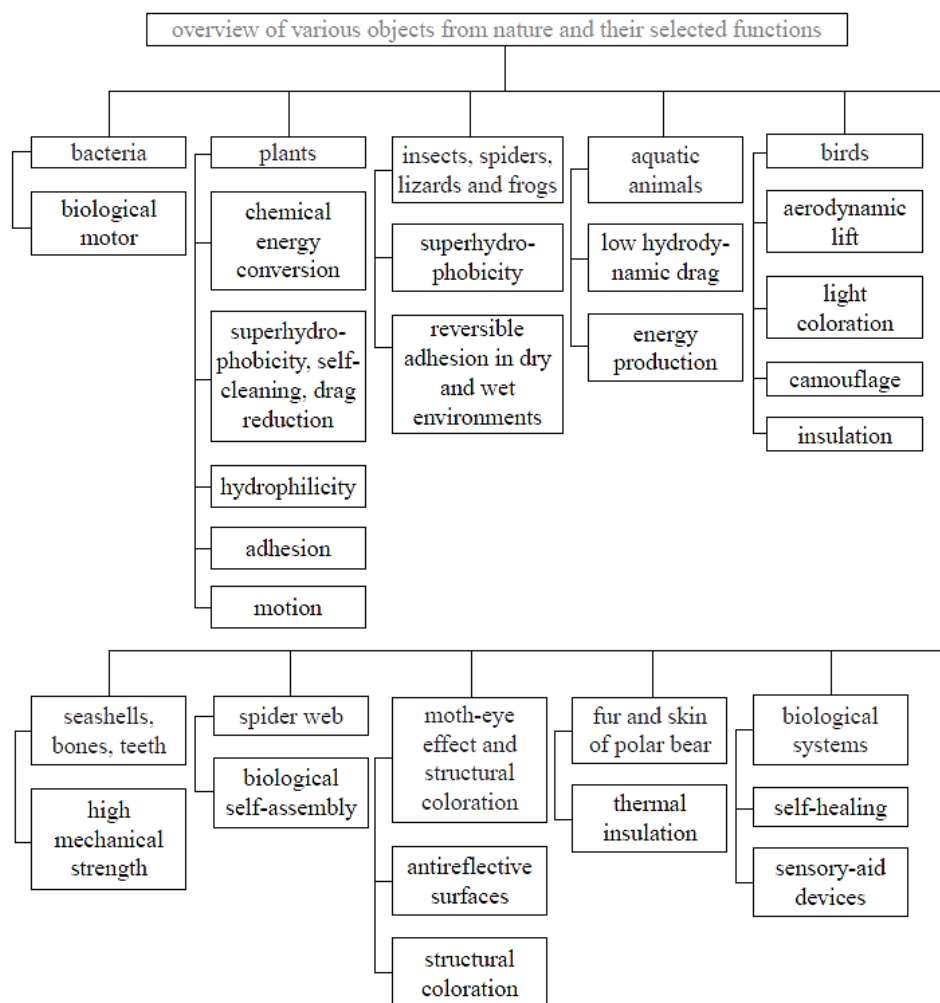


Figure 9. Overview of some existent organisms in nature that somehow inspired the scientific community due to their properties of commercial interest. Retrieved from reference ¹¹⁶.

This evolution has accrued over centuries extremely efficient natural materials which have attracted the attention of scientists and engineers that are inspired by this overwhelming biodiversity of nature-derived designs and aim to mimic such processes and features to basic and applied sciences, a field known as “biomimetics”^{116,117}. This word, derived from the Greek word biomimesis, was coined by polymath Otto Schmitt in 1957, a doctoral researcher that developed a physical device that aimed to mimic the electrical action of nerves^{116,118}. Still, Schmitt was not the first to analyze Nature in this prism and try to replicate interesting natural features for designing new materials or technologies. The story of Leonardo da Vinci is well-known until today, in particular his engineering skills and sketches of flying machines based on the flight of birds¹¹⁹. Also, the first successful airplane built by the Wright brothers was allegedly inspired from observations of pigeons in flight¹²⁰. In another example, George de Mestral noticed how hooked burs of plants latched onto the fur of his dog or to people’s clothing. After a detailed microscopic inspection, he observed the presence of tiny microscopic hooks at the end of burr’s spines and later on was able to replicate these microstructures synthetically. This invention is what is now popularly known as Velcro and highlights the promise of bioinspired approaches for a wide range of applications¹²¹. In summary, the idea that Nature has already solved many of the problems that researchers are trying to tackle fuels biomimetic trends in the biomedical fields. Animals, plants and microbes all represent successful engineering design and some of their unique features can be used as templates to advance the design of novel materials with improved properties over current alternatives. The follow subsections highlight some of these interesting bioinspired approaches seeking to mimic specific features found in natural structures or organisms.

2.2.1. Nacre

The shell of most gastropods and bivalve mollusks possesses three main layers: the outer one (periostracum), composed of hardened protein, the middle one (prismatic), composed of columnar calcite, and finally the inner one (nacre) composed by aragonite and organic material. While the peripheral layers are brittle and hard, providing the resistance to penetration from external impact, nacre gives the shell toughness, by allowing dissipation of mechanical energy (Figure 10)¹²². Nacre, also known as mother of pearl, is a natural biomineralized CaCO₃ composite made of 95 wt.% of brittle aragonite platelets, and only 5

Chapter 2: Introduction

wt.% of organic materials, such as proteins and polysaccharides. This material is now identified as an outstanding model for high-performance materials, such as strength, toughness and stiffness^{122,123}. These remarkable mechanical properties have been investigated using a variety of particular techniques including tension, shear, three and four point bending and compression^{124–129}.

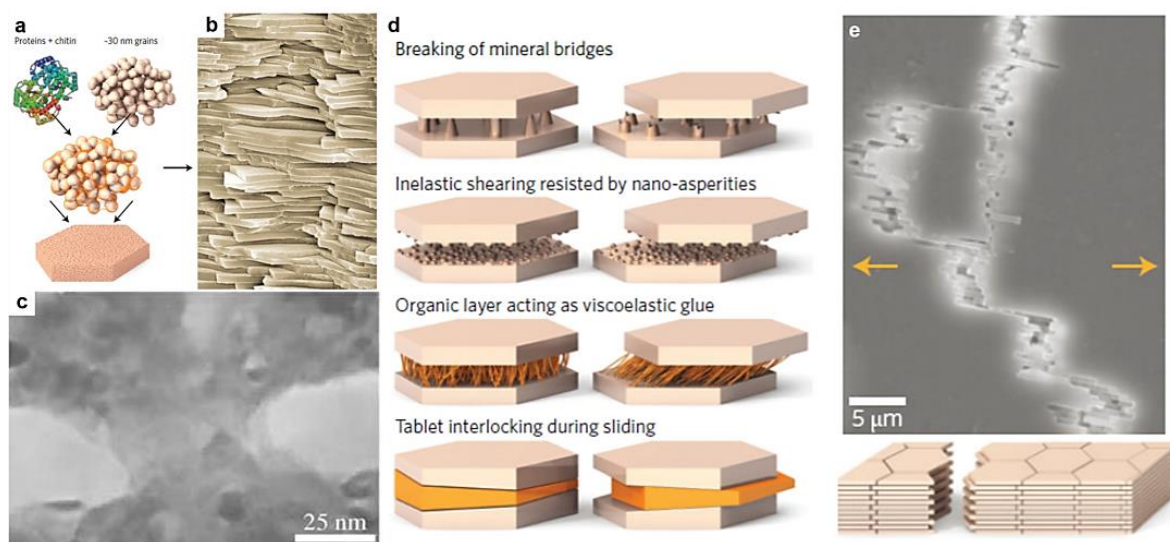


Figure 10. Nacre hierarchical microarchitecture and its toughening mechanism. **a)** Network of CaCO₃ platelets glued together by a biopolymer. **b)** Brick-and-mortar architecture. **c)** Mineral bridges immersed in the polymer layer. **d)** Sketch of the toughening mechanism of nacre. **e)** Crack propagation mechanism within nacre showing obvious crack deflection. Retrieved from reference¹³⁰.

Inspired by both these structural and mechanical features, the scientific community have attempted several approaches to mimic the nacre-nature and produce bioinspired nacre-like structures¹³¹. Overall, nacre bioinspired materials lie in one of three categories: (i) mimicking the layered structure; (ii) mimicking its mineralization process; (iii) mimicking its inorganic and organic composition¹²². Nanocellulose-based films with CaCO₃ generated a lamellar material similar to nacre and with excellent mechanical properties in terms of stiffness and plasticity¹³². Alternatively, PVA/GO multilayered films have achieved a brick-and-mortar microstructure resembling nacre with improved mechanical properties as well as electrical conductivity and biocompatibility¹³³. Recently, this layered structure also inspired the design of flexible macroscopic ribbon fibers made from ultralong hydroxyapatite nanowires and sodium polyacrylate. In this study, the fibers achieved remarkable flexibility and the authors suggest applications in smart wearable devices or biomedical engineering¹³⁴.

2.2.2. Lobster cuticle

The large-sized crustacean American lobster (*Homarus americanus*) is the heaviest crustacean in the world. This marine organism has a characteristic hierarchical biological structure designed to resist mechanical loads. This is due to its crustacean cuticle, which is one of the oldest natural materials for structural and armor applications¹³⁵. The cuticle is a chitin-based continuous tissue that is locally modified to exhibit a transition in mechanical properties between mineralized skeletal elements and interconnecting arthrodistal membranes (Figure 11)¹³⁶. The flexibility of cuticle in terms of dramatically altering its physical properties derives from a high structural and compositional freedom, a key factor for enabling motility while offering protection from predators¹³⁶.

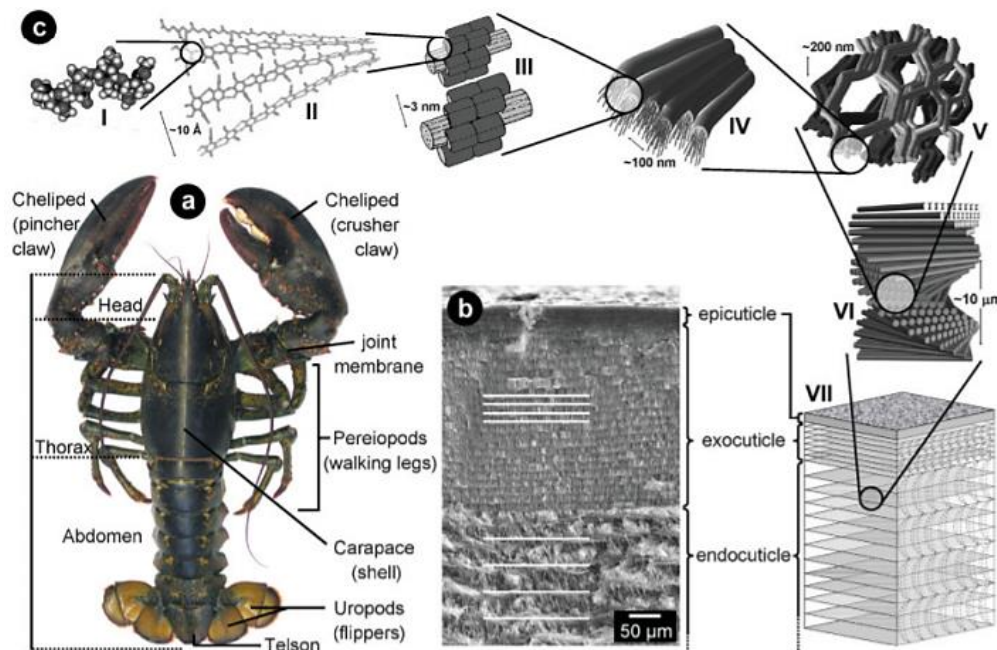


Figure 11. Hierarchical microstructure of lobster cuticle. **a)** American lobster (*Homarus americanus*) morphology. **b)** SEM image of the cuticle cross-section, showing the different layers. **c)** Hierarchical organization: (I) N-acetyl-glucosamine molecules forming (II) anti-parallel α -chitin chains. (III) nanofibrils formed of chitin molecules wrapped with proteins, which cluster to form (IV) chitin-protein fibers. (V) All fibers are oriented in the same direction. (VI) Typical twisted plywood structure chitin-protein fibers. (VII) Three-layered cuticle. Retrieved from reference¹³⁷.

Chapter 2: Introduction

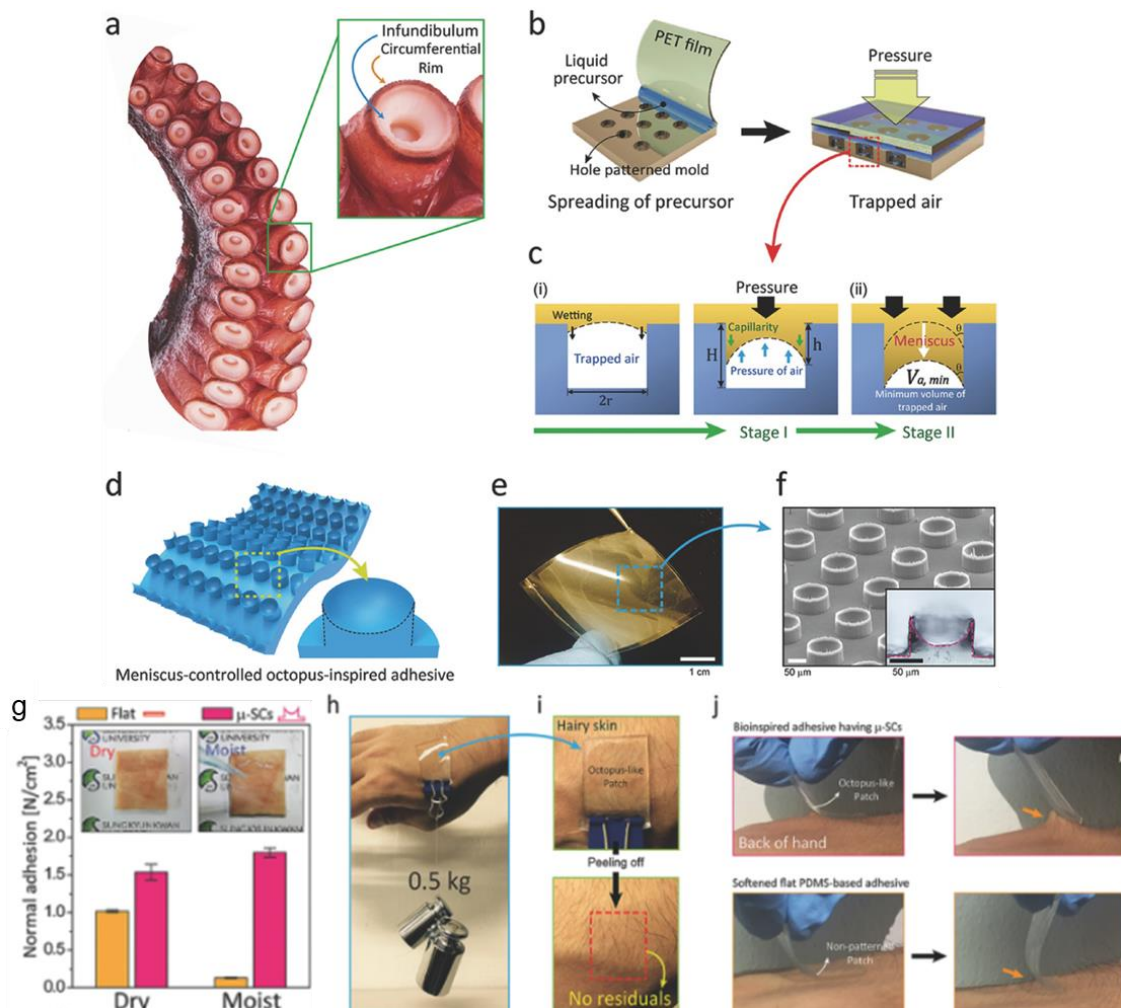
The cuticle is a multilayered chitin-protein based composite, which is further hardened by incorporation of nanoscale biomineralized particles, such as calcite and amorphous calcium carbonate that can be found aligned along the organic fibers¹³⁸. Macroscopically, the cuticle consists in two main layers, the epicuticle, which is a thin waxy layer that acts as a diffusion barrier to the environment, and the procuticle, which can be divided into an exocuticle and endocuticle, both designed to resist mechanical loads (Figure 11b)¹³⁷. Recently, inspired by these structural properties found in arthropods exoskeletons, researchers have been attempting to unveil this chitin-based hierarchical structure. João and co-workers produced chitosan/crystalline chitin nanowhiskers films for biomimetic tuning of the material mechanical properties by modulating the ratio of chitin/chitosan¹³⁹. In another study, Oh and colleagues explored the calcium-triggered disassembly of chitin nanofibrils, inspired by the natural presence of such divalent cations throughout most load-bearing chitin structures, such as chitin¹⁴⁰. Moving forward, advanced applications exploiting this interesting cuticle layered structure could yield novel materials with distinct mechanical behaviors.

2.2.3. Octopus

The octopus is a soft-bodied eight-limbed Cephalopod that inhabits the ocean. The interior surfaces of its limbs are covered with circular adhesive suckers that octopuses use to anchor themselves to a substrate or to grasp and manipulate objects¹⁴¹. Octopus' suckers have a unique hierarchical dome-like structure capable of reversible adhesion in dry and wet conditions, as well as slippery, rough and irregular surfaces. Thus, unsurprisingly, the great adhesive properties of the octopus' sucker have been gathering increased attention lately via multiple bioinspired approaches aiming to replicate its adhesive features.

Lee and colleagues mimicked the pressure-induced adhesion of octopus' suckers by combining a thermoresponsive pNIPAM polymeric layer and an elastomeric PDMS microcavity for developing a smart adhesive pad with enabled switchable adhesiveness in response to temperature stimuli¹⁴². Alternatively, Chen and co-workers developed a PDMS nanosucker capable of efficiently adhering to a porcine heart¹⁴³. More recently, Baik and co-workers developed meniscus-controlled octopus-inspired adhesive patch with unfoldable 3D microtips in micropillars inspired by the rim and infundibulum of the characteristic octopus' suction cup (Figure 12)¹⁴⁴. The octopus-like sucker patch experienced an enhanced pulling strength on pig skin in both dry and moist conditions due to increased suction stress.

Notably, this bioinspired patch exhibited higher pull-off and peel-off strengths than flat suckers on hairy pigskin in dry, moist and underwater conditions. Also, this octopus-inspired patch can withstand a total weight of 0.5 kg while attached to a rough skin covered with hairs. The authors suggest that this adhesive patch design may advance typical patches for wound healing and smart skin/organ attachable medical devices.



Chapter 2: Introduction

The same research group has also recently developed an octopus-inspired carbon-based conducting polymer composite to generate an adhesive electronic patch for biosignal monitoring¹⁴⁵. The resulting stretchable electronic patch was water-resistant, skin-adhesive, ultra-thin and light-weight, as well as capable of measuring electrocardiogram and bending motions of a human wrist even underwater.

Octopus-inspired adhesive systems are extremely promising because artificial suckers can only be used on flat targets, however the human tissues and wounds are practically irregular at the millimeter/micrometer scale, not to mention the lack of effectiveness of the suckers in wet surfaces. Thus, advancing octopus biomimetic adhesive materials will undoubtedly create novel bioadhesive strategies for biomedical applications in the near future.

References

1. Tang, Z., Wang, Y., Podsiadlo, P. & Kotov, N. A. Biomedical applications of layer-by-layer assembly: From biomimetics to tissue engineering. *Adv. Mater.* **18**, 3203–3224 (2006).
2. Borges, J., Rodrigues, L. C., Reis, R. L. & Mano, J. F. Layer-by-layer assembly of light-responsive polymeric multilayer systems. *Adv. Funct. Mater.* **24**, 5624–5648 (2014).
3. Villiers, M. M. de, Otto, D. P., Strydom, S. J. & Lvov, Y. M. Introduction to nanocoatings produced by layer-by-layer (LbL) self-assembly. *Adv. Drug Deliv. Rev.* **63**, 701–715 (2011).
4. Langmuir, I. The constitution and fundamental properties of solids and liquids. II. Liquids. *J. Am. Chem. Soc.* **39**, 1848–1906 (1917).
5. Langmuir, I. The mechanism of the surface phenomena of flotation. *Trans. Faraday Soc.* **15**, 62–74 (1920).
6. Blodgett, K. B. Monomolecular films of fatty acids on glass. *J. Am. Chem. Soc.* **56**, 495 (1934).
7. Michel, M., Toniazzi, V., Ruch, D. & Ball, V. Deposition Mechanisms in Layer-by-Layer or Step-by-Step Deposition Methods: From Elastic and Impermeable Films to Soft Membranes with Ion Exchange Properties. *ISRN Mater. Sci.* **2012**, 1–13 (2012).
8. Schwartz, D. K. Langmuir-Blodgett film structure. *Surf. Sci. Rep.* **27**, 241–334 (1997).
9. Keeney, M. *et al.* Nanocoating for biomolecule delivery using layer-by-layer self-assembly. *J. Mater. Chem. B* (2015).
10. Iler, R. K. Multilayers of colloidal particles. *J. Colloid Interface Sci.* **21**, 569–594 (1966).

11. Nicolau, y. F., davied, s., genoud, f., nechtschein, m. & travers, j. . Polyaniline, polypyrrole, poly(3-nethylthiophene) and polybithiophene layer-by-layer deposited thin films. *Synth. Met.* **43**, 1491–1494 (1991).
12. Decher, G. & Schmitt, J. Fine-Tuning of the film thickness of ultrathin multilayer films composed of consecutively alternating layers of anionic and cationic polyelectrolytes. *Prog. Colloid Polym. Sci.* **89**, 160–164 (1992).
13. Ariga, K., McShane, M., Lvov, Y. M., Ji, Q. & Hill, J. P. Layer-by-layer assembly for drug delivery and related applications. *Expert Opin. Drug Deliv.* **8**, 633–644 (2011).
14. Sousa, M. P. *et al.* Bioinspired multilayer membranes as potential adhesive patches for skin wound healing. *Biomaterials Science* **6**, 1962–1975 (2018).
15. Silva, J. M. M. da. Nanostructured 3D Constructs based on chitosan and chondroitin sulphate multilayers for cartilage tissue enngineering. (Universidade do Minho, 2011).
16. Moura, D. *et al.* High performance free-standing films by layer-by-layer assembly of graphene flakes and ribbons with natural polymers. *J. Mater. Chem. B* **4**, 7718–7730 (2016).
17. Richardson, J. J. *et al.* Innovation in Layer-by-Layer Assembly. *Chem. Rev.* **116**, 14828–14867 (2016).
18. Andreeva, D. V., Fix, D., Mohwald, H. & Shchukin, D. G. Self-Healing Anticorrosion Coatings Based on pH-Sensitive Polyelectrolyte/Inhibitor Sandwichlike Nanostructures. *Adv. Mater.* **20**, 2789–2794 (2008).
19. Shchukin, D. G. *et al.* Layer-by-Layer Assembled Nanocontainers for Self-Healing Corrosion Protection. *Adv. Mater.* **18**, 1672–1678 (2006).
20. Wijeratne, S. *et al.* Layer-by-Layer Deposition with Polymers Containing Nitrilotriacetate, A Convenient Route to Fabricate Metal- and Protein-Binding Films. *ACS Appl. Mater. Interfaces* **8**, 10164–10173 (2016).
21. Wu, Y. *et al.* From ultratough artificial nacre to elastomer: Poly(n-butyl acrylate) grafted graphene oxide nanocomposites. *Compos. Part A Appl. Sci. Manuf.* **88**, 156–164 (2016).
22. Xiong, R., Hu, K., Zhang, S., Lu, C. & Tsukruk, V. V. Ultrastrong Freestanding Graphene Oxide Nanomembranes with Surface-Enhanced Raman Scattering Functionality by Solvent-Assisted Single-Component Layer-by-Layer Assembly. *ACS Nano* **10**, 6702–6715 (2016).
23. Naseri-Nosar, M. & Ziora, Z. M. Wound dressings from naturally-occurring polymers: A review on homopolysaccharide-based composites. *Carbohydr. Polym.* **189**, 379–398 (2018).
24. Wang, B., Zhao, L., Zhu, W., Fang, L. & Ren, F. Mussel-inspired nano-multilayered coating on magnesium alloys for enhanced corrosion resistance and antibacterial property. *Colloids Surfaces B Biointerfaces* **157**, 432–439 (2017).
25. Gentile, P., Carmagnola, I., Nardo, T. & Chiono, V. Layer-by-layer assembly for biomedical applications in the last decade. *Nanotechnology* **26**, 422001–422022 (2015).
26. Choi, I. *et al.* PH-controlled exponential and linear growing modes of layer-by-layer

- assemblies of star polyelectrolytes. *J. Am. Chem. Soc.* **133**, 9592–9606 (2011).
27. Spicer, C. D., Pashuck, E. T. & Stevens, M. M. Achieving Controlled Biomolecule-Biomaterial Conjugation. *Chem. Rev.* **118**, 7702–7743 (2018).
 28. Lundin, M., Solaqa, F., Thormann, E., MacAkova, L. & Blomberg, E. Layer-by-layer assemblies of chitosan and heparin: Effect of solution ionic strength and pH. *Langmuir* **27**, 7537–7548 (2011).
 29. Silva, J. M., García, J. R., Reis, R. L., García, A. J. & Mano, J. F. Tuning cell adhesive properties via layer-by-layer assembly of chitosan and alginate. *Acta Biomater.* **51**, 279–293 (2017).
 30. Boddohi, S. & Kipper, M. J. Engineering nanoassemblies of polysaccharides. *Adv. Mater.* **22**, 2998–3016 (2010).
 31. Sinha, V. R. & Kumria, R. Polysaccharides in colon-specific drug delivery. *Int. J. Pharm.* **224**, 19–38 (2001).
 32. Mizrahy, S. & Peer, D. Polysaccharides as building blocks for nanotherapeutics. *Chem. Soc. Rev.* **41**, 2623–2640 (2012).
 33. Miao, T., Wang, J., Zeng, Y., Liu, G. & Chen, X. Polysaccharide-Based Controlled Release Systems for Therapeutics Delivery and Tissue Engineering: From Bench to Bedside. *Adv. Sci.* **5**, (2018).
 34. Iqbal, N. *et al.* Recent concepts in biodegradable polymers for tissue engineering paradigms: a critical review. *Int. Mater. Rev.* 1–36 (2018).
 35. Liu, J., Willför, S. & Xu, C. A review of bioactive plant polysaccharides: Biological activities, functionalization, and biomedical applications. *Bioact. Carbohydrates Diet. Fibre* **5**, 31–61 (2015).
 36. Li, Y., Wang, X. & Sun, J. Layer-by-layer assembly for rapid fabrication of thick polymeric films. *Chem. Soc. Rev.* **41**, 5998–6009 (2012).
 37. Silva, J. M. *et al.* Tailored freestanding multilayered membranes based on chitosan and alginate. *Biomacromolecules* **15**, 3817–3826 (2014).
 38. Alonso-Sande, M., Teijeiro-Osorio, D., Remuñán-López, C. & Alonso, M. J. Glucomannan, a promising polysaccharide for biopharmaceutical purposes. *Eur. J. Pharm. Biopharm.* **72**, 453–462 (2009).
 39. Crini, G. Recent developments in polysaccharide-based materials used as adsorbents in wastewater treatment. *Prog. Polym. Sci.* **30**, 38–70 (2005).
 40. García-González, C. A., Alnaief, M. & Smirnova, I. Polysaccharide-based aerogels - Promising biodegradable carriers for drug delivery systems. *Carbohydr. Polym.* **86**, 1425–1438 (2011).
 41. Pitarresi, G., Calabrese, R., Palumbo, F. S., Licciardi, M. & Giammona, G. Polysaccharide/polyaminoacid composite scaffolds for modified DNA release. *Int. J. Pharm.* **382**, 7–14 (2009).
 42. Spizzirri, U. G. *et al.* Antioxidant-polysaccharide conjugates for food application by eco-friendly grafting procedure. *Carbohydr. Polym.* **79**, 333–340 (2010).
 43. Francis Suh, J. K. & Matthew, H. W. T. Application of chitosan-based polysaccharide

- biomaterials in cartilage tissue engineering: A review. *Biomaterials* **21**, 2589–2598 (2000).
44. Silva, J. M., Caridade, S. G., Reis, R. L. & Mano, J. F. Polysaccharide-based freestanding multilayered membranes exhibiting reversible switchable properties. *R. Soc. Chem.* **12**, 1200–1209 (2016).
 45. Singh, R., Shitiz, K. & Singh, A. Chitin and chitosan: biopolymers for wound management. *Int. Wound J.* **14**, 1276–1289 (2017).
 46. G. Sandri, S. R., Bonferoni, M. C., Ferrari, F., Mori, M. & Caramella, C. The role of chitosan as a mucoadhesive agent in mucosal drug delivery. *J. Drug Deliv. Sci. Technol.* **22**, 275–284 (2012).
 47. Lee, K. Y. & Mooney, D. J. Alginate: Properties and biomedical applications. *Prog. Polym. Sci.* **37**, 106–126 (2012).
 48. Saranraj, P. & Naidu, M. A. Hyaluronic Acid Production and its Applications - A Review. *Int. J. Pharm. Biol. Arch.* **4**, 853–859 (2013).
 49. Han, D., Yan, L., Chen, W., Li, W. & Bangal, P. R. Cellulose/graphite oxide composite films with improved mechanical properties over a wide range of temperature. *Carbohydr. Polym.* **83**, 966–972 (2011).
 50. Mano, J. F. *et al.* Natural origin biodegradable systems in tissue engineering and regenerative medicine: present status and some moving trends. *J. R. Soc. Interface* **4**, 999–1030 (2007).
 51. Abir, F., Barkhordarian, S. & Sumpio, B. E. Efficacy of Dextran Solutions in Vascular Surgery. *Vasc. Endovascular Surg.* **38**, 483–491 (2004).
 52. Lin, Q. *et al.* Heparin/collagen multilayer as a thromboresistant and endothelial favorable coating for intravascular stent. *J. Biomed. Mater. Res. Part A* **96A**, 132–141 (2011).
 53. Cherg, W.-J. *et al.* Hemocompatibility and adhesion of heparin/dopamine and heparin/collagen self-assembly multilayers coated on a titanium substrate. *Appl. Surf. Sci.* **463**, 732–740 (2019).
 54. du Souich, P., García, A. G., Vergés, J. & Montell, E. Immunomodulatory and anti-inflammatory effects of chondroitin sulphate. *J. Cell. Mol. Med.* **13**, 1451–1463 (2009).
 55. Borges, J. & Mano, J. F. Molecular interactions driving the layer-by-layer assembly of multilayers. *Chem. Rev.* **114**, 8883–8942 (2014).
 56. Richardson, J. J., Bjornmalm, M. & Caruso, F. Technology-driven layer-by-layer assembly of nanofilms. *Science (80-.)*. **348**, aaa2491-aaa2491 (2015).
 57. Reuther, J. F., Dahlhauser, S. D. & Anslyn, E. Van. Tunable Orthogonal Reversible Covalent (TORC) Bonds: Dynamic Chemical Control over Molecular Assembly. *Angew. Chemie Int. Ed.* (2018).
 58. Costa, R. R., Custódio, C. A., Arias, F. J., Rodríguez-Cabello, J. C. & Mano, J. F. Layer-by-layer assembly of chitosan and recombinant biopolymers into biomimetic coatings with multiple stimuli-responsive properties. *Small* **7**, 2640–2649 (2011).

Chapter 2: Introduction

59. Wood, K. C., Chuang, H. F., Batten, R. D., Lynn, D. M. & Hammond, P. T. Controlling interlayer diffusion to achieve sustained, multiagent delivery from layer-by-layer thin films. *Proc. Natl. Acad. Sci.* **103**, 10207–10212 (2006).
60. Xiang, Y., Lu, S. & Jiang, S. P. Layer-by-layer self-assembly in the development of electrochemical energy conversion and storage devices from fuel cells to supercapacitors. *Chem. Soc. Rev.* **41**, 7291–7321 (2012).
61. Rivera, M. C., Pinheiro, A. C., Bourbon, A. I., Cerqueira, M. A. & Vicente, A. A. Hollow chitosan/alginate nanocapsules for bioactive compound delivery. *Int. J. Biol. Macromol.* **79**, 95–102 (2015).
62. Ribeiro, C. *et al.* Preparation of Well-Dispersed Chitosan/Alginate Hollow Multilayered Microcapsules for Enhanced Cellular Internalization. *Molecules* **23**, 625 (2018).
63. Correia, C. R., Sher, P., Reis, R. L. & Mano, J. F. Liquified chitosan–alginate multilayer capsules incorporating poly(L-lactic acid) microparticles as cell carriers. *Soft Matter* **9**, 2125–2130 (2013).
64. Shchukin, D. G., Patel, A. A., Sukhorukov, G. B. & Lvov, Y. M. Nanoassembly of Biodegradable Microcapsules for DNA Encasing. *J. Am. Chem. Soc.* **126**, 3374–3375 (2004).
65. Quinn, J. F., Johnston, A. P. R., Such, G. K., Zelikin, A. N. & Caruso, F. Next generation, sequentially assembled ultrathin films: Beyond electrostatics. *Chem. Soc. Rev.* **36**, 707–718 (2007).
66. Kharlampieva, E., Koziyovskaya, V. & Sukhishvili, S. A. Layer-by-layer hydrogen-bonded polymer films: From fundamentals to applications. *Adv. Mater.* **21**, 3053–3065 (2009).
67. DeLongchamp, D. M. & Hammond, P. T. Highly Ion Conductive Poly(ethylene oxide)-Based Solid Polymer Electrolytes from Hydrogen Bonding Layer-by-Layer Assembly. *Langmuir* **20**, 5403–5411 (2004).
68. Sukhishvili, S. A. & Granick, S. Layered, Erasable Polymer Multilayers Formed by Hydrogen-Bonded Sequential Self-Assembly. *Macromolecules* **35**, 301–310 (2002).
69. Lee, H., Mensire, R., Cohen, R. E. & Rubner, M. F. Strategies for Hydrogen Bonding Based Layer-by-Layer Assembly of Poly(vinyl alcohol) with Weak Polyacids. *Macromolecules* **45**, 347–355 (2012).
70. Zhang, Y., Guan, Y., Yang, S., Xu, J. & Han, C. C. Fabrication of Hollow Capsules Based on Hydrogen Bonding. *Adv. Mater.* **15**, 832–835 (2003).
71. Kozlovskaya, V. *et al.* Hydrogen-bonded LbL shells for living cell surface engineering. *Soft Matter* **7**, 2364–2372 (2011).
72. Zhou, B. *et al.* Vacuum-assisted layer-by-layer electrospun membranes: antibacterial and antioxidative applications. *RSC Adv.* **4**, 54517–54524 (2014).
73. Adatoz, E. B., Hendessi, S., Ow-Yang, C. W. & Demirel, A. L. Restructuring of poly(2-ethyl-2-oxazoline)/tannic acid multilayers into fibers. *Soft Matter* **14**, 3849–3857 (2018).
74. Paramasivam, G., Vergaelen, M., Ganesh, M.-R., Hoogenboom, R. & Sundaramurthy,

- A. Hydrogen bonded capsules by layer-by-layer assembly of tannic acid and poly(2-n-propyl-2-oxazoline) for encapsulation and release of macromolecules. *J. Mater. Chem. B* **5**, 8967–8974 (2017).
75. Zhao, Y.-N., Gu, J., Jia, S., Guan, Y. & Zhang, Y. Zero-order release of polyphenolic drugs from dynamic, hydrogen-bonded LBL films. *Soft Matter* **12**, 1085–1092 (2016).
 76. Takemoto, Y., Ajiro, H. & Akashi, M. Hydrogen-Bonded Multilayer Films Based on Poly(N-vinylamide) Derivatives and Tannic Acid. *Langmuir* **31**, 6863–6869 (2015).
 77. Monfared, A., Ghaee, A. & Ebrahimi-Barough, S. Fabrication of tannic acid/poly(N-vinylpyrrolidone) layer-by-layer coating on Mg-based metallic glass for nerve tissue regeneration application. *Colloids Surfaces B Biointerfaces* **170**, 617–626 (2018).
 78. Zangi, R., Hagen, M. & Berne, B. J. Effect of ions on the hydrophobic interaction between two plates. *J. Am. Chem. Soc.* **129**, 4678–4686 (2007).
 79. Ten Wolde, P. R. Hydrophobic interactions: An overview. *J. Phys. Condens. Matter* **14**, 9445–9460 (2002).
 80. Guyomard, A., Muller, G. & Glinel, K. Buildup of multilayers based on amphiphilic polyelectrolytes. *Macromolecules* **38**, 5737–5742 (2005).
 81. Qian, Y. *et al.* Surface modification of nanofibrous matrices via layer-by-layer functionalized silk assembly for mitigating the foreign body reaction. *Biomaterials* **164**, 22–37 (2018).
 82. An, Q., Huang, T. & Shi, F. Covalent layer-by-layer films: chemistry, design, and multidisciplinary applications. *Chem. Soc. Rev.* **47**, 4061–5098 (2018).
 83. Kim, S.-H. *et al.* Tissue adhesive, rapid forming, and sprayable ECM hydrogel via recombinant tyrosinase crosslinking. *Biomaterials* **178**, 401–412 (2018).
 84. Yang, G. *et al.* Assessment of the characteristics and biocompatibility of gelatin sponge scaffolds prepared by various crosslinking methods. *Sci. Rep.* **8**, 1616 (2018).
 85. Silva, J. M. *et al.* PH Responsiveness of Multilayered Films and Membranes Made of Polysaccharides. *Langmuir* **31**, 11318–11328 (2015).
 86. Micheau, C., Bauduin, P., Diat, O. & Faure, S. Specific Salt and pH Effects on Foam Film of a pH Sensitive Surfactant. *Langmuir* **29**, 8472–8481 (2013).
 87. Zhang, L., Zheng, M., Liu, X. & Sun, J. Layer-by-layer assembly of salt-containing polyelectrolyte complexes for the fabrication of dewetting-induced porous coatings. *Langmuir* **27**, 1346–1352 (2011).
 88. Zhang, Z. *et al.* Salt plays a pivotal role in the temperature-responsive aggregation and layer-by-layer assembly of polymer-decorated gold nanoparticles. *Chem. Mater.* **25**, 4297–4303 (2013).
 89. Gong, X. & Gao, C. Influence of salt on assembly and compression of PDADMAC/PSSMA polyelectrolyte multilayers. *Phys. Chem. Chem. Phys.* **11**, 11577–11586 (2009).
 90. Milkova, V. & Radeva, T. Effect of ionic strength and molecular weight on electrical properties and thickness of polyelectrolyte bi-layers. *Colloids Surfaces A Physicochem. Eng. Asp.* **424**, 52–58 (2013).

Chapter 2: Introduction

91. Salomäki, M., Vinokurov, I. A. & Kankare, J. Effect of temperature on the buildup of polyelectrolyte multilayers. *Langmuir* **21**, 11232–11240 (2005).
92. Nohria, R. *et al.* Humidity sensor based on ultrathin polyaniline film deposited using layer-by-layer nano-assembly. *Sensors Actuators, B Chem.* **114**, 218–222 (2006).
93. Huang, H. C. & Zacharia, N. S. Layer-by-layer rose petal mimic surface with oleophilicity and underwater oleophobicity. *Langmuir* **31**, 714–720 (2015).
94. McAloney, R. A., Sinyor, M., Dudnik, V. & Cynthia Goh, M. Atomic force microscopy studies of salt effects on polyelectrolyte multilayer film morphology. *Langmuir* **17**, 6655–6663 (2001).
95. Rydzek, G. *et al.* Electrochemical nanoarchitectonics and layer-by-layer assembly: From basics to future. *Nano Today* **10**, 138–167 (2015).
96. Martins, N. I. *et al.* Multilayered membranes with tuned well arrays to be used as regenerative patches. *Acta Biomater.* **57**, 313–323 (2017).
97. Gomes, T. D. *et al.* Adhesive free-standing multilayer films containing sulfated levan for biomedical applications. *Acta Biomater.* **69**, 183–195 (2018).
98. Sousa, M. P., Cleymand, F. & Mano, J. F. Elastic chitosan / chondroitin sulfate multilayer membranes. *Biomed. Mater.* **11**, 35008 (2016).
99. Caridade, S. G. *et al.* Free-standing polyelectrolyte membranes made of chitosan and alginate. *Biomacromolecules* **14**, 1653–1660 (2013).
100. Caridade, S. G. *et al.* Myoconductive and osteoinductive free-standing polysaccharide membranes. *Acta Biomater.* **15**, 139–149 (2015).
101. Silva, M. *et al.* Biomedical films of graphene nanoribbons and nanoflakes with natural polymers. *RSC Adv.* **7**, 27578–27594 (2017).
102. Gu, Y., Huang, X., Wiener, C. G., Vogt, B. D. & Zacharia, N. S. Large-scale solvent driven actuation of polyelectrolyte multilayers based on modulation of dynamic secondary interactions. *ACS Appl. Mater. Interfaces* **7**, 1848–1858 (2015).
103. Chiarelli, P. A. *et al.* Controlled fabrication of polyelectrolyte multilayer thin films using spin-assembly. *Adv. Mater.* **13**, 1167–1171 (2001).
104. Jinhan, C., Char, K., Hong, J.-D. & Lee, K.-B. Fabrication of Highly Ordered Multilayer Films Using a Spin Self-Assembly Method. *Adv. Mater.* **13**, 1076–1078 (2001).
105. Schlenoff, J. B., Dubas, S. T. & Farhat, T. Sprayed polyelectrolyte multilayers. *Langmuir* **16**, 9968–9969 (2000).
106. Izquierdo, A., Ono, S. S., Voegel, J. C., Schaaf, P. & Decher, G. Dipping versus spraying: Exploring the deposition conditions for speeding up layer-by-layer assembly. *Langmuir* **21**, 7558–7567 (2005).
107. Merrill, M. H. & Sun, C. T. Fast, simple and efficient assembly of nanolayered materials and devices. *Nanotechnology* **20**, 075606 (2009).
108. Mulhearn, W. D., Kim, D. D., Gu, Y. & Lee, D. Facilitated transport enhances spray layer-by-layer assembly of oppositely charged nanoparticles. *Soft Matter* **8**, 10419–10427 (2012).

109. Alongi, J., Carosio, F., Frache, A. & Malucelli, G. Layer by Layer coatings assembled through dipping, vertical or horizontal spray for cotton flame retardancy. *Carbohydr. Polym.* **92**, 114–119 (2013).
110. Guven, S. *et al.* Multiscale assembly for tissue engineering and regenerative medicine. *Trends Biotechnol.* **33**, 269–279 (2015).
111. Gentile, P. *et al.* Functionalised nanoscale coatings using layer-by-layer assembly for imparting antibacterial properties to polylactide-co-glycolide surfaces. *Acta Biomater.* **21**, 35–43 (2015).
112. Lai, Y. T. *et al.* Structure of a designed protein cage that self-assembles into a highly porous cube. *Nat. Chem.* **6**, 1065–1071 (2014).
113. Zhang, Y., Arugula, M. A., Wales, M., Wild, J. & Simonian, A. L. A novel layer-by-layer assembled multi-enzyme/CNT biosensor for discriminative detection between organophosphorus and non-organophosphorus pesticides. *Biosens. Bioelectron.* **67**, 287–295 (2015).
114. Hong, C. Y. *et al.* Semipermeable Functional DNA-Encapsulated Nanocapsules as Protective Bioreactors for Biosensing in Living Cells. *Anal. Chem.* **89**, 5389–5394 (2017).
115. Wang, J. *et al.* Genipin Inhibits LPS-Induced Inflammatory Response in BV2 Microglial Cells. *Neurochem. Res.* **42**, 2769–2776 (2017).
116. Bhushan, B. Biomimetics: lessons from nature-an overview. *Philos. Trans. R. Soc. A Math. Phys. Eng. Sci.* **367**, 1445–1486 (2009).
117. Barthelat, F. Biomimetics for next generation materials. *Philos. Trans. R. Soc.* **365**, 2907–2919 (2007).
118. Vincent, J. F. V., Bogatyreva, O. A., Bogatyrev, N. R., Bowyer, A. & Pahl, A.-K. Biomimetics: its practice and theory. *J. R. Soc. Interface* **3**, 471–482 (2006).
119. Yurtkuran, S., Kirli, G. & Taneli, Y. Learning from Nature: Biomimetic Design in Architectural Education. *Procedia - Soc. Behav. Sci.* **89**, 633–639 (2013).
120. Thakoor, S. *et al.* Review: The Benefits and Applications of Bioinspired Flight Capabilities. *J. Robot. Syst.* **20**, 687–706 (2003).
121. Andrews, H. G. & Badyal, J. P. S. Bioinspired hook surfaces based upon a ubiquitous weed (*Galium aparine*) for dry adhesion. *J. Adhes. Sci. Technol.* **28**, 1243–1255 (2014).
122. Rodrigues, J. R., Alves, N. M. & Mano, J. F. Nacre-inspired nanocomposites produced using layer-by-layer assembly: Design strategies and biomedical applications. *Mater. Sci. Eng. C* **76**, 1263–1273 (2017).
123. Barthelat, F. & Zhu, D. A novel biomimetic material duplicating the structure and mechanics of natural nacre. *J. Mater. Res.* **26**, 1203–1215 (2011).
124. Currey, J. D. Mechanical properties of mother of pearl in tension. *Proc. R. Soc. London - Biol. Sci.* **196**, 443–463 (1977).
125. Barthelat, F., Tang, H., Zavattieri, P. D., Li, C. M. & Espinosa, H. D. On the mechanics of mother-of-pearl: A key feature in the material hierarchical structure. *J. Mech. Phys.*

- Solids* **55**, 306–337 (2007).
126. Menig, R., Meyers, M. H., Meyers, M. A. & Vecchio, K. S. Quasi-static and dynamic mechanical response of *Haliotis rufescens* (abalone) shells. *Acta Mater.* **48**, 2383–2398 (2000).
 127. Wang, R. Z., Suo, Z., Evans, A. G., Yao, N. & Aksay, I. A. Deformation mechanisms in nacre. *J. Mater. Res.* **16**, 2485–2493 (2001).
 128. Barthelat, F., Li, C.-M., Comi, C. & Espinosa, H. D. Mechanical properties of nacre constituents and their impact on mechanical performance. *J. Mater. Res.* **21**, 1977–1986 (2006).
 129. Jackson, A. P., Vincent, J. F. V. & Turner, R. M. The Mechanical Design of Nacre. *Proc. R. Soc. B Biol. Sci.* **234**, 415–440 (1988).
 130. Zhao, H., Yang, Z. & Guo, L. Nacre-inspired composites with different macroscopic dimensions: strategies for improved mechanical performance and applications. *NPG Asia Mater.* **10**, 1–22 (2018).
 131. Cheng, Q., Jiang, L. & Tang, Z. Bioinspired layered materials with superior mechanical performance. *Acc. Chem. Res.* **47**, 1256–1266 (2014).
 132. Farhadi-Khouzani, M. *et al.* A CaCO₃/nanocellulose-based bioinspired nacre-like material. *J. Mater. Chem. A* **5**, 16128–16133 (2017).
 133. Li, Y. Q., Yu, T., Yang, T. Y., Zheng, L. X. & Liao, K. Bio-Inspired nacre-like composite films based on graphene with superior mechanical, electrical, and biocompatible properties. *Adv. Mater.* **24**, 3426–3431 (2012).
 134. Yang, R.-L., Zhu, Y.-J., Chen, F.-F., Qin, D.-D. & Xiong, Z.-C. Bioinspired Macroscopic Ribbon Fibers with a Nacre-Mimetic Architecture Based on Highly Ordered Alignment of Ultralong Hydroxyapatite Nanowires. *ACS Nano* (2018).
 135. Nikolov, S. *et al.* Revealing the Design Principles of High-Performance Biological Composites Using Ab initio and Multiscale Simulations: The Example of Lobster Cuticle. *Adv. Mater.* **22**, 519–526 (2010).
 136. Fabritius, H.-O. *et al.* Functional adaptation of crustacean exoskeletal elements through structural and compositional diversity: a combined experimental and theoretical study. *Bioinspir. Biomim.* **11**, 055006 (2016).
 137. Fabritius, H. O., Sachs, C., Triguero, P. R. & Raabe, D. Influence of structural principles on the mechanics of a biological fiber-based composite material with hierarchical organization: The exoskeleton of the lobster *homarus americanus*. *Adv. Mater.* **21**, 391–400 (2009).
 138. Sachs, C., Fabritius, H. & Raabe, D. Hardness and elastic properties of dehydrated cuticle from the lobster *Homarus americanus* obtained by nanoindentation. *J. Mater. Res.* **21**, 1987–1995 (2006).
 139. João, C. F. C. *et al.* Bio-inspired production of chitosan/chitin films from liquid crystalline suspensions. *Carbohydr. Polym.* **155**, 372–381 (2017).
 140. Oh, D. X. *et al.* Chiral nematic self-assembly of minimally surface damaged chitin nanofibrils and its load bearing functions. *Sci. Rep.* **6**, 23245 (2016).

141. Tramacere, F. *et al.* The Morphology and Adhesion Mechanism of Octopus vulgaris Suckers. *PLoS One* **8**, e65074 (2013).
142. Lee, H. *et al.* Octopus-Inspired Smart Adhesive Pads for Transfer Printing of Semiconducting Nanomembranes. *Adv. Mater.* **28**, 7457–7465 (2016).
143. Chen, Y.-C. & Yang, H. Octopus-Inspired Assembly of Nanosucker Arrays for Dry/Wet Adhesion. *ACS Nano* **11**, 5332–5338 (2017).
144. Baik, S., Kim, J., Lee, H. J., Lee, T. H. & Pang, C. Highly Adaptable and Biocompatible Octopus-Like Adhesive Patches with Meniscus-Controlled Unfoldable 3D Microtips for Underwater Surface and Hairy Skin. *Adv. Sci.* **5**, 1800100 (2018).
145. Chun, S. *et al.* Conductive and Stretchable Adhesive Electronics with Miniaturized Octopus-Like Suckers against Dry/Wet Skin for Biosignal Monitoring. *Adv. Funct. Mater.* **1805224**, (2018).

Chapter 3: Materials and Methods

3.1. Materials

Chitosan (CHT) (M_w 40–150 kDa, deacetylation degree $\geq 92.6\%$ and viscosity of 16–30 cP) was supplied by Chitoceuticals. Alginic acid sodium salt (ALG) (viscosity of 4–12 cP, 1% in H₂O at 25 °C), N-Hydroxysuccinimide (NHS, 98%), N-(3-Dimethylaminopropyl)-N'-ethylcarbodiimide hydrochloride (EDC) (purity, $\geq 98.0\%$ (AT)), methacrylic anhydride (purity~94%), methacrylic acid 99%, 2-Hydroxy-4'-(2-Hydroxyethoxy)-2-methylpropiophenone 98% (Irgacure 2959), and hydrochloric acid (37% PA) were purchased from Sigma Aldrich. Phosphate buffered saline (PBS) was obtained from Thermo Fisher Scientific, while acetic acid was acquired from Chem-Lab and sodium hydrogen carbonate from Fisher. Spectra/Por®1 dialysis membrane (cutoff 6–8 kDa) and Spectra/Por®3 dialysis membrane (cutoff 3.5 kDa) were purchased from SpectrumLabs. Finally, sodium acetate trihydrate was obtained from Sharlau and sodium chloride from LabChem.

3.2. Methods

3.2.1. Synthesis of Methacrylated Polysaccharides

3.2.1.1. Modification of Alginate with Methacrylic Anhydride

Methacrylated alginate (ALG-MA) was prepared following a standard procedure (Figure 13)^{1,2}. Briefly, ALG was dissolved at 2.0% (w/v) in distilled water, at room temperature, with vigorous mechanical stirring. Then, 2 molar equivalents of methacrylic anhydride (MAN) per alginate repeating units were added dropwise to the solution that was then incubated for 24 h at 5 °C, in the dark. The pH of the mixture was periodically adjusted to 8 by dropwise addition of concentrated aqueous NaOH (5.0 M) in order to neutralize the MAN formed during the reaction. Afterwards, the reaction mixture was dialyzed against water using 3.5 kDa cutoff dialysis membranes, for 5 days (changing water 3 times per day).

The resulting solution was frozen at -80 °C, followed by freeze-drying and stored at 4 °C until further use. The relative degree of substitution that is, the amount of methacrylate moieties was assessed by proton nuclear magnetic resonance (¹H NMR) spectroscopy by comparing the areas of the signals arising from the vinyl protons of the inserted moieties with the signal from the anomeric proton of the guluronic acid block (G-units)³. This value

was still multiplied by a correction factor that is, the relative number of G-units, because of the presence of mannuronic acid (M-units).

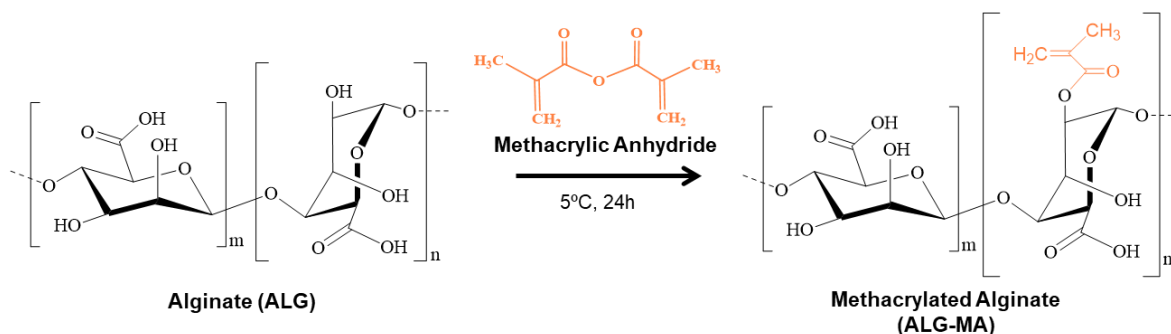


Figure 13. Schematic representation of the chemical modification of alginate (ALG) with methacrylate moieties.

3.2.1.2. Modification of Chitosan with Methacrylic Acid

The modification of CHT was performed following a procedure described in the literature (Figure 14)⁴. Briefly, Chitosan was dissolved at 0.25% (w/v) in acetic acid 0.05 M (pH 5.5) at room temperature, overnight. Afterwards, 2.9×10^{-2} mol of methacrylic acid (MAc) (corresponding to 2 molar equivalents per CHT repeating units) was added dropwise to the CHT solution under mechanical stirring. Then 4.4×10^{-2} mol of EDC ([EDC] = 1.5 [MAc]) was added to the mixture, followed by the addition of NHS ([NHS] = [EDC]) after 15 min. The reaction was carried out at room temperature during 24h. The resulting modified CHT solution was dialyzed, using 6-8 kDa cutoff dialysis membranes, against 0.05 M NaHCO_3 (3 shifts), 0.001 M HCl (2 shifts), 0.1 M NaCl (3 shifts) and finally deionized water (5/6 shifts). The purified CHT solution was lyophilized over a week and stored at 4°C , protected from light until further use. The DS was determined by ^1H NMR analysis by comparing the characteristic peaks of the vinyl protons from the methacrylate moieties, with the reference peak of the anomeric proton of the chitosan backbone and also was corrected taking into account the deacetylation degree of the CHT precursor biopolymer.

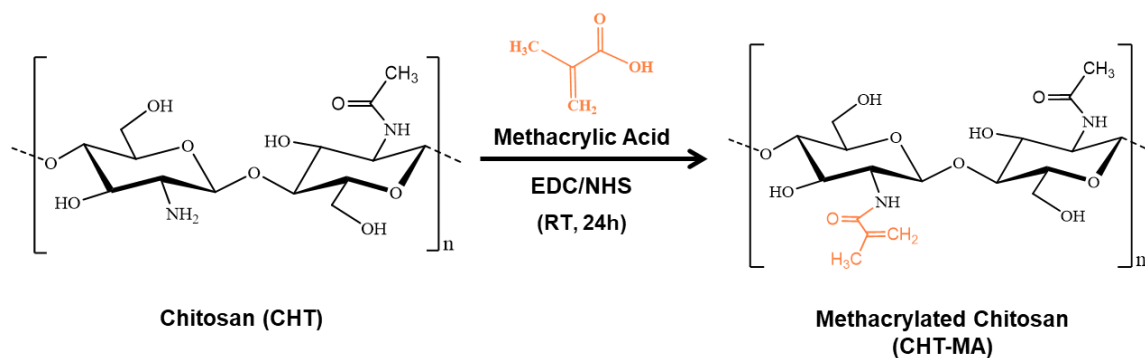


Figure 14. Schematic representation of the chemical modification of chitosan (CHT) with methacrylate moieties.

3.2.2. Characterization of the modified polysaccharides

The successful synthesis of both modified polysaccharides was evaluated by two different techniques. The proton nuclear magnetic resonance (^1H NMR) analyses were recorded at 70 °C on a Bruker Advance III 400 MHz spectrometer. All samples characterized were previously dissolved in 800 μl of D_2O and then transferred to 300 MHz NMR glass tubes (Sigma-Aldrich) and then analyzed. The spectra acquisition main parameters consisted of 256 scans, 32 dummy scans, and 18 s relaxation delay. For the data processing, a software called MestReNova was used. On the other hand, the Fourier Transformed Infrared spectroscopy was performed on dried samples using the attenuated total reflectance (ATR-FTIR) method through a Bruker Tensor 27 spectrometer. The spectra of all samples were recorded at a 2 cm^{-1} resolution for a total of 256 scans in the spectral width of 4000 to 400 cm^{-1} . All data were processed in OPUS software.

3.2.3. Film Assembly

3.2.3.1. Zeta Potential

To understand the impact of electrostatic forces of each solution, CHT, ALG, CHT-MA and ALG-MA (1 mg mL^{-1} and 0.5 mg mL^{-1} each) containing 0.15 M NaCl were dissolved into acetate buffer. The pH of all solutions was adjusted to 5.5. The ζ -potential of each solution was determined using a Malvern Zetasizer Nano ZS equipment (Malvern Instruments Ltd., Malvern, United Kingdom) at 25 °C.

3.2.3.2. Quartz crystal microbalance with dissipation monitoring

The build-up process of CHT/ALG and CHT-MA/ALG-MA multilayer films was evaluated using a quartz crystal microbalance with dissipation monitoring (QCM-D, Q-Sence), with sensor crystals coated with gold, excited at a fundamental frequency of 5 MHz as well as at 15, 25, 35, 45 and 55 MHz corresponding to the 3rd, 5th, 7th, 9th and 11th overtones, respectively.

Fresh polyelectrolyte solutions were prepared by dissolution of CHT, ALG, CHT-MA and ALG-MA in 0.15 M NaCl to yield a final concentration of 0.5 mg mL⁻¹ for each one. The CHT solution was injected into the system for 6 min to allow the adsorption equilibrium at the crystal's surface. The acetate buffer solution was then pumped during 4 min as a rinsing step in order to remove the unbound molecules. In third place, the ALG solution was pumped into the system for 6 min, and then the acetate buffer for the next 4 min, and so on in order to complete the desired number of layers. The CHT-MA/ALG-MA bilayers deposition were injected in the same conditions as the last ones.

3.2.3.3. Production of multilayered films

The main goal of this project is to produce FS multilayered membranes based on CHT and ALG multilayers alternately deposited with CHT-MA and ALG-MA multilayers. However, as controls, standard membranes with only CHT and ALG multilayers and other ones with CHT-MA and ALG-MA were also fabricated.

The production of all the different conditions of multilayered FS membranes was achieved using the LbL methodology with the help of a dipping robot, illustrated in Figure 15. Polypropylene (PP) substrates were immersed in alternated polyelectrolyte solutions with a rinsing solution between each of them. Polyelectrolyte solutions were obtained by firstly dissolving 0.15 M NaCl (pH = 5.5) in the rinsing solution (buffer acetate) and then added the different polymers (1 mg mL⁻¹). These conditions were verified for CHT, ALG, CHT-MA and ALG-MA. Moreover, the deposition time for each 4 polyelectrolytes was 4 min and 4 min for rinsing solution.

At the end four different types of FS membranes were produced, multilayered membranes containing CHT and ALG (CHT/ALG)₂₀₀, membranes containing the pendant methacrylic groups (CHT-MA/ALG-MA)₂₀₀ and also two types of intercalated membranes with

multilayers alternately deposited with CHT and ALG and CHT-MA and ALG-MA, ones of 10 bilayers each $[(\text{CHT}/\text{ALG})_{10}(\text{CHT-MA}/\text{ALG-MA})_{10}]_{200}$ or simplified $(10/10)_{200}$ and the other ones with 25 bilayers each $[(\text{CHT}/\text{ALG})_{25}(\text{CHT-MA}/\text{ALG-MA})_{25}]_{200}$ or $(25/25)_{200}$. Finally, the different types of FS multilayered membranes were then characterized.

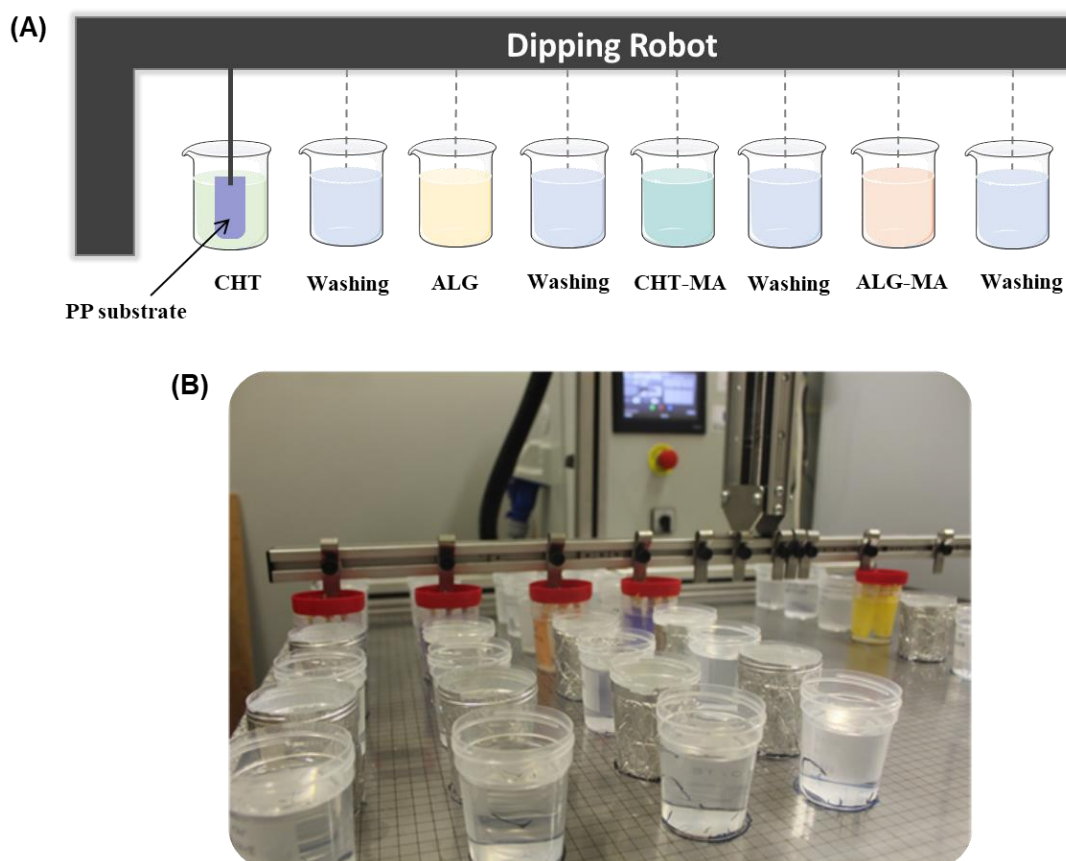


Figure 15. Dipping robot used for LbL assembly. (A) illustration of the steps during the dipping coating. (B) Real photograph of the dipping robot used to produce freestanding (FS) membranes.

3.2.3.4. Photocrosslinking

To promote the photocrosslinking different solutions with both polysaccharides mixed with irgacure 2959 were prepared, which is a typical member of highly efficient photoinitiators used in photocleavage reactions that involves its excited states and dissociates into free radicals upon UV light irradiation through an α -cleavage reaction⁵. The photocrosslinking of the methacrylate-modified polymers was tested by exposing the different solutions to an UV/ozone precleaned system under 185 and 254 nm UV lights at 4.6 mW/cm². So, the produced FS membranes were immersed, for 15 min, into a solution of 0.5% (w/v) of

irgacure dissolved in water/ethanol (volume ratio 1:1). After that, they were exposed to UV radiation for 5 min and then were washed with deionized water to remove the excess of the irgacure. After well dried the membranes were ready to be tested out.

3.2.3.5. Scanning electron microscopy

The cross-section of the freestanding membranes was visualized through scanning electron microscopy (SEM, S4100, Hitachi, Japan), operating at 4 kV. All samples were previously sputtered with a conductive gold layer, using a sputter coater. Cross-sections were produced with liquid nitrogen. However, aiming to evaluate the cross-section microstructures, membranes were lyophilized until occurred spontaneous fractures.

3.2.3.6. Water uptake ability

The water uptake ability of all different types of freestanding multilayered membranes was determined by immersing dry samples, previously weighted, in a phosphate buffered saline solution (PBS) at pH = 7.4 up to 10 min at room temperature (RT). The swollen FS samples were removed at pre-determined time points ($t = 15$ s, 30 s, 45 s, 1 min, 2 min, 5 min and 10 min) from the immersion. After removing the excess of water with the help of a filter paper, the membranes were immediately weighed with an analytical balance. The water uptake was calculated based on equation (1), where W_w corresponds to the weight of swollen and W_d to dried FS weight.

$$\text{Water uptake (\%)} = \frac{W_w - W_d}{W_d} \times 100 \quad (1)$$

3.2.3.7. Mechanical test

Tensile tests were performed to investigate the produced membranes under tension, by using a Shimadzu MMT-101N (Shimadzu Scientific Instruments, Japan) with a load cell of 100 N and a crosshead speed of $1 \text{ mm} \cdot \text{min}^{-1}$, illustrated in Figure 16. For that, two sets of membranes were produced for mechanical assays: one without any treatment and other one was previously swelled in water, frozen in liquid nitrogen, lyophilized overnight and stored

until further analysis. Prior to mechanical tests, both sets of samples were immersed in PBS during 2h. The thickness of all samples was measured using a micrometer with a precision of 1 μm . The mechanical tests were made at room temperature (RT) with a gauge length of 5 mm.

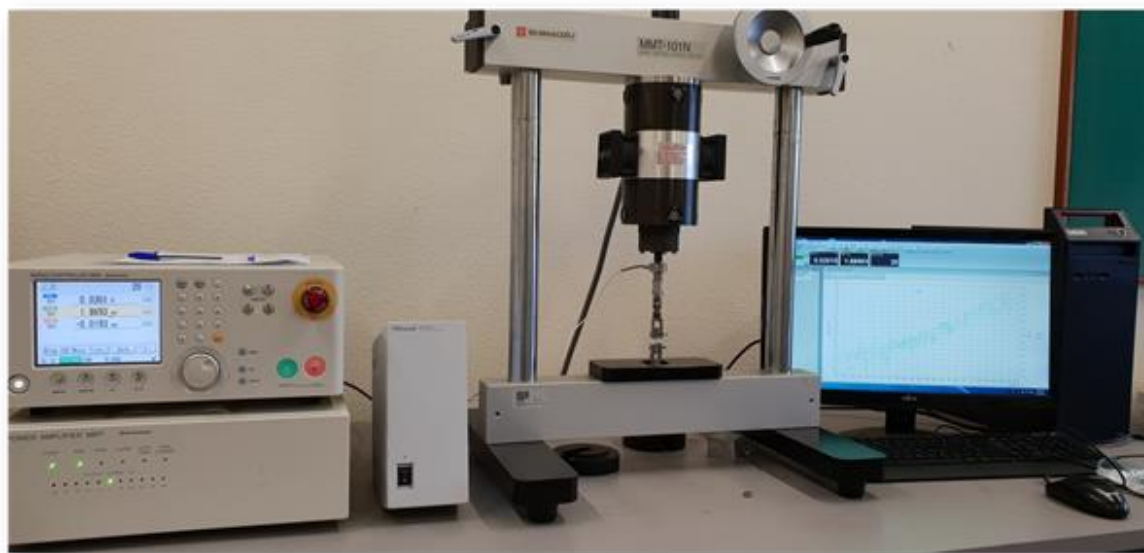


Figure 16. Real-time photograph of the Shimadzu MMT-101N, used to performed tensile tests in the membranes.

The young's modulus (E) is the mechanical property that measures the stiffness of a solid material. For that this was obtained by dividing the tensile strength (Stress – σ) for elongation (Strain – ϵ) in the elastic part (linear) of the physical stress-strain curve, as shown in equation (2), see Figure 17.

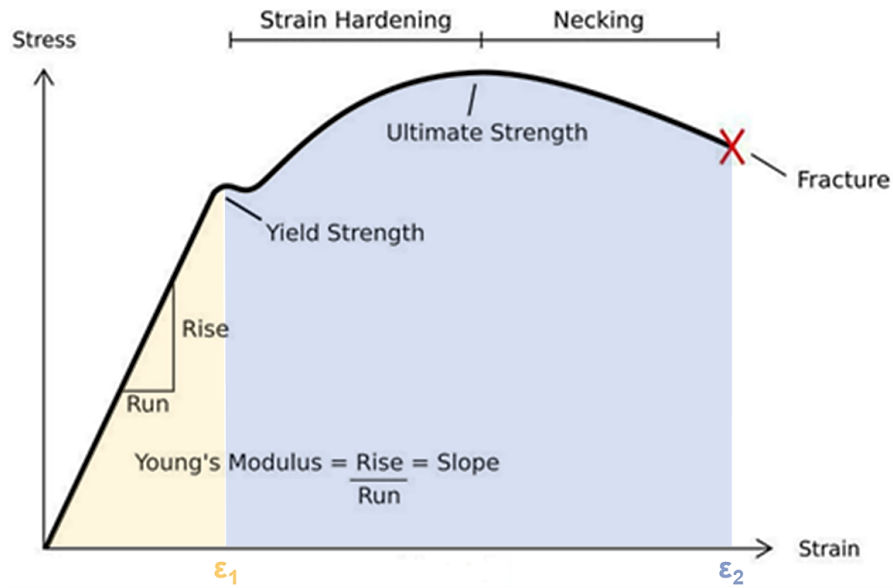


Figure 17. Stress-strain curve. Young's modulus is obtained by the slope in elastic linear part. Ultimate Strength represents the maximum value of stress that any material could suffer, leading to its fracture. Adapted from reference ⁶.

$$Young's\ Modulus\ (Pa) = \frac{Stress(\sigma)}{Strain\ (\epsilon)} \quad (2)$$

However, to calculate these values it was necessary to perform secondary equations, which was the case of stress and strain, presented below.

The stress (σ , Pa) applied to a specific material is obtained by divided the force at each point (F, N) by the cross-sectional area (A).

$$Stress\ (\sigma, Pa) = \frac{F}{A} = \frac{F}{width \times thickness} \quad (3)$$

Strain (ϵ , adimensional) is the measure of how much deformation one material could suffer compared to its original length. Simplifying, strain is the ratio of extension (ΔL , m) to original length (L, m).

$$\text{Strain } (\varepsilon, \text{adimensional}) = \frac{\Delta L}{L} = \frac{\Delta L}{\text{gauge length}} \quad (4)$$

In addition, the strain energy density (U , J/m^3) was also evaluated, and corresponds to the area under the stress-strain curve (energy stored per unit of volume), as we can see in the equation below.

$$\text{Energy } \left(U, \frac{\text{J}}{\text{m}^3} \right) = A_{\varepsilon_1} + A_{\varepsilon_2} = \left(\frac{1}{2} \times \frac{F}{A} \times \frac{\Delta L(0, \varepsilon_1)}{L} \right) + \left(\int_{\varepsilon_1}^{\varepsilon_2} \sigma \, dx \right) \quad (5)$$

References

1. Smeds, K. A. *et al.* Photocrosslinkable polysaccharides for in situ hydrogel formation. *J. Biomedical Mater. Res.* **54**, 115–121 (2001).
2. Zhou, S., Bismarck, A. & Steinke, J. H. G. Ion-responsive alginate based macroporous injectable hydrogel scaffolds prepared by emulsion templating. *J. Mater. Chem. B* **1**, 4736–4745 (2013).
3. Mignon, A. *et al.* Combinatory approach of methacrylated alginate and acid monomers for concrete applications. *Carbohydr. Polym.* **155**, 448–455 (2017).
4. Diolosà, M. *et al.* Use of methacrylate-modified chitosan to increase the durability of dentine bonding systems. *Biomacromolecules* **15**, 4606–4613 (2014).
5. Liu, M., Li, M.-D., Xue, J. & Phillips, D. L. Time-Resolved Spectroscopic and Density Functional Theory Study of the Photochemistry of Irgacure-2959 in an Aqueous Solution. *J. Phys. Chem.* **118**, 8701–8707 (2014).
6. Figari, P. Steps to Analyzing a Material's Properties From Its Stress/Strain Curve. *Instructables* (2015). Available at URL: <https://www.instructables.com/id/Steps-to-Analyzing-a-Materials-Properties-from-its/>

Chapter 4: Results and Discussion

**4.1. Bioinspired approach to Tune Mechanical Properties of
Multilayered Freestanding Membranes for Skin
Regenerative Patches**

Subchapter 4.2.

This subchapter is based on the article entitled
“Bioinspired Approach to Tune Mechanical Properties of Multilayered Freestanding Membranes
for Skin Regenerative Patches”
(manuscript in preparation)

Bioinspired approach to Tune Mechanical Properties of Multilayered Freestanding Membranes for skin regenerative patches

Fernandes, E.A.¹, Patrício, S.G^{2#}, and Mano, J.F.^{2#}

¹ Department of Materials Engineering and Ceramics, University of Aveiro, Campus Universitário de Santiago, 3810-193, Aveiro, Portugal

² Department of Chemistry, CICECO – Aveiro Institute of Materials, University of Aveiro, Campus Universitário de Santiago, 3810-193, Aveiro, Portugal

Corresponding Author:

E-mail: sgpatricio@ua.pt; jmano@ua.pt

Abstract

Understanding the several mechanisms present in nature is an elegant way for developing novel materials with sophisticated properties. Jellyfish is a free-swimming marine organism with a particular umbrella-shaped bell, that contains a tough, yet gelatinous matrix called mesoglea. Inspired by this porous structure with high mechanical properties, the design of a new multilayered free-standing membrane with marine-derived biopolymers was envisioned. To reach this purpose, Chitosan (CHT) and Alginate (ALG) were initially modified with pendant methacrylic groups (MA). Afterwards, aiming to recapitulate the jellyfish structure, two types of intercalated (CHT/ALG/CHT-MA/ALG-MA) membranes were produced by selective photocrosslinking. Deposition conditions of the polymers were studied through zeta potential measurements and quartz crystal microbalance with dissipation monitoring analysis. Moreover, mechanical tests revealed higher elasticity for intercalated membranes. Interestingly, scanning electron microscopy showed distinct stratification for the bioinspired intercalated membranes when compared to unmodified CHT/ALG controls.

Keywords: Biomimetics, Layer-by-Layer assembly, marine-origin polysaccharides, mechanical properties modulation, photocrosslinking.

1. Introduction

Ever since the pioneering work of Decker and his coworkers, Layer-by-Layer (LbL) has shown to be an easy and efficient way for fabricating hierarchical films. This versatile method is based on the sequential deposition of multivalent materials over an underlying substrate, coordinated by electrostatic and/or non-electrostatic forces^{1,2}. This technique stands out because it allows precise control over structural thickness, mechanical properties, surface charge and innumerable material combinations over any type of substrate^{2,3}. Interestingly, such multilayered films, when deposited on specific substrates with intrinsic low surface energy, can be easily removed without resorting to post-processing steps, thus allowing the production of freestanding (FS) membranes⁴. Moreover, these membranes can be used across several research fields with different applications such as biomimetic membranes for regenerative medicine, biomaterial scaffolds for tissue engineering, as well as drug delivery and cell coating techniques⁵⁻⁷.

Natural polymers represent attractive building blocks for LbL constructs not only due to their variable polyelectrolyte nature, wide availability and significant number of functional groups for chemical functionalization but also intrinsic biocompatibility/biodegradability and bioactivity features⁸⁻¹⁰. Several studies have been reported the design of biofunctional FS membranes by using natural based polysaccharides¹¹⁻¹⁴. However, a major drawback is their high hydration levels and low mechanical strength causing poor cell adhesion. To overcome these limitations, several strategies have been employed in order to modulate the bulk mechanical properties of multilayered FS membranes, thus improving biological performance. A common approach consists in the chemical post-assembly treatment by using crosslinking agents as glutaraldehyde or genipin for amine-based multilayers and EDC/NHS or calcium chloride in the case of multilayers with carboxylic moieties¹⁵⁻¹⁸. Recently, the incorporation of graphene derivatives into the multilayered membranes has also emerged as another alternative to tailor mechanical properties^{19,20}. Among all strategies, genipin has been more explored in chitosan and alginate multilayers because of their higher efficiency low cytotoxic effects and ability to tune cell adhesion^{2,21}. Despite the improvement of the biological performance, genipin crosslinking mostly allows the membrane stiffness enhancement, while the maximum tensile strain related with the biomaterial elastic stretching decreases significantly. This is a critical issue for soft tissue

engineering constructs like skin since its biological functions rely on the mechanical properties of the dermis, in particular in the elasticity and resistance to stretch²². However, scarce studies have exploited the design of high-performing biomaterials with tailored elastic properties. Recently, Sousa M.P *et al.* developed a mussel-inspired freestanding membranes based in chitosan, alginate and hyaluronic acid functionalized with dopamine groups. Such molecules provided adhesiveness behavior to the freestanding membranes, which improved drastically the stiffness and elastic stretching properties of the biomaterial, thus leading to a high-performing cellular response and wound healing process¹³. In fact, the development of high-performing biomaterials inspired in naturally systems have conquered new horizons in tissue engineering and regenerative medicine fields^{23,24}. In this work hierarchical self-supported membranes based in the electrostatic interaction of intercalated CHT/ALG pair of layers and CHT and ALG bilayers previously functionalized with methacrylated pendant groups (CHT-MA/ALG-MA) were successfully produced by LbL assembly, (Figure 18). After detachment from the underlying substrate, hierarchical freestanding membranes were exposed to UV light in order to promote the photocrosslinking of the methacrylated moieties. We hypothesized that the photocrosslinking treatment combined with lyophilization cycles could generate interconnected porous CHT-MA/ALG-MA multilayers interlayered with stratified CHT/ALG pair of layers, which could broadly disperse stress near a crack tip, as the jellyfish gel. Emulating the jellyfish's mesoglea porous anisotropic structure represents a new attempt to modulate mechanical properties of CHT/ALG freestanding membranes herein reported for the first time. Moreover, the effect of photocrosslinking methacrylate moieties within FS membranes was evaluated not only over the mechanical properties but also correlated with water uptake ability and microstructural features.

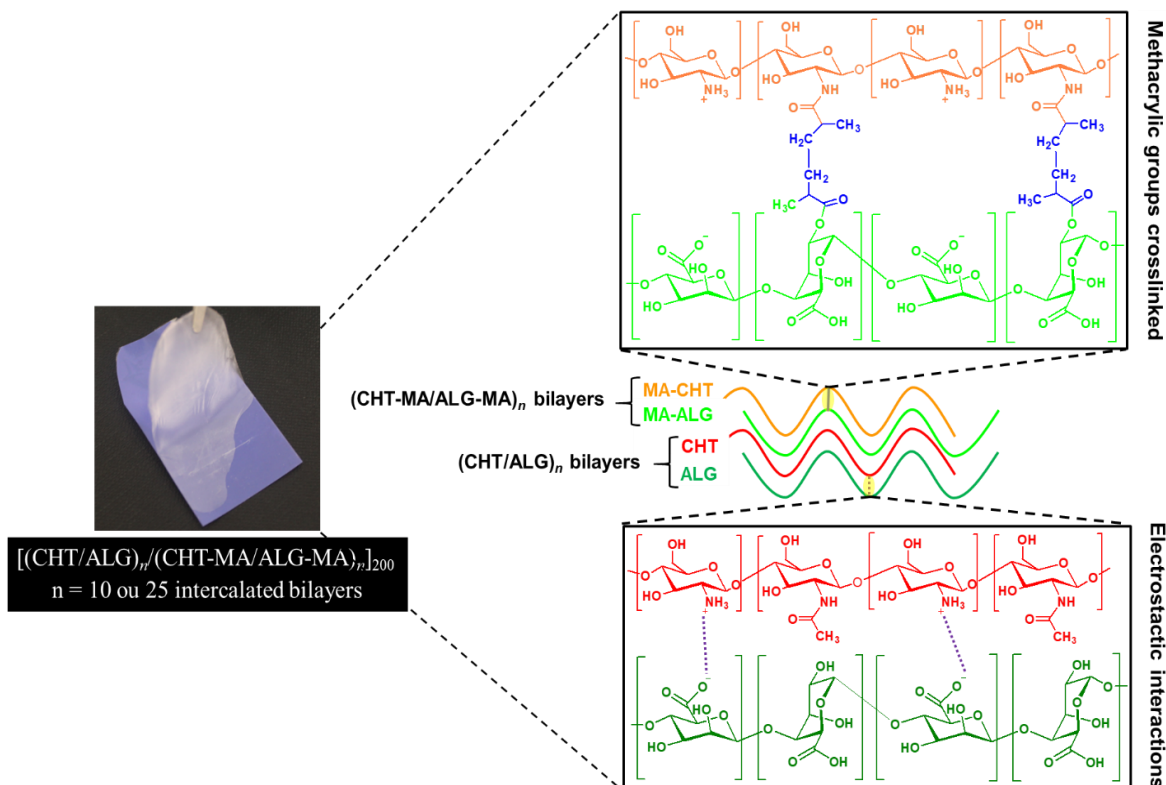


Figure 18. Scheme of the multilayered rearrangements within the membrane after UV light exposure (photocrosslinking). Electrostatic interactions are combined with covalent bonds arising from photocrosslinking of methacrylate groups.

2. Materials and Methods

2.1. Materials

Chitosan (CHT) (Mw40–150 kDa, deacetylation degree $\geq 92.6\%$ and viscosity of 16–30 cP) was supplied by Chitoceuticals. Alginic acid sodium salt (ALG) (viscosity of 4–12 cP, 1% in H₂O at 25 °C), N-Hydroxysuccinimide (NHS, 98%), N-(3-Dimethylaminopropyl)-N'-ethylcarbodiimide hydrochloride (EDC) (purity, $\geq 98.0\%$ (AT)), methacrylic anhydride (purity~94%), methacrylic acid 99%, 2-Hydroxy-4'-(2-Hydroxyethoxy)-2-methylpropiophenone 98% (Irgacure 2959), and hydrochloric acid (37% PA) were purchased from Sigma Aldrich. Phosphate buffered saline (PBS) was obtained from Thermo Fisher Scientific, while acetic acid was acquired from Chem-Lab and sodium hydrogen carbonate from Fisher. Spectra/Por®1 dialysis membrane (cutoff 6–8 kDa) and Spectra/Por®3 dialysis membrane (cutoff 3.5 kDa) were purchased from SpectrumLabs.

Finally, sodium acetate trihydrate was obtained from Sharlau and sodium chloride from LabChem.

2.2. Synthesis of methacrylated polysaccharides

2.2.1 Modification of alginate with methacrylic anhydride

Methacrylated alginate (ALG-MA) was prepared following a standard procedure^{25,26}. Briefly, ALG was dissolved at 2.0 % (w/v) in distilled water, at room temperature, with vigorous mechanical stirring. Then, 2 molar equivalents of methacrylic anhydride (MAN) per alginate repeating units were added dropwise to the solution that was then incubated for 24 h at 5 °C, in the dark. The pH of the mixture was periodically adjusted to 8 by dropwise addition of concentrated aqueous NaOH (5.0 M) in order to neutralize the MAN formed during the reaction. Afterwards, the reaction mixture was dialyzed against water using 3.5 kDa cutoff dialysis membranes, for 5 days (changing water 3 times per day).

The resulting solution was frozen at -80 °C, followed by freeze-drying and stored at 4 °C until further use. The relative degree of substitution (DS) that is, the amount of methacrylate moieties was assessed by proton nuclear magnetic resonance (¹H NMR) spectroscopy by comparing the areas of the signals arising from the vinyl protons of the inserted moieties with the signal from the anomeric proton of the guluronic acid block (G-units)²⁷. This value was still multiplied by a correction factor that is, the relative number of G-units, because of the presence of mannuronic acid (M-units). All synthesis steps are illustrated in Figure S1.†

2.2.2. Modification of chitosan with methacrylic acid

The modification of CHT was performed following a procedure described in the literature²⁸. Briefly, Chitosan was dissolved at 0.25% (w/v) in acetic acid 0.05 M (pH 5.5) at room temperature, overnight. Afterwards, 2.9×10^{-2} mol of methacrylic acid (MAc) (corresponding to 2 molar equivalents per CHT repeating units) was added dropwise to the CHT solution under mechanical stirring. Then 4.4×10^{-2} mol of EDC ([EDC] = 1.5 [MAc]) was added to the mixture, followed by the addition of NHS ([NHS] = [EDC]) after 15 min. The reaction was carried out at room temperature during 24h. The resulting modified CHT solution was dialyzed, using 6-8 kDa cutoff dialysis membranes, against 0.05 M NaHCO₃ (3 shifts), 0.001 M HCl (2 shifts), 0.1 M NaCl (3 shifts) and finally deionized water (5/6 shifts). The purified

CHT solution was lyophilized over a week and stored at 4 °C, protected from light until further use. The DS was determined by ^1H NMR analysis by comparing the characteristic peaks of the vinyl protons from the methacrylate moieties, with the reference peak of the anomeric proton of the chitosan backbone and also was corrected taking into account the deacetylation degree of the CHT precursor biopolymer. All synthesis steps are illustrated in Figure S1†.

2.3. Proton nuclear magnetic resonance spectroscopy

^1H NMR analyses were recorded at 70 °C on a Bruker Advance III 400 MHz spectrometer. All the samples characterized were previously dissolved in 800 μl of D_2O and then transferred to 300 MHz NMR glass tubes (Sigma-Aldrich). The spectra acquisition main parameters consisted of 256 scans, 32 dummy scans, and 18 s relaxation delay. For the data processing was used a software called MestReNova.

2.4. Attenuated total reflectance – Fourier transform spectroscopy

Fourier Transformed Infrared spectra were performed on dried samples using the attenuated total reflectance (ATR-FTIR) method through a Bruker Tensor 27 spectrometer. The spectra of all samples were recorded at a 2 cm^{-1} resolution for a total of 256 scans in the spectral width of 4000 to 400 cm^{-1} . All data were processed in OPUS software.

2.5. Quartz crystal microbalance with dissipation monitoring

The build-up process of CHT/ALG and CHT-MA/ALG-MA multilayer films was evaluated using a quartz crystal microbalance with dissipation monitoring (QCM-D, Q-Sence), with sensor crystals coated with gold, excited at a fundamental frequency of 5 MHz as well as at 15, 25, 35, 45 and 55 MHz corresponding to the 3rd, 5th, 7th, 9th and 11th overtones, respectively.

Fresh polyelectrolyte solutions were prepared by dissolution of CHT, ALG, CHT-MA and ALG-MA in 0.15 M NaCl to yield a final concentration of 0.5 mg mL^{-1} for each one. The CHT solution was injected into the system for 6 min to allow the adsorption equilibrium at the crystal's surface. The acetate buffer solution was then pumped during 4 min as a rinsing

step in order to remove the unbound molecules. In third place, the ALG solution was pumped into the system for 6 min, and then the acetate buffer for the next 4 min, and so on in order to complete the desired number of layers. The CHT-MA/ALG-MA bilayers deposition were injected in the same conditions as the last ones. The electrical charge of all polyelectrolyte solutions was evaluated by measuring their zeta potential with a Malvern Zetasizer Nano ZS equipment (Malvern Instruments Ltd., Malvern, United Kingdom).

2.6. Production of multilayered films

The main goal of this project is to produce FS multilayered membranes based on CHT and ALG multilayers alternately deposited with CHT-MA and ALG-MA multilayers.

The production of all the different conditions of multilayered FS membranes was achieved using the LbL methodology with the help of a dipping robot, illustrated in figure S1.† PP substrates were immersed in alternated polyelectrolyte solutions with a rising solution between each of them. Polyelectrolyte solutions were obtained by firstly dissolving 0.15 M NaCl (pH = 5.5) in the rising solution (buffer acetate) and then added the different polymers (1 mg mL⁻¹). These conditions were verified for CHT, ALG, CHT-MA and ALG-MA. The deposition time for all polyelectrolytes was 4 min and 4 min for rising solution.

At the end four different types of FS membranes were produced, multilayered membranes containing CHT and ALG (CHT/ALG)₂₀₀, membranes containing the pendant methacrylic groups (CHT-MA/ALG-MA)₂₀₀ and also two types of intercalated membranes with multilayers alternately deposited with CHT and ALG and CHT-MA and ALG-MA, ones of 10 bilayers each [(CHT/ALG)₁₀(CHT-MA/ALG-MA)₁₀]₂₀₀ or simplified (10/10)₂₀₀ and the other ones with 25 bilayers each [(CHT/ALG)₂₅(CHT-MA/ALG-MA)₂₅]₂₀₀ or (25/25)₂₀₀ (see Figure S2†). To promote the photocrosslinking, different solutions with both polysaccharides mixed with irgacure 2959 were prepared, which is a typical member of highly efficient photoinitiators used in photocleavage reactions that involves its excited states and dissociates into free radicals upon UV light irradiation through an α -cleavage reaction²⁹. The photocrosslinking of the methacrylate-modified polymers was tested by exposing the different membranes to an UV/ozone precleaned system under 185 and 254 nm UV lights at 4.6 mW/cm². So, the produced FS membranes were immersed, for 15 min, into a solution of 0.5% (w/v) of irgacure dissolved in water/ethanol (volume ratio 1:1). After that

were exposed to UV radiation for 5 min and then were washed with deionized water to remove the excess of the irgacure. After well dried, the membranes were ready to be tested out. Finally, the different types of FS multilayered membranes obtained were then characterized.

2.7. Water uptake ability

The water uptake ability of all different types of freestanding multilayered membranes was determined by immersing dry samples, previously weighted, in a phosphate buffered saline solution (PBS) at pH = 7.4 up to 10 min at room temperature (RT). The swollen FS samples were removed at pre-determined time points ($t = 15$ s, 30 s, 45 s, 1 min, 2 min, 5 min and 10 min) from the immersion. After removing the excess of water with the help of a filter paper, the membranes were immediately weighed with an analytical balance. The water uptake was calculated based on equation (1), where W_w corresponds to the weight of swollen and W_d to dried FS weight.

$$\text{Water uptake (\%)} = \frac{W_w - W_d}{W_d} \times 100 \quad (1)$$

2.8. Mechanical tests

Tensile tests were performed using a Shimadzu MMT-101N (Shimadzu Scientific Instruments, Japan) with a load cell of 100 N and a crosshead speed of $1 \text{ mm} \cdot \text{min}^{-1}$. Two sets of membranes were produced for mechanical assays: one without any treatment and other one was previously swelled in water, frozen in liquid nitrogen, lyophilized overnight and stored until further analysis. Prior to mechanical tests, both sets of samples were immersed in PBS during 2h. The thickness of all samples was measured using a micrometer with a precision of $1 \text{ } \mu\text{m}$. The mechanical tests were made at room temperature (RT) with a gauge length of 5 mm.

2.9. Scanning electron spectroscopy

The cross-section of the FS membranes was visualized through scanning electron microscopy (SEM, S4100, Hitachi, Japan), operating at 4 kV. All samples were previously sputtered with a conductive gold layer, using a sputter coater. Cross-sections were produced with liquid nitrogen. However, aiming to evaluate the cross-section microstructures, membranes were lyophilized until occurred spontaneous fractures.

3. Results and Discussion

3.1. Synthesis and Characterization of Modified Polysaccharides

Herein, CHT and ALG biopolymers were also modified with pendant methacrylic groups to introduce covalent bonds within the membrane nanostratification. The addition of covalent bonds in the bilayers could add improved mechanical properties and establish a more porous-like character. Briefly, methacrylated ALG (ALG-MA) was obtained by esterification of hydroxyl groups with methacrylic anhydride, whereas methacrylated CHT (CHT-MA) was achieved by EDC/NHS conjugation of the carboxyl group in methacrylic acid with the amine-containing CHT polymer.

3.1.1. Methacrylated Alginate

The synthesis of ALG-MA proceeded as before described in the Methods Section 3.2.1.1. The modified polysaccharide was then characterized by ¹H NMR and ATR-FTIR.

The proton NMR spectrum of the synthesized polymer is in agreement with literature reports and exhibits the characteristic peaks of both reaction components (Figure 19)²⁶. The peaks obtained at $\delta=6.64$ ppm and $\delta=6.21$ ppm are typical of the methacrylic protons, which corresponds to the methylene protons. On the other hand, at $\delta=2.37$ ppm is represented the methyl group peak, also characteristic of the methacrylic group. In addition, the peak at $\delta=5.09$ ppm is assigned to the anomeric protons of the glucose ring of alginate. At the end, an 8% DS of the synthesized ALG-MA was obtained, calculated as previously described.

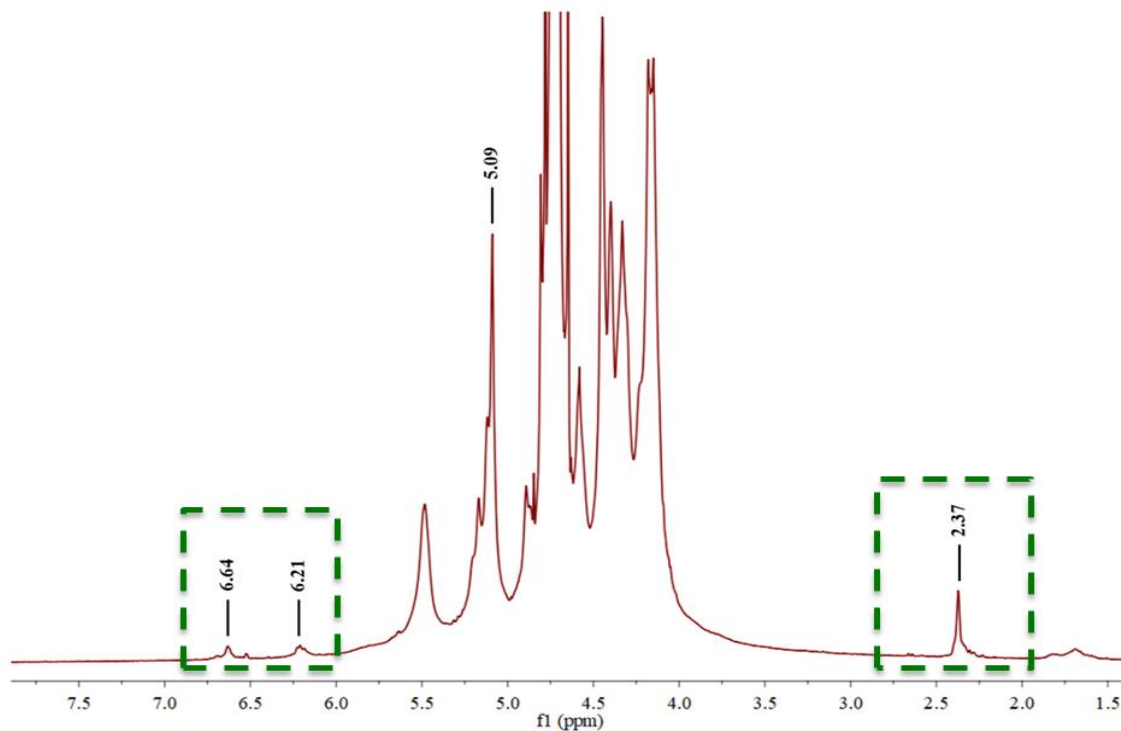


Figure 19. ^1H NMR spectrum of ALG-MA in D_2O at $70\text{ }^\circ\text{C}$.

Adding to ^1H NMR characterization, the ATR-FTIR spectra also validates that the successful modification occurred on ALG-MA (Figure 20). The initial analysis of the individual reagents reveals a band centered at 3283 cm^{-1} , which is assigned to **O-H** stretching and at 2920 cm^{-1} , and it is only observed in ALG and ALG-MA. At 2920 cm^{-1} it is shown a peak related to **C-H** stretching vibration in both ALG-MA and ALG. Regarding MAN, the characteristic band attached at 2992 cm^{-1} is related to unsaturated **C-H** stretching, on the other hand at 2930 and 2855 cm^{-1} is represented the saturated **C-H** stretching³⁰. In addition, the antisymmetric CO_2^- stretch is visible at 1599 (ALG-MA) and 1595 cm^{-1} (ALG), on the other hand, the peaks intensity at 1406 (ALG-MA) and 1405 cm^{-1} (ALG) are related to the symmetric CO_2^- stretch. For the MAN, the carboxyl stretching (**C=O**) is represented by the peaks at 1802 , 1746 and 1721 cm^{-1} ³⁰. As for the CHT-MA, **C=O** stretch is represented at 1734 cm^{-1} , which occurred by the incorporation of the methacrylic group into the alginate chain. Therefore, the antisymmetric **C-O-C** stretch vibration band is found at 1027 and 1026 cm^{-1} , for ALG-MA and ALG, respectively. Also, it is noted at 1026 cm^{-1} the skeletal vibration of ALG. Finally, the peaks at 812 (ALG-MA) and 814 cm^{-1} (ALG) are attributed to the **C-H** vibration of the pyranose (ring of the alginate) group.

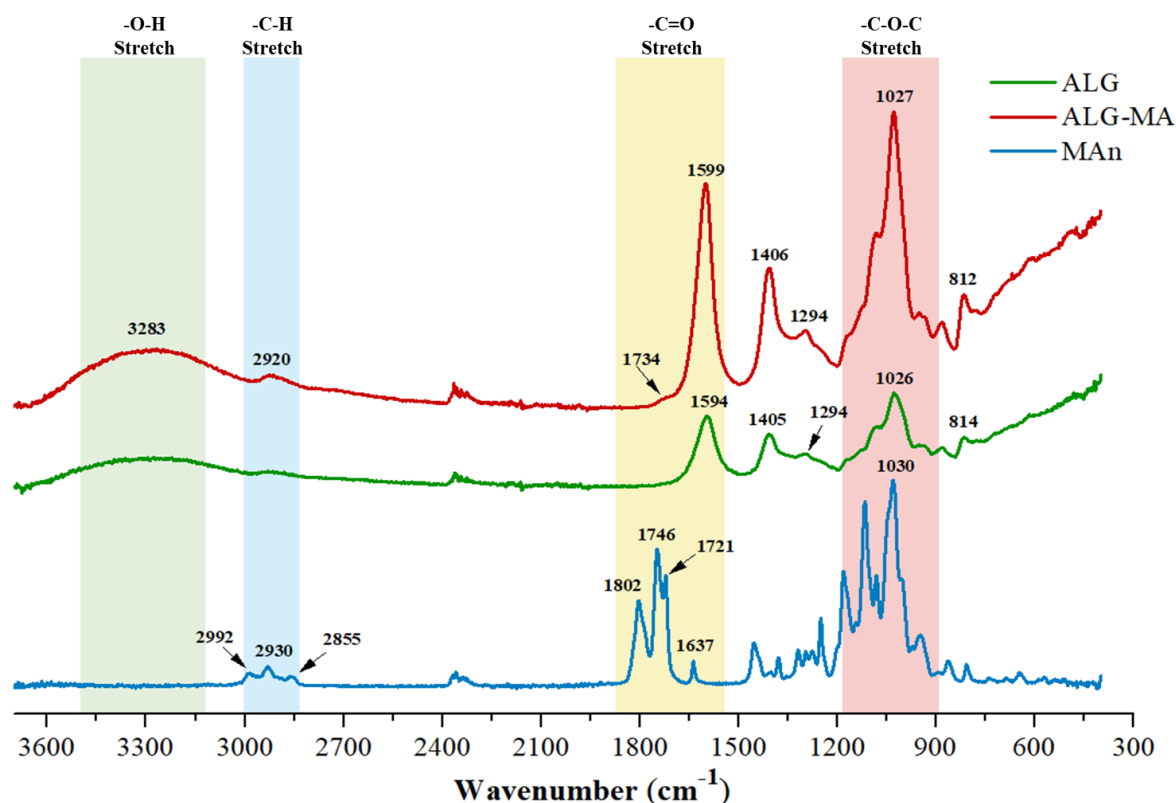


Figure 20. ATR-FTIR spectra of ALG-MA and its reaction components.

3.1.2. Methacrylated Chitosan

Methacrylic moieties have been attached through carbodiimide chemistry onto the chitosan chain following the procedure already reported in the Methods Section 3.2.1.2. The presence of side-chain moieties was verified and quantified by means of ^1H NMR and ATR-FTIR. The ^1H NMR spectrum of the CHT-MA is represented in Figure 21. As the spectrum demonstrates, all the characteristic peaks of the synthesized polymer are in agreement with those already reported in literature³¹. In detail, the two peaks around $\delta=6.19$ ppm and $\delta=5.98$ ppm are characteristic to the vinyl protons of the inserted moieties. In addition, the anomeric protons of the polysaccharide chain are observed from $\delta=5.06$ ppm to $\delta=5.162$ ppm. Moreover, the signal of the methyl groups of the acetyl moieties on CHT is assigned at $\delta=2.50$ ppm and the presence of the methyl group of the methacrylate moiety on the polymer chain is observed at $\delta=2.40$ ppm. The DS of the modified CHT was about 12%, calculated as before described.

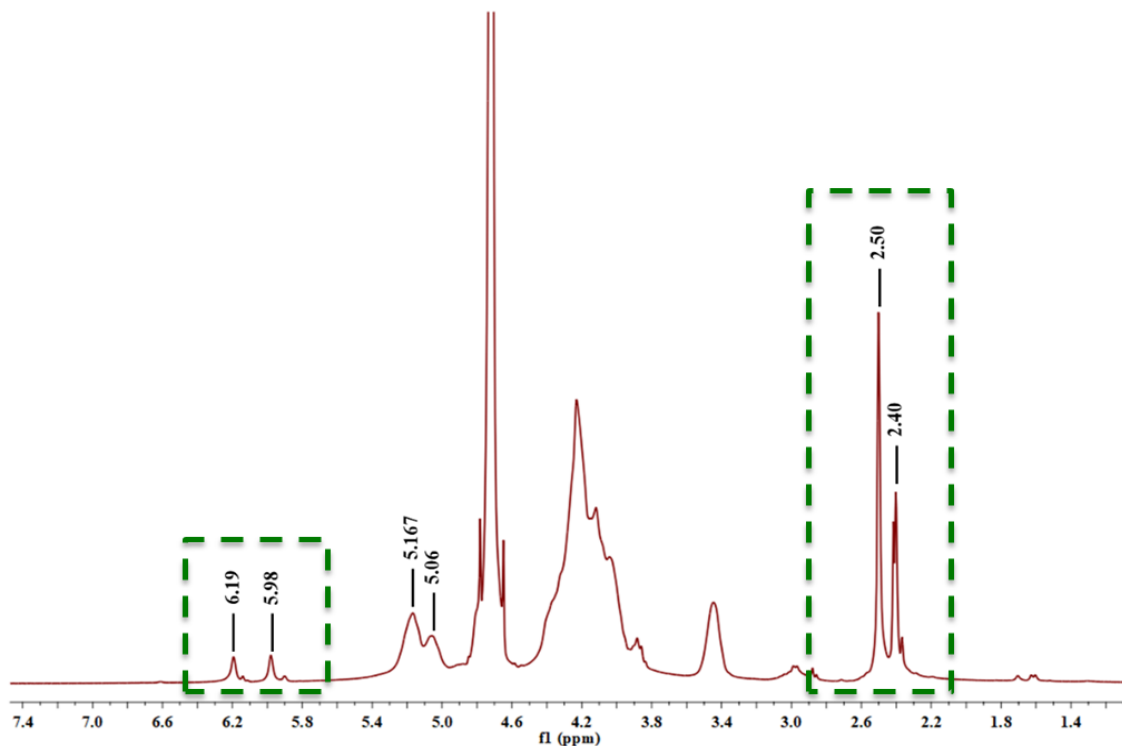


Figure 21. ^1H NMR spectrum of CHT-MA in D_2O at $70\text{ }^\circ\text{C}$.

Adding to ^1H NMR characterization, the ATR-FTIR spectra were acquired to assure the successful modification of the CHT-MA (Figure 22). At a primarily look, it is easily observed a broad and strong band centred at 3294 cm^{-1} for CHT-MA, as similarly observed in CHT spectrum, which corresponds to the stretching vibration of **O-H**, the extension vibration of **N-H** and intermolecular hydrogen bonds of polysaccharide^{32,33}. It is also evident the bands at 2885 and 2868 cm^{-1} which are assigned to **C-H** stretching vibrations in CHT-MA and CHT, respectively³². As for MA, the peaks at 2962 and 2929 cm^{-1} represent the stretch of the CH_2 and CH_3 , respectively. In addition, the strong band at 1689 cm^{-1} correspond to the stretch vibration of carboxyl group (**C=O**) in MA spectrum. Moreover, at 1591 cm^{-1} it is evidenced the amide stretching vibration characteristic the CHT spectrum³². As for the CHT-MA, it is important to emphasize the peaks at 1641 and 1548 cm^{-1} which are assigned to the stretching vibration of carboxyl group (**C=O**) and amide, respectively, where the first one was inherited from MA and the second one from CHT. The ATR-FTIR data also shows a peak at 1632 cm^{-1} which represent the **C=C** stretching due to the vinyl unsaturation present in MA monomer³⁴. The skeletal vibration of **C-O** stretching it is observed at 1062 and 1028 cm^{-1} , for CHT-MA and at 1024 cm^{-1} , for CHT. Also, the absorption bands at 1152 (CHT-MA) and 1149 cm^{-1} (CHT) can be attributed to asymmetric

stretching of the C-O-C bridge. Furthermore, the signal 898 and 891 cm^{-1} resembles to the C-H bending out of the plane of the ring of monosaccharides ³⁵.

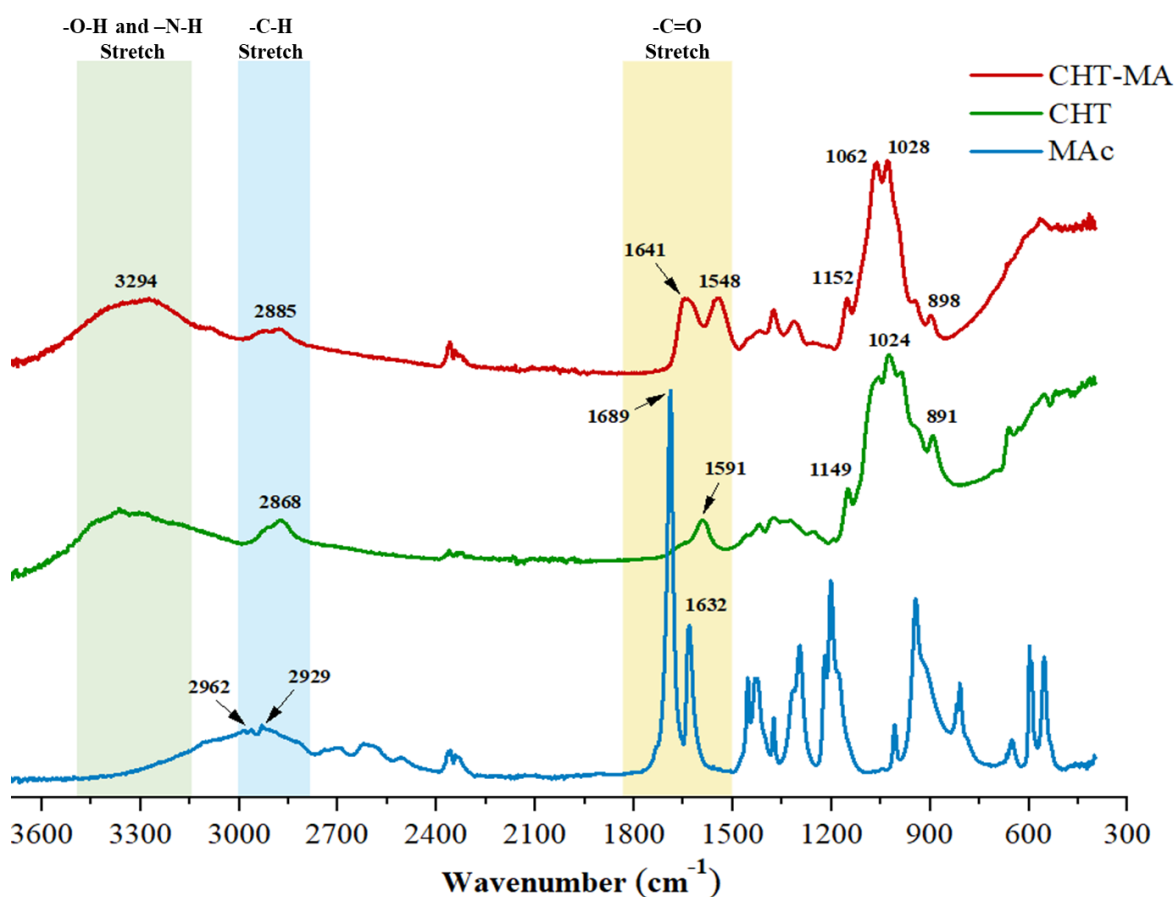


Figure 22. ATR-FTIR spectra of CHT-MA and its reaction components.

3.2. Build-up of multilayered films

The LbL approaches are mainly based on electrostatic interactions, as reported in literature ³. In this regard, prior to QCM-D monitoring, the zeta potential of all polyelectrolytes was measured under working conditions (pH=5.5 at RT and 0.15 M NaCl). As expected ALG presents a negative charge (-23.1 ± 0.4 mV) as well as ALG-MA (-18.8 ± 0.3 mV) while CHT (19.6 ± 0.3 mV) and CHT-MA (13.6 ± 0.3 mV) exhibit positive electrical charge. These results confirm the cationic and anionic nature of CHT-MA and ALG-MA, respectively, even after chemical functionalization (Figure 23B). In this sense, we hypothesize that the positively charged CHT-MA and the negatively charged ALG-MA could be successfully self-assembled by electrostatic-driving forces, in a similar way of CHT/ALG multilayers.

Chapter 4: Results and Discussion

Afterwards, the possible buildup of CHT-MA/ALG-MA multilayered films, through the sequential adsorption of the oppositely charged polymers, was assessed *in situ* with the QCM-D technique by applying an alternating electric field across the gold-coated quartz crystal sensor. In parallel, QCM-D monitoring of CHT/ALG multilayered films was also performed as the control system.

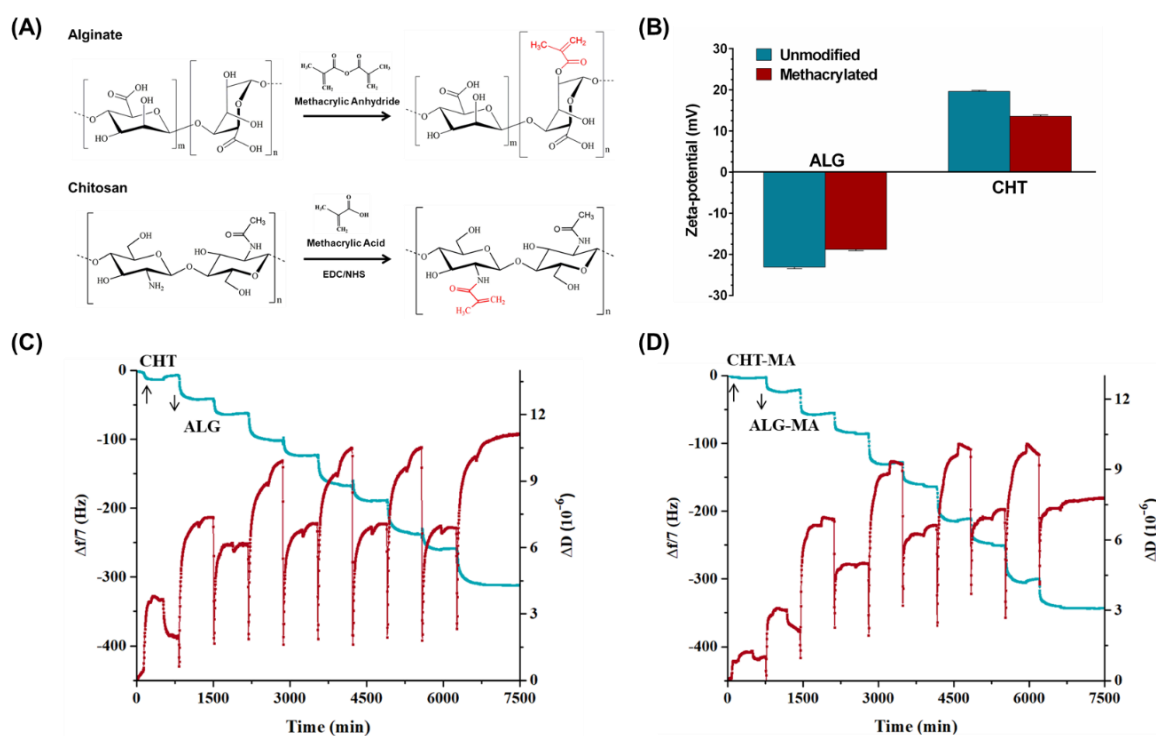


Figure 23. Overview of the synthesis route, electrokinetic potential and thin film deposition. **(A)** Chemical modification of alginate (ALG) and chitosan (CHT) to their methacrylated (MA) counterparts. **(B)** Zeta-potential analysis of ALG and CHT after methacrylation. **(C, D)** QCM-D analysis of build-up assemblies of **(C)** CHT/ALG, and **(D)** CHT-MA/ALG-MA up to 5 deposition layers in 0.15 M NaCl, normalized frequency Δf_7 (blue) and dissipation ΔD_7 (red), obtained at seventh overtone.

Figure 23C and 23D show the normalized frequency (Δf_n) and dissipation factor (ΔD) variations obtained at the 7th overtone ($n = 7$) during the construction of five bilayers of CHT/ALG and CHT-MA/ALG-MA films, respectively, onto the gold-plated quartz crystal substrates. The decrease on normalized frequency after each deposition steps is related with the increased mass over the gold-coated quartz crystals, indicating the successful deposition of polyelectrolytes at every stage of the adsorption process as well the gradual growth of both multilayered films. In this sense, we hypothesize that CHT/ALG and CHT-MA/ALG-MA multilayers can be assembled in fashion modes to produce hierarchical FS membranes.

Moreover, comparing both systems, CHT/ALG and CHT-MA/ALG-MA films present similar Δ_f values after the deposition of 5 bilayers, suggesting that the introduction of the MA pendant groups doesn't cause any change in the build-up of CHT-MA/ALG-MA films. Concerning the energy dissipation, this one increases after each layer deposition, indicating the non-rigid behavior as well as the viscoelastic nature of the absorbed materials, which is a characteristic of soft and hydrated films.

Usually, QCM-D data are also used to estimate the thickness variations of the multilayered films at each adsorption step, by using Voigt-based viscoelastic models^{13,36}. The cumulative thickness evolution also allows to predict the film growth mode and can be extrapolated for flat freestanding membranes with variable number of bilayers. However, in our study, the calculation of the film thickness doesn't give any reliable information, since the hierarchically structured membranes, that will be further produced, will be exposed to UV light to induce photocrosslinking of methacrylate moieties. The photocrosslinking process may produce some changes in the internal structure of the membranes, affecting the total thickness of the system.

3.3. Production of the freestanding membranes

With the confirmation of successful deposition of the chosen polyelectrolytes by QCM-D experiments, the next step was to carry out the FS membranes production. For that, a dipping robot was used to fabricate the FS multilayered membranes over a low surface energy substrate (PP substrate). The process was repeated for 200 times at RT and consisted in a consecutive and sequential absorption of polyelectrolytes by immersing in according washing and polyelectrolyte solutions. At the end, four different types of FS membranes were obtained, after drying at RT and via a simple detachment from the underlying PP substrate: the standard (CHT/ALG)₂₀₀ and (CHT-MA/ALG-MA)₂₀₀ membranes, as well as the hierarchically structured (10/10)₂₀₀ and (25/25)₂₀₀ membranes. It should point out that (CHT-MA/ALG-MA)₂₀₀ membranes seemed more thinner than the other membranes, after removing from the substrate. Afterwards, all types of produced membranes were immersed in Irgacure solution for 15 min and photocrosslinked under UV light during 5 min. An overall schematic of all the necessary steps for producing photocrosslinked FS multilayered membranes are presented in detail in Figure S1†.

3.4. ATR-FTIR analysis

In order to prove the photocrosslinked reaction of methacrylate groups, ATR-FTIR analysis of one of the hierarchically structured membranes was performed before and after UV irradiation treatment. Figure 24 shows the ATR-FTIR spectra of (CHI/ALG)₂₀₀, exposed to UV, as well as the hierarchal (10/10)₂₀₀ membranes, before and after photo-crosslinking. At a primarily look, these spectra, as expected, shares similarities with the CHT, ALG, ALG-MA and CHT-MA ones, which is the case of the large **O-H** stretching band between 3500 and 3000 cm⁻¹ (represented in the green region), the **C-H** stretching vibrations between 3000 and 2700 cm⁻¹, (in blue region) and the antisymmetric **C-O-C** stretch vibrations band centered at around 1000 cm⁻¹. Moreover, at 1590 cm⁻¹ (CHT/ALG)₂₀₀ and 1594 cm⁻¹ (10/10)₂₀₀ after UV curation it is evidenced the amide stretching vibrations characteristic of the CHT spectrum³². In the other hand, the peaks intensity at 1406 (CHT/ALG)₂₀₀, 1408 cm⁻¹ (10/10)₂₀₀ and (10/10)₂₀₀ after UV are related to the symmetric CO₂⁻ stretch, characteristic of ALG. However, the most notorious peaks are centered at 1604 and 1558 cm⁻¹, represented in the (10/10)₂₀₀ spectrum, which are assigned to the stretching vibration of carboxyl groups (**C=O**) and amide, respectively, where the first one was inherited from MA and the second one from CHT. After photocrosslinking, the peak at 1604 cm⁻¹ decreases drastically in (10/10)₂₀₀, which confirms that the consumption of the double bonds of methacrylic groups from CHT-MA/ALG-MA layers. Thus, it's expected that MA photocrosslinking could allow the formation of interconnected layers through the covalent bonding.

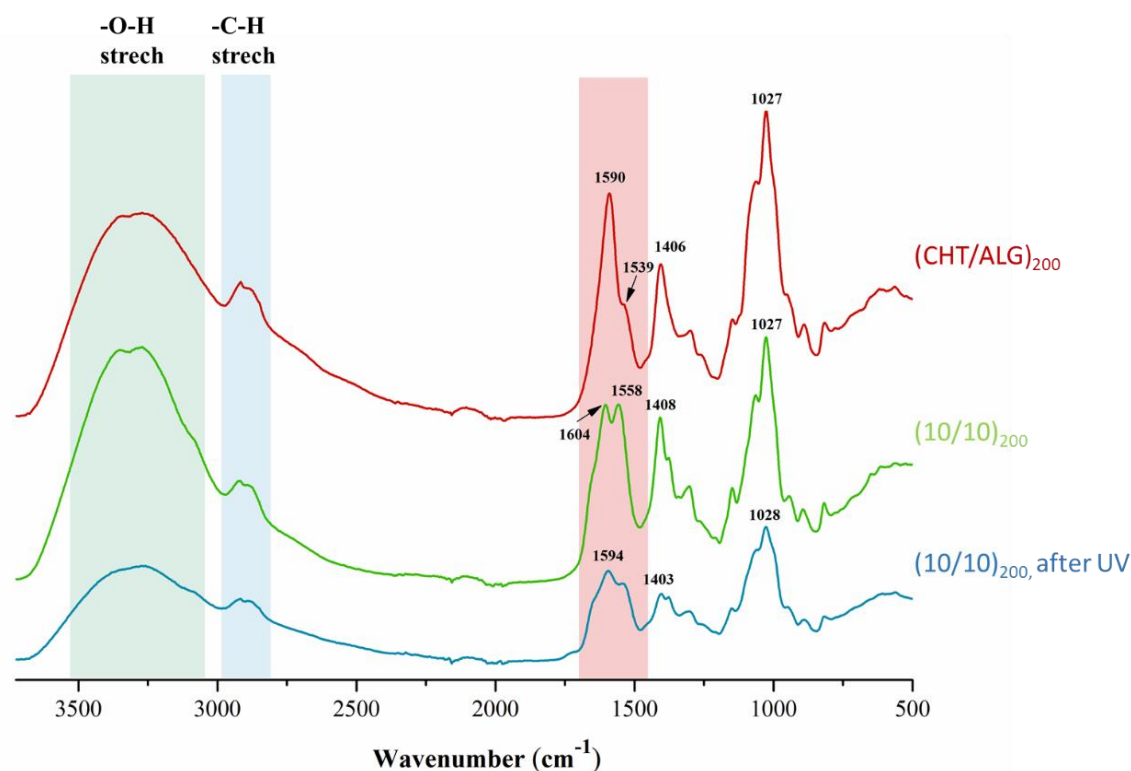


Figure 24. ATR-FTIR spectra of the FS membranes made of (CHT/ALG)₂₀₀ exposed to UV light, red line, (10/10)₂₀₀, green line, and (10/10)₂₀₀ after UV, blue line. The relevant area, after photocrosslinking, is represented in the red band.

3.5. Water uptake ability

FS membranes based in CHT and ALG derivatives are composed by polyelectrolytes with abundant hydrophilic groups such as hydroxyl, amine, and carboxyl groups, which can promote water-uptake^{9,18}. The water uptake profiles of the different FS multilayered membranes were evaluated for up to 10 min in PBS solution at physiological conditions (pH = 7.4, RT). The results obtained are demonstrated in Figure 25A. At a first look, it is possible to observe appreciable water uptake ability across all FS membranes, and all of them seem to reach maximum water content in few seconds, except (CHT-MA/ALG-MA)₂₀₀ membranes that reaches the equilibrium after 1 min. In fact, these membranes present highest water contents, which can be explained by the likely porous structure created upon photocrosslinking. Interestingly, the hierarchical membranes composed by intercalated layers of CHT/ALG and CHT-MA/ALG-MA exhibit lower hydration levels than (CHT-MA/ALG-MA)₂₀₀ showing a water uptake ability quite similar to the (CHT/ALG)₂₀₀

membranes, although slightly higher. The hierarchical structured membranes are composed by both CHT/ALG and CHT-MA/ALG-MA bilayers, which is expected a water uptake ability limited by the swelling behavior of the control membranes. However, for thicker intercalation block (25/25)₂₀₀ membranes, a lower water uptake was observed. Therefore, increasing the number of bilayers in each intercalated block seems to affect the water uptake ability of the hierarchical membranes.

3.6. Mechanical tests

To analyze the mechanical properties of the hierarchical membranes, tensile tests were performed in hydrated samples in order to mimic the physiological environment (Figure 25 B-E). Moreover, tensile tests of the control membranes, (CHT/ALG)₂₀₀ and (CHT-MA/ALG-MA)₂₀₀, were also realized. Otherwise, to evaluate the effect of the lyophilization to promote the formation of open porous within the MA photocrosslinked layers, it was also performed mechanical assays on FS membranes previously frozen and dried by lyophilization. Interestingly, the frozen and lyophilization processes slightly increase the Young's modulus (E) of the photocrosslinked membranes, even the (CHT/ALG)₂₀₀ system. Nevertheless, with or without lyophilization, the (CHT/ALG)₂₀₀ standard membranes exhibit the highest Young's modulus than the hierarchical ones. This observation corroborates the water uptake results, where the (CHT/ALG)₂₀₀ membranes have presented lower hydration levels. In fact, when FS membranes have higher ability to retain more water like the hierarchical membranes, a stiffness decrease was already observed due to the increase of water mobility that causes a kind of plasticization phenomena^{21,37}. Furthermore, it's expected the introduction of MA photocrosslinked moieties promotes the formation of interconnected porous interlayers, thus retaining much more water than the standard (CHT/ALG)₂₀₀ membranes. Indeed, the plasticization effect in hierarchical structured membranes is corroborated by the decrease of the ultimate tensile strength meaning that hierarchical membranes are more elastic and stretchable than the (CHT/ALG)₂₀₀ probably because of the well-organized microstructure that contributes for more efficient stress dispersion. Moreover, the strain energy absorbed until membrane rupture is higher for the hierarchical structured systems, in particular for the interlayered (10/10)₂₀₀ membranes and after the frozen/lyophilization processes which also seems to play a relevant role in pore formation.

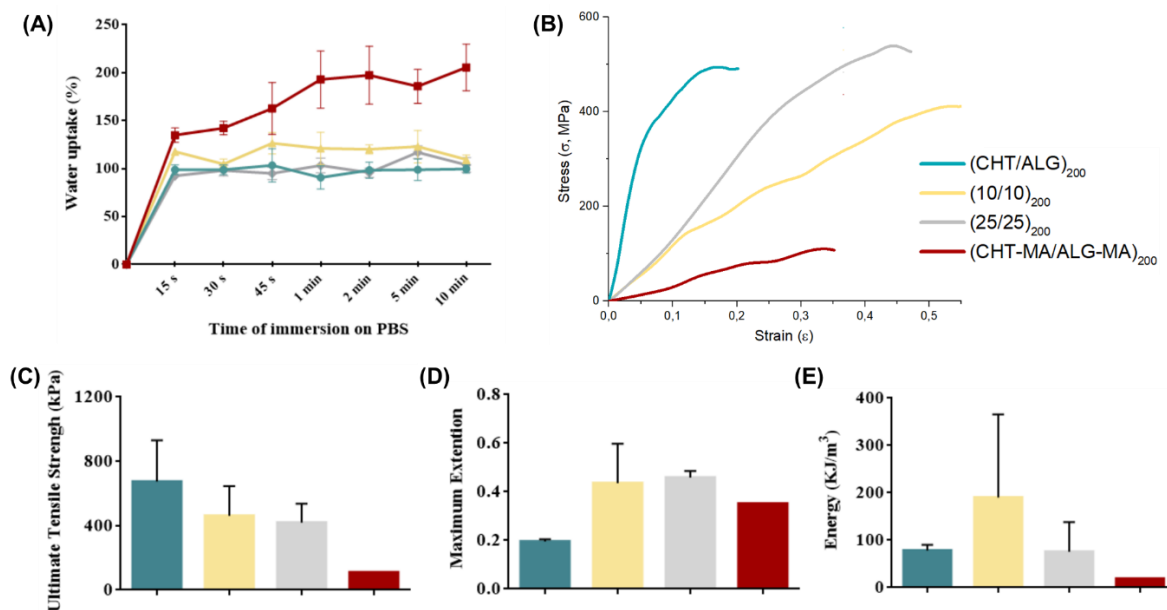


Figure 25. (A) Water uptake measurements of (CHT/ALG)₂₀₀, (CHT-MA/ALG-MA)₂₀₀, (10/10)₂₀₀ and (25/25)₂₀₀ FS multilayered membranes immersed in PBS solution for 10 min. (B-D) Mechanical assays performed through tensile tests in (CHT/ALG)₂₀₀, (CHT-MA/ALG-MA)₂₀₀, (10/10)₂₀₀ and (25/25)₂₀₀ membranes, previously swelled in water, frozen in liquid nitrogen and then lyophilized overnight. After that, were hydrated in 2h of PBS solution. (B) Representative stress-strain curves. (C) Ultimate tensile strength. (D) Maximum extension. (E) Strain energy density.

3.7. Scanning electron microscopy analysis

In order to observe the microstructural morphology of the cross-section membranes, SEM analysis was also performed. Figure 26 A and B show the cross-section of (CHT/ALG)₂₀₀ and (25/25)₂₀₀ lyophilized membranes, respectively. Such samples were fractured in liquid nitrogen. Comparing both cross-sections is possible to observe the hierarchical structure of (25/25)₂₀₀ membrane composed by 4 blocks: 25 bilayers of CHT/ALG interlayered with 25 bilayers of CHT-MA/ALG-MA, repeated 2 times. Despite the clear observation of the well-organized structure, the fracture in liquid nitrogen doesn't allow to inspect the cross-section morphology. To achieve this purpose, some samples were left under lyophilization until complete fracture. In Figure 26C is possible to confirm that liquid nitrogen created an artefact effect on the morphology. Herein, the cross-section of (CHT/ALG)₂₀₀ show a quite internal homogeneous morphology as confirmed at higher magnification (Figure 26D). Interestingly, at the same magnification, the cross-section of the hierarchically structured (10/10)₂₀₀ membrane (Figure 26E) presents two distinct regions. At the bottom of the image

Chapter 4: Results and Discussion

is possible to observe a kind of stratification, which morphology is quite similar to the (CHT/ALG)₂₀₀ membranes. Moreover, at the top, a porous interconnected network is clearly visible. This confirms that the photocrosslinked MA moieties are able to create a multilayered porous structure after lyophilization. The hierarchically structure composed by linear stratification regions interlayered with porous interconnected networks, in a similar way of the jellyfish anisotropic structure (Figure 26F). Such hierarchical structure supports the mechanical results aforementioned, where the membrane becomes less brittle and more stretchable, which allows the stress dispersion across it.

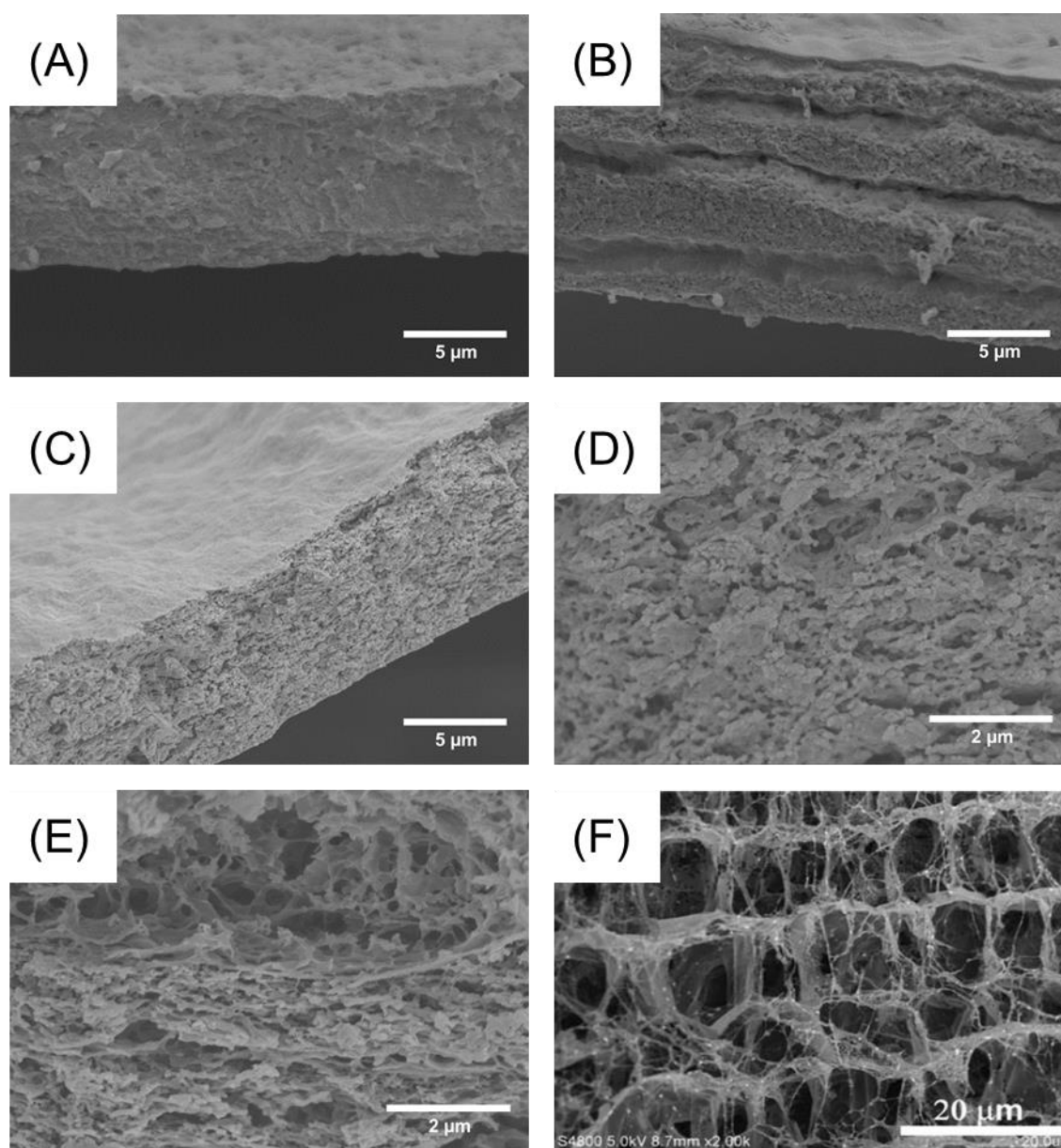


Figure 26. SEM images of multilayered membranes structure. (A, B) Lyophilized membranes cross-sections which were fractured with liquid nitrogen, (A) (CHT/ALG)₂₀₀ and (B) (25/25)₂₀₀. (C–E) Cross-section of the

freeze-dried multilayered membranes fractured during the freeze-drying process. (CHT/ALG)₂₀₀ membranes at (C) low and (D) high magnification comparing with the (E) intercalated (10/10)₂₀₀. (F) SEM micrographs of freeze-dried jellyfish mesoglea at low magnification showing a layered porous structure³⁸.

4. Conclusions

In this work, easily detachable membranes based on CHT and ALG derivatives were successfully obtained via LbL. The introduction of the photocrosslinkable methacrylic groups into the FS membranes allowed the development of hierarchically structured FS membranes which shown a layered porous structure arising from the photocrosslinkable moieties combined with homogeneous stratification layers. This bioinspired hierarchical design exhibits interesting elastic stretching behavior due to the well-organized structure, finding particular applicability in soft tissue regeneration. Despite the proof-of-concept of the bioinspired approach, this novel strategy requires further improvements to be used as an effective methodology to modulate the mechanical properties of FS membranes.

References

1. Decher, G. & Schmitt, J. Fine-Tuning of the film thickness of ultrathin multilayer films composed of consecutively alternating layers of anionic and cationic polyelectrolytes. *Prog. Colloid Polym. Sci.* **89**, 160–164 (1992).
2. Silva, J. M., García, J. R., Reis, R. L., García, A. J. & Mano, J. F. Tuning cell adhesive properties via layer-by-layer assembly of chitosan and alginate. *Acta Biomater.* **51**, 279–293 (2017).
3. Borges, J. & Mano, J. F. Molecular interactions driving the layer-by-layer assembly of multilayers. *Chem. Rev.* **114**, 8883–8942 (2014).
4. Caridade, S. G. *et al.* Myoconductive and osteoinductive free-standing polysaccharide membranes. *Acta Biomater.* **15**, 139–149 (2015).
5. Larking, A. L., Davis, R. M. & Rajagopalan, P. Biocompatible, Detachable, and Free-Sanding Polyelectrolyte Multilayer Films. *Biomacromolecules* **11**, 2788–2796 (2010).
6. Ariga, K., McShane, M., Lvov, Y. M., Ji, Q. & Hill, J. P. Layer-by-layer assembly for drug delivery and related applications. *Expert Opin. Drug Deliv.* **8**, 633–644 (2011).
7. Fukuda, Y. *et al.* Layer-by-layer cell coating technique using extracellular matrix facilitates rapid fabrication and function of pancreatic β -cell spheroids. *Biomaterials* **160**, 82–91 (2018).
8. Liu, J., Willför, S. & Xu, C. A review of bioactive plant polysaccharides: Biological activities, functionalization, and biomedical applications. *Bioact. Carbohydrates Diet.*

- Fibre* **5**, 31–61 (2015).
9. Almodóvar, J., Place, L. W., Gogolski, J., Erickson, K. & Kipper, M. J. Layer-by-Layer Assembly of Polysaccharide-Based Polyelectrolyte Multilayers: A Spectroscopic Study of Hydrophilicity, Composition, and Ion Pairing. *Biomacromolecules* **12**, 2755–2765 (2011).
 10. Basu, A., Kunduru, K. R., Abteu, E. & Domb, A. J. Polysaccharide-Based Conjugates for Biomedical Applications. *Bioconjug. Chem.* **26**, 1396–1412 (2015).
 11. Sousa, M. P., Gonzalez de Torre, I., Oliveira, M. B., Rodríguez-Cabello, J. C. & Mano, J. F. Biomimetic click assembled multilayer coatings exhibiting responsive properties. *Mater. Today Chem.* **4**, 150–163 (2017).
 12. Gomes, T. D. *et al.* Adhesive free-standing multilayer films containing sulfated levan for biomedical applications. *Acta Biomater.* **69**, 183–195 (2018).
 13. Sousa, M. P. *et al.* Bioinspired multilayer membranes as potential adhesive patches for skin wound healing. *Biomaterials Science* **6**, 1962–1975 (2018).
 14. Sousa, M. P., Caridade, S. G. & Mano, J. F. Control of Cell Alignment and Morphology by Redesigning ECM-Mimetic Nanotopography on Multilayer Membranes. *Adv. Healthc. Mater.* 1601462 (2017). doi:10.1002/adhm.201601462
 15. Martins, G. V., Merino, E. G., Mano, J. F. & Alves, N. M. Crosslink Effect and Albumin Adsorption onto Chitosan/Alginate Multilayered Systems: An in situ QCM-D Study. *Macromol. Biosci.* **10**, 1444–1455 (2010).
 16. Pinto, E. M., Barsan, M. M. & Brett, C. M. A. Mechanism of Formation and Construction of Self-Assembled Myoglobin/Hyaluronic Acid Multilayer Films: An Electrochemical QCM, Impedance, and AFM Study. *J. Phys. Chem. B* **114**, 15354–15361 (2010).
 17. Gaudière, F. *et al.* Genipin-cross-linked layer-by-layer assemblies: Biocompatible microenvironments to direct bone cell fate. *Biomacromolecules* **15**, 1602–1611 (2014).
 18. Silva, J. M., Caridade, S. G., Oliveira, N. M., Reis, R. L. & Mano, J. F. Chitosan–alginate multilayered films with gradients of physicochemical cues. *J. Mater. Chem. B* **3**, 4555–4568 (2015).
 19. Moura, D. *et al.* High performance free-standing films by layer-by-layer assembly of graphene flakes and ribbons with natural polymers. *J. Mater. Chem. B* **4**, 7718–7730 (2016).
 20. Silva, C. *et al.* Nanostructured Biopolymer/Few-Layer Graphene Freestanding Films with Enhanced Mechanical and Electrical Properties. *Macromol. Mater. Eng.* **303**, 1700316 (2018).
 21. Silva, J. M. *et al.* Tailored freestanding multilayered membranes based on chitosan and alginate. *Biomacromolecules* **15**, 3817–3826 (2014).
 22. Achterberg, V. F. *et al.* The Nano-Scale Mechanical Properties of the Extracellular Matrix Regulate Dermal Fibroblast Function. *J. Invest. Dermatol.* **134**, 1862–1872 (2014).
 23. Sanchez, C., Arribart, H. & Guille, M. M. G. Biomimetism and bioinspiration as tools

- for the design of innovative materials and systems. *Nat. Mater.* **4**, 277–288 (2005).
24. Shin, H., Jo, S. & Mikos, A. G. Biomimetic materials for tissue engineering. *Biomaterials* **24**, 4353–4364 (2003).
 25. Smeds, K. A. *et al.* Photocrosslinkable polysaccharides for in situ hydrogel formation. *J. Biomedial Mater. Res.* **54**, 115–121 (2001).
 26. Zhou, S., Bismarck, A. & Steinke, J. H. G. Ion-responsive alginate based macroporous injectable hydrogel scaffolds prepared by emulsion templating. *J. Mater. Chem. B* **1**, 4736–4745 (2013).
 27. Mignon, A. *et al.* Combinatory approach of methacrylated alginate and acid monomers for concrete applications. *Carbohydr. Polym.* **155**, 448–455 (2017).
 28. Diolosà, M. *et al.* Use of methacrylate-modified chitosan to increase the durability of dentine bonding systems. *Biomacromolecules* **15**, 4606–4613 (2014).
 29. Liu, M., Li, M.-D., Xue, J. & Phillips, D. L. Time-Resolved Spectroscopic and Density Functional Theory Study of the Photochemistry of Irgacure-2959 in an Aqueous Solution. *J. Phys. Chem.* **118**, 8701–8707 (2014).
 30. Tarducci, C., Schofield, W. C. E., Badyal, J. P. S., Brewer, S. A. & Willis, C. Synthesis of cross-linked ethylene glycol dimethacrylate and cyclic methacrylic anhydride polymer structures by pulsed plasma deposition. *Macromolecules* **35**, 8724–8727 (2002).
 31. Diolosà, M. *et al.* Use of methacrylate-modified chitosan to increase the durability of dentine bonding systems. *Biomacromolecules* **15**, 4606–4613 (2014).
 32. Lawrie, G. *et al.* Interactions between alginate and chitosan biopolymers characterized using FTIR and XPS. *Biomacromolecules* **8**, 2533–2541 (2007).
 33. Song, C., Yu, H., Zhang, M., Yang, Y. & Zhang, G. Physicochemical properties and antioxidant activity of chitosan from the blowfly *Chrysomya megacephala* larvae. *Int. J. Biol. Macromol.* **60**, 347–354 (2013).
 34. García, D. M. *et al.* Synthesis and characterization of poly(methacrylic acid) hydrogels for metoclopramide delivery. *Eur. Polym. J.* **40**, 1637–1643 (2004).
 35. Queiroz, M. F., Melo, K. R. T., Sabry, D. A., Sasaki, G. L. & Rocha, H. A. O. Does the use of chitosan contribute to oxalate kidney stone formation? *Mar. Drugs* **13**, 141–158 (2015).
 36. Martins, N. I. *et al.* Multilayered membranes with tuned well arrays to be used as regenerative patches. *Acta Biomater.* **57**, 313–323 (2017).
 37. Sousa, M. P., Cleymand, F. & Mano, J. F. Elastic chitosan / chondroitin sulfate multilayer membranes. *Biomed. Mater.* **11**, 35008 (2016).
 38. An, S. *et al.* Bio-inspired, colorful, flexible, defrostable light-scattering hybrid films for the effective distribution of LED light. *Nanoscale* **9**, 9139–9147 (2017).

Supplementary information

Bioinspired approach to Tune Mechanical Properties of Multilayered Freestanding Membranes for skin regenerative patches

Fernandes, E.A.¹, Patrício, S.G^{2#}, and Mano, J.F.^{2#}

¹ Department of Materials Engineering and Ceramics, University of Aveiro, Campus Universitário de Santiago, 3810-193, Aveiro, Portugal

² Department of Chemistry, CICECO – Aveiro Institute of Materials, University of Aveiro, Campus Universitário de Santiago, 3810-193, Aveiro, Portugal

Corresponding Author:

E-mail: sgpatricio@ua.pt; jmano@ua.pt

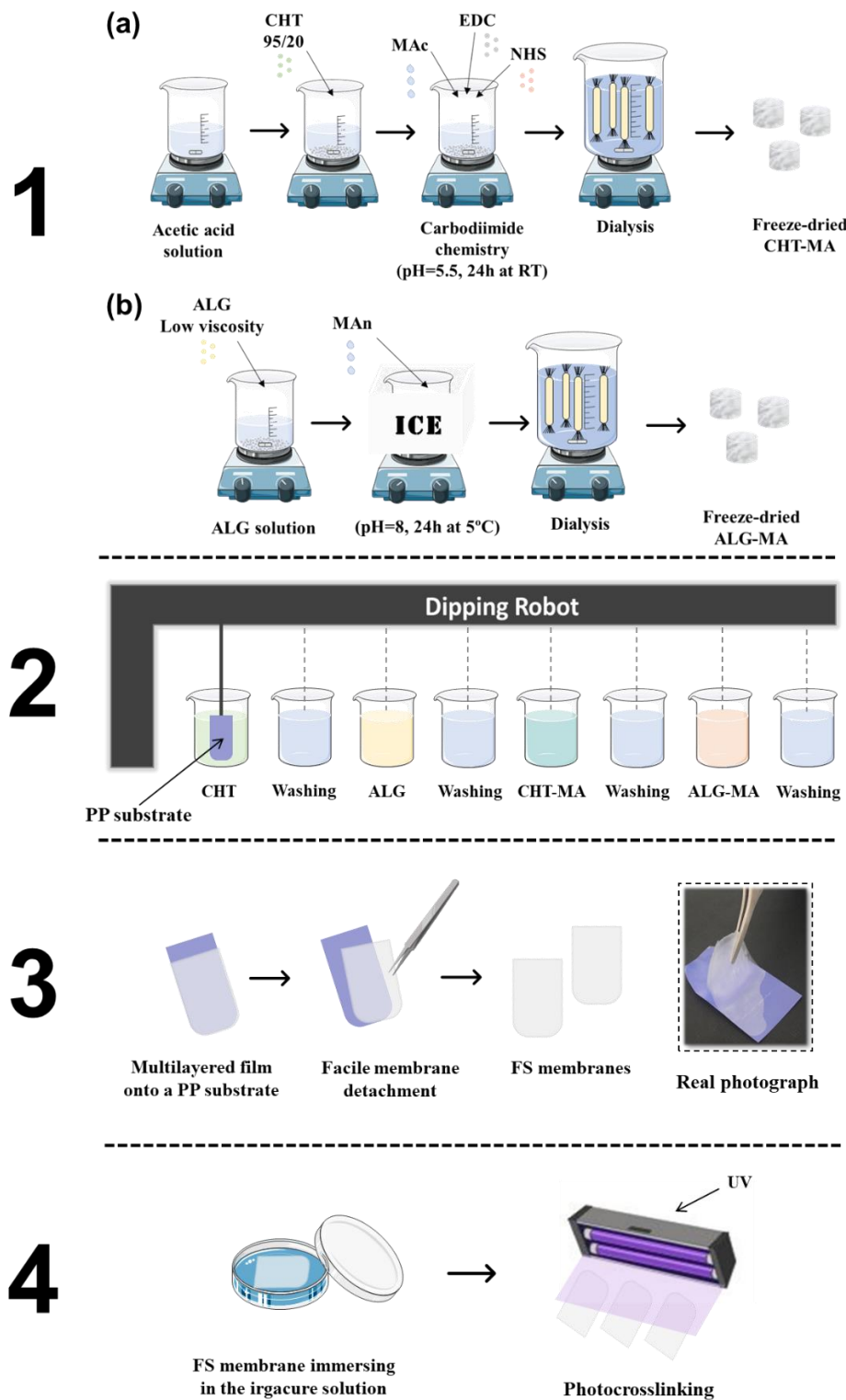


Figure S1†. Overview of steps needed to achieve the bioinspired membranes. **(1)** Schematic representation of the synthesis of the ALG-MA (a) and CHT-MA (b). **(2)** LbL assembly using the dipping robot equipment. **(3)** Detachment method employed to obtain the FS multilayered membranes and a real photograph of the procedure performed in the intercalated membrane (10/10)₂₀₀. **(4)** Photocrosslinking of the FS membranes.

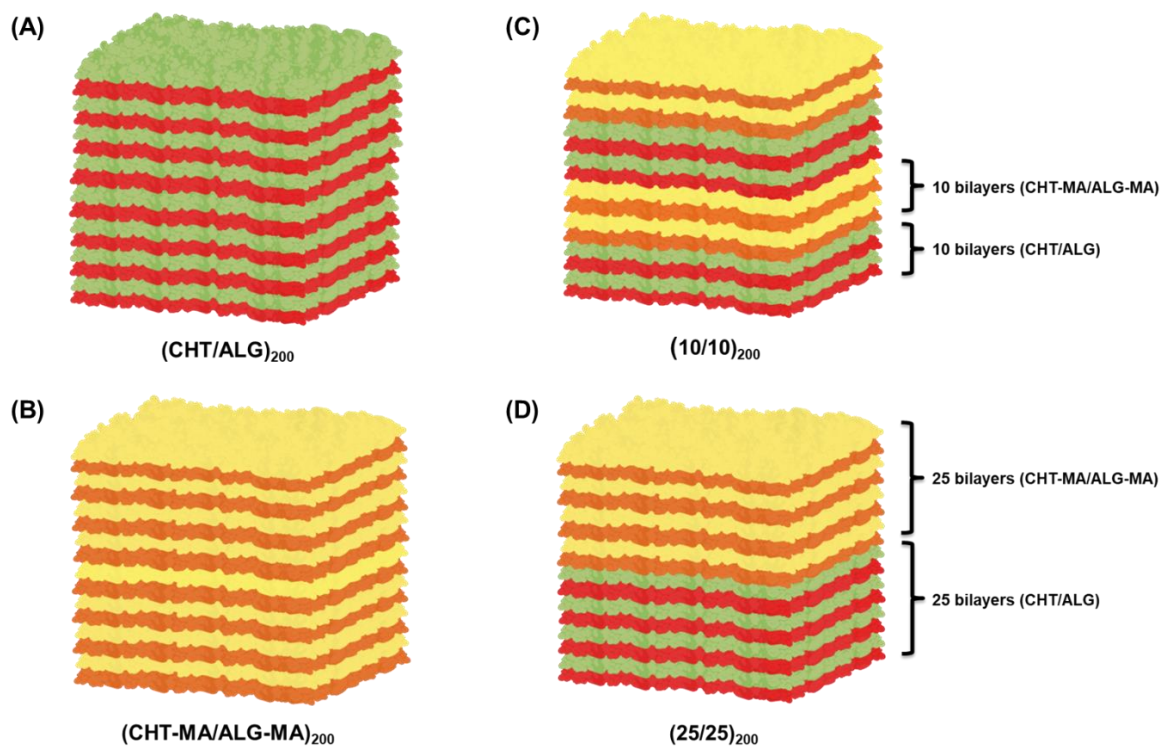


Figure S2†. All types of the produced FS multilayered membranes. **(A-B)** Control membranes: **(A)** multilayered membranes containing CHT and ALG $(\text{CHT}/\text{ALG})_{200}$ and **(B)** membranes containing the pendant methacrylic groups $(\text{CHT-MA}/\text{ALG-MA})_{200}$. **(C-D)** Intercalated membranes with multilayers alternately deposited with CHT and ALG and CHT-MA and ALG-MA, **(C)** ones with 10 bilayers each $(10/10)_{200}$ and **(D)** ones with 25 bilayers each $(25/25)_{200}$.

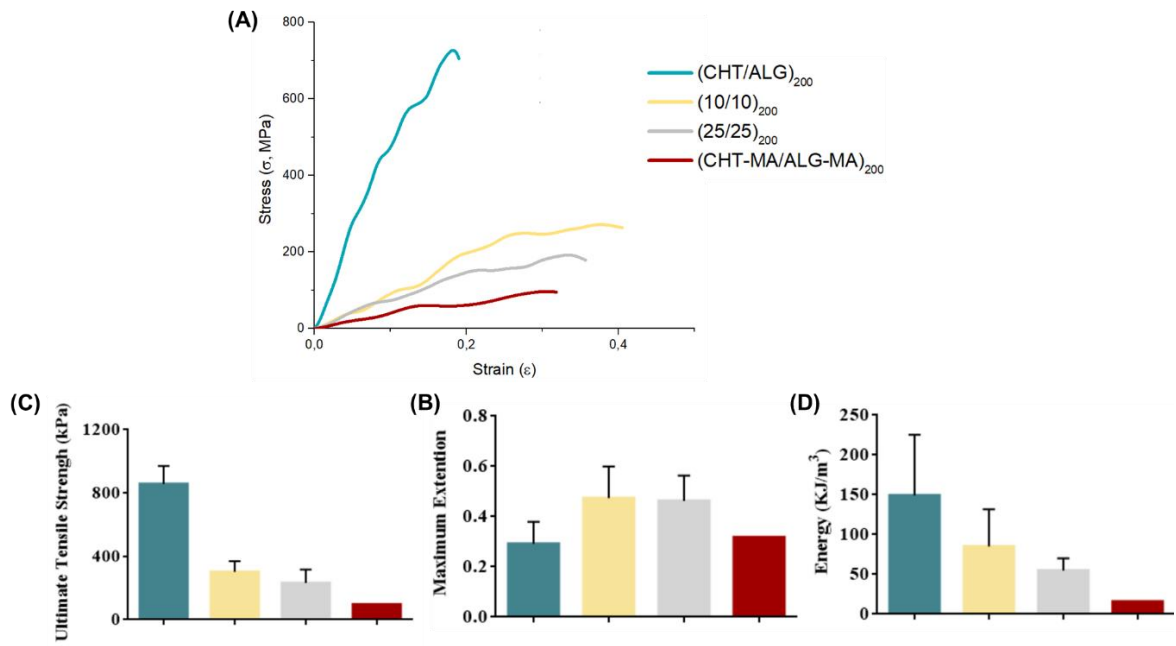


Figure S3†. Mechanical assays performed through tensile tests in (CHT/ALG)₂₀₀, (CHT-MA/ALG-MA)₂₀₀, (10/10)₂₀₀ and (25/25)₂₀₀ membranes (without lyophilization), hydrated in 2h of PBS solution. **(A)** Representative stress-strain curves. **(B)** Ultimate tensile strength. **(C)** Maximum extension. **(D)** Strain energy density.

Chapter 5: General Conclusions and Future Perspectives

Regenerative medicine is an established research field with tremendous potential for improving the quality of life at a worldwide-level. Successful applications in this field should be able to heal or replace damaged tissues effectively. Moreover, this type of medicine is the result of intertwining several novel and thriving areas, including tissue engineering. Currently, the number of clinically approved therapies using biomaterials for tissue engineering is increasing but its translation and effectiveness of these applications is still slow.

Among the polysaccharide agents, CHT and ALG are two of the most studied so far, by taking advantage of their available functional groups that allow easy chemical modification. By modifying the structure, researchers can attempt to tailor their properties for desired applications. In this work, easily detachable membranes made of naturally-available CHT and ALG were successfully obtained via LbL immersive assembly. The introduction of photocrosslinkable pendant methacrylic groups in both biopolymers allowed for rapid interlayer crosslinking of the bioinspired membranes upon UV exposure. The water uptake ability of FS membranes seems to peak within just a few seconds after immersion. However, (CHT-MA/ALG-MA)₂₀₀ showed a later equilibrium (after 1 min). Indeed, this last membrane presented the highest water ability. On the contrary, unmodified (CHT/ALG)₂₀₀ presented the lowest values. As for the intercalated multilayered membranes, (25/25)₂₀₀ showed lower water content value than (10/10)₂₀₀. Differences in swelling capacities across membranes may reflect important changes in the stability of the multilayered film as well as its microscopic structural organization and porosity. Indeed, this was confirmed by SEM microstructural analysis of the various conditions. As for the mechanical tests, the (CHT/ALG)₂₀₀ membranes, with or without freeze-drying process, showed the highest Young's modulus, whereas methacrylated membranes experienced decreased Young's modulus, and these results corroborate the water uptake studies. On the other hand, all modified intercalated (10/10)₂₀₀ and (25/25)₂₀₀ membranes, as well as the modified control membranes (CHT-MA/ALG-MA)₂₀₀, showed a decrease in the ultimate tensile strength, which suggests that the methacrylic modification could induce more elastic behavior of the multilayered films.

Overall, the obtained results suggest that the chemical modification with methacrylic pendant groups on the biopolymers has a significant effect on its physicochemical properties. In fact, whereas in the ALG-MA the modification occurred between hydroxyls, in CHT-MA the EDC/NHS mediated modification occurred at primary amines. This resulted in a significantly reduced charge of CHT-MA, when compared to unmodified CHT. Meanwhile, the impact of the modification on the charge of ALG-MA was not as evident, as it can be observed in the obtained zeta-potential analysis of the several polysaccharides. Because this LbL assembly process is mostly driven by electrostatic forces during immersion, film build-up might be hindered by the reduction of electrostatic forces due to modification. Although the introduced covalent bonds upon photocrosslinking are stronger than the non-covalent electrostatic forces between CHT and ALG, this was done in a post covalent conversion methodology. Thus, the multilayered films that are formed before the crosslinking could be weaker than unmodified ones due to reduced electrostatic interactions driving a less compact assembly. This hypothesis could explain the increased swelling capacities, as well as significantly more elastic behavior over unmodified membranes. As future alternatives for improving this system, two approaches are envisioned. Firstly, carry out CHT modification with methacrylic groups via its hydroxyl group and not the primary amine that determines strong electrostatic forces with the ALG carboxyl group. Such modification should not affect the polymer charge as significantly as the amine-modification approach here studied. Hence, the films developed this way could experience stronger electrostatic forces during layer build-up and then experience improved stiffness when photocrosslinked. Secondly, implementing different bioconjugation strategies other than the methacrylic modification, because the latter directs the system towards a post covalent conversion strategy. Using pendant clickable groups with fast reaction kinetics that can react *in situ* during layer build-up would allow for a different assembly process named consecutive covalent fabrication. In this approach, the multilayered films would be covalently crosslinked throughout the entire dipping process, which could help mitigate the key role of electrostatic forces for driving LbL assembly. Moving forward, the different strategies here present can yield multilayered membranes with a wide range of mechanical properties that could be interesting for biomedical applications.